



1

2 Non-Destructive Carabao Mango Sorter and Grader based on Physical Characteristics  
3 using Machine Learning

4

---

5 A Thesis  
6 Presented to the Faculty of the  
7 Department of Electronics and Computer Engineering  
8 Gokongwei College of Engineering  
9 De La Salle University

10

---

11 In Partial Fulfillment of the  
12 Requirements for the Degree of  
13 Bachelor of Science in Computer Engineering

14

---

15 by

16 BANAL Kenan A.  
17 BAUTISTA Francis Robert Miguel F.  
18 HERMOSURA Don Humphrey L.  
19 SALAZAR Daniel G.

20 November, 2025



# De La Salle University

21

## THESIS APPROVAL SHEET

22

This thesis entitled **Non-Destructive Carabao Mango Sorter and Grader based on Physical Characteristics using Machine Learning**, prepared and submitted by:

24

BANAL, Kenan A.

25

BAUTISTA, Francis Robert Miguel F.

26

HERMOSURA, Don Humphrey L.

27

SALAZAR, Daniel G.

28

29

with group number AISL-1-2425-C5 in partial fulfillment of the requirements for the degree of **Bachelor of Science in Computer Engineering, (BS-CPE)** has been examined and is recommended for acceptance and approval.

30

31

32

33

### PANEL OF EXAMINERS

34

---

**Dr. Donabel de Veas Abuan**

35

*Chair*

36

37

---

**Dr. Alexander Co Abad**

38

*Member*

39

---

**Engr. Dino Dominic F. Ligutan**

40

*Member*

41

---

**Dr. Reggie C. Gustilo**

39

*Adviser*

40

Date: \_\_\_\_\_

41



De La Salle University

42  
43  
44  
45

2025

All Rights Reserved. No part of this publication may be reproduced, stored in an information retrieval system, or transmitted, in any form or by any means, electronic, mechanical, by photocopying, scanning, recording, or otherwise, except under the terms of the applicable law.



46

## ACKNOWLEDGMENT

47  
48  
49  
50  
51  
52  
53  
54  
55  
56  
57  
58  
59

We would like to first acknowledge God the almighty for blessing and guiding us in this thesis paper and to our Family members for their support and encouragement. Furthermore, we would like to take our current adviser Dr. Reggie C. Gustilo for his support, guidance, and patience throughout our thesis. We would also like to thank our previous adviser Dr. Ana Antoniette Illahi for helping us with the thesis proposal and the proposal defense. Furthermore, we would like to thank our external advisor Dr. Cecilia Reyes for giving her experience insight and guidance in research related to Carabao mangoes in the Philippines. Moreover, we would like to thank our panelists Dr. Donabel de Veas Abuan, Dr. Alexander Co Abad, and Engr. Dino Ligutan for their comments and suggestions to improve our thesis. Additionally, we would like to thank our previous panelist member Engr. Jose Martin Maningo for giving advise during the thesis proposal defense. Lastly, we would like to thank the farmers Jerry Bravante, Ivan Joseph Palma, Ailen Q. Redome, and Jesus Redome for participating in our thesis paper and sharing their experience in mango farming.



60

## ABSTRACT

61 Current machine learning systems for Carabao mango sorting and grading primarily classify  
62 mangoes based on individual physical characteristics such as size, bruises, and ripeness.  
63 However, limited research has explored systems that can prioritize these characteristics  
64 according to user-defined preferences with customizable weighting. This study introduces  
65 a flexible Carabao mango grading and sorting system that integrates machine learning with  
66 a user-adjustable weighting mechanism, enabling dynamic prioritization or exclusion of  
67 ripeness, size, and bruises based on specific requirements. Different machine learning  
68 methods were evaluated for classifying ripeness and bruises separately. The dataset con-  
69 sisted of both publicly available images and researchers' own Carabao mango images, with  
70 a data split of 70-15-15 for training, validation, and testing, respectively. Convolutional  
71 Neural Network (CNN) models, particularly EfficientNetV2, achieved optimal performance  
72 for ripeness and bruise classification with accuracy scores of 98% and 99%, respectively.  
73 To validate these results, a comparative analysis between the best-performing model and  
74 expert evaluations was conducted, yielding an overall agreement accuracy of 79%. For size  
75 classification, two approaches (Computer Vision and Object Detection) were assessed for  
76 estimating mango length and width. Faster Region-based Convolutional Neural Network  
77 (Faster R-CNN) demonstrated the best overall performance, with measured length and  
78 width differences of 13.57% and 3.24% from the ground truth, respectively. Finally, the  
79 image acquisition system, consisting of an Raspberry Pi (RPi) with a camera module and  
80 conveyor belt setup, successfully demonstrated the proposed grading and sorting process



# De La Salle University

81 using the developed linear grading formula.

82 *Index Terms*—Machine Learning, Carabao mango, Bruises, Ripeness, Microcontrollers.



## TABLE OF CONTENTS

84	<b>Thesis Approval Sheet</b>	ii
85	<b>Acknowledgment</b>	iv
86	<b>Abstract</b>	v
87	<b>Table of Contents</b>	vii
88	<b>List of Figures</b>	xiii
89	<b>List of Tables</b>	xv
90	<b>Abbreviations and Acronyms</b>	xvi
91	<b>Notations</b>	xvii
92	<b>Glossary</b>	xviii
93	<b>Listings</b>	xix
94	<b>Chapter 1 INTRODUCTION</b>	1
95	1.1 Background of the Study . . . . .	2
96	1.2 Prior Studies . . . . .	4
97	1.3 Problem Statement . . . . .	5
98	1.4 Objectives and Deliverables . . . . .	6
99	1.4.1 General Objective (GO) . . . . .	6
100	1.4.2 Specific Objectives (SOs) . . . . .	6
101	1.4.3 Expected Deliverables . . . . .	7
102	1.5 Significance of the Study . . . . .	9
103	1.5.1 Technical Benefit . . . . .	10
104	1.5.2 Social Impact . . . . .	11
105	1.5.3 Environmental Welfare . . . . .	11
106	1.6 Assumptions, Scope, and Delimitations . . . . .	11
107	1.6.1 Assumptions . . . . .	11
108	1.6.2 Scope . . . . .	12
109	1.6.3 Delimitations . . . . .	12



110	<b>Chapter 2 LITERATURE REVIEW</b>	<b>14</b>
111	2.1 Existing Work . . . . .	15
112	2.1.1 Deep Learning Classification Algorithms . . . . .	19
113	2.2 Lacking in the Approaches . . . . .	20
114	2.3 Summary . . . . .	21
115	<b>Chapter 3 THEORETICAL CONSIDERATIONS</b>	<b>23</b>
116	3.1 Introduction . . . . .	24
117	3.2 Relevant Theories and Models . . . . .	24
118	3.3 Technical Background . . . . .	25
119	3.4 Conceptual Framework Background . . . . .	25
120	3.5 Software Concepts . . . . .	26
121	3.5.1 Thresholding . . . . .	26
122	3.5.2 Object Size Calculation . . . . .	27
123	3.5.3 Convolutional Neural Network . . . . .	28
124	3.6 Hardware Concepts . . . . .	28
125	3.6.1 Camera Module . . . . .	28
126	3.6.2 4 Channel Relay . . . . .	29
127	3.6.3 Gear Ratio . . . . .	30
128	3.7 Summary . . . . .	30
129	<b>Chapter 4 DESIGN CONSIDERATIONS</b>	<b>31</b>
130	4.1 Introduction . . . . .	32
131	4.2 Engineering Standards . . . . .	32
132	4.2.1 Eletirical Certifications . . . . .	32
133	4.2.2 Safety of Machinery . . . . .	32
134	4.2.3 Safety Requirements for Technology Equipment . . . . .	33
135	4.2.4 Open-source Software Compliance . . . . .	33
136	4.3 System Architecture . . . . .	33
137	4.4 Hardware Considerations . . . . .	35
138	4.4.1 General Prototype Framework . . . . .	35
139	4.4.2 Prototype Flowchart . . . . .	36
140	4.4.3 Prototype 3D Model . . . . .	38
141	4.4.4 Hardware Specifications . . . . .	38
142	4.4.4.1 Raspberry Pi . . . . .	38
143	4.4.4.2 Raspberry Pi Camera . . . . .	41
144	4.4.4.3 DC Motor . . . . .	43
145	4.4.4.4 MicroSD Card . . . . .	44
146	4.4.4.5 LED Lights . . . . .	45
147	4.4.4.6 Power Supply . . . . .	46



148	4.4.4.7	4 Channel Relay Module . . . . .	48
149	4.4.4.8	RPi Power Supply . . . . .	49
150	4.4.4.9	Mini Conveyor Single Narrow . . . . .	51
151	4.4.4.10	Mini Conveyor Double Narrow . . . . .	52
152	4.5	Software Considerations . . . . .	53
153	4.5.1	PyTorch . . . . .	53
154	4.5.2	OpenCV . . . . .	53
155	4.5.3	CustomTkinter . . . . .	54
156	4.6	User Interface . . . . .	54
157	4.7	Summary . . . . .	54
158	<b>Chapter 5</b>	<b>METHODOLOGY</b>	<b>56</b>
159	5.1	Introduction . . . . .	59
160	5.2	Research Approach . . . . .	59
161	5.3	Hardware Design . . . . .	59
162	5.4	Software Design . . . . .	60
163	5.4.1	Machine Learning Methods . . . . .	62
164	5.4.2	Optimizer . . . . .	62
165	5.4.3	Data Loading Optimization . . . . .	63
166	5.4.4	Data Transfer Optimization . . . . .	63
167	5.4.5	Mixed Precision Training . . . . .	64
168	5.4.6	Adaptive learning Rate Schedulers . . . . .	64
169	5.4.7	CrossEntropy Loss with Label Smoothing . . . . .	65
170	5.4.8	Early Stopping and Checkpointing . . . . .	65
171	5.4.9	Input Resolution . . . . .	65
172	5.4.10	Regularization . . . . .	66
173	5.5	Data Collection Methods . . . . .	66
174	5.6	Testing and Evaluation Methods . . . . .	69
175	5.6.1	Data Augmentation and Splitting . . . . .	71
176	5.6.2	Comparative Test of CNN Models . . . . .	74
177	5.6.3	Benchmarking Best CNN Model on +10k Mango Dataset . . . . .	75
178	5.6.4	Classification Report . . . . .	76
179	5.6.4.1	Confusion Matrix . . . . .	77
180	5.6.4.2	Precision . . . . .	79
181	5.6.4.3	Recall . . . . .	79
182	5.6.4.4	F1 Score . . . . .	79
183	5.6.4.5	Accuracy . . . . .	79
184	5.6.5	Ripeness Training and Testing . . . . .	80
185	5.6.5.1	Green . . . . .	81



186	5.6.5.2	Yellow_Green . . . . .	81
187	5.6.5.3	Yellow . . . . .	81
188	5.6.6	Bruises Training and Testing . . . . .	82
189	5.6.6.1	Stem End Rots . . . . .	82
190	5.6.6.2	Dendritic Spot . . . . .	82
191	5.6.6.3	Anthracnose . . . . .	83
192	5.6.6.4	Sapburn . . . . .	83
193	5.6.6.5	Skin Browning . . . . .	83
194	5.6.6.6	Lenticel Spot . . . . .	83
195	5.6.7	Size Determination . . . . .	84
196	5.6.7.1	Real World Dimensions . . . . .	84
197	5.6.7.2	Object Detection . . . . .	85
198	5.6.7.3	Calibration by Getting the Pixels per cm . . . . .	85
199	5.7	Mango Formula with User Priority . . . . .	86
200	5.8	Summary . . . . .	87
201	<b>Chapter 6 RESULTS AND DISCUSSIONS</b>		<b>91</b>
202	6.1	Training and Testing Results of the Model . . . . .	94
203	6.1.1	Ripeness Classification Results . . . . .	94
204	6.1.1.1	Naive Bayes . . . . .	94
205	6.1.1.2	KMeans . . . . .	96
206	6.1.1.3	KNN . . . . .	96
207	6.1.1.4	CNN . . . . .	98
208	6.1.2	Bruises Classification Results . . . . .	102
209	6.1.2.1	CNN . . . . .	102
210	6.2	Achieving the Highest Accuracy in CNN Models . . . . .	105
211	6.2.1	Analysis of Table 6.9 . . . . .	105
212	6.2.2	Analysis of Table 6.8 and Table 6.7 . . . . .	110
213	6.2.3	Analysis of Confusion Matrix together with Validation Loss and Accuracy . . . . .	113
214	6.2.3.1	Ripeness Classification . . . . .	114
215	6.2.3.2	Bruises Classification . . . . .	119
216	6.3	Comparative Analysis: Model Performance vs. Expert Benchmark . . . . .	124
217	6.3.1	Expert Evaluation Methodology . . . . .	125
218	6.3.2	Comparative Results . . . . .	125
219	6.4	Size Determination Results . . . . .	129
220	6.4.1	Method 1: Real World Object Size Calculation via Foreground Masking and Thresholding . . . . .	129
221	6.4.2	Method 2: Object Detection using Faster-RCNN . . . . .	133



224	6.4.2.1	Training and Testing . . . . .	133
225	6.4.2.2	Calibration to the Prototype . . . . .	134
226	6.4.3	Test Comparison Between Both Methods . . . . .	135
227	6.5	Formula with User Priority . . . . .	138
228	6.6	Physical Prototype . . . . .	142
229	6.6.1	Version 1: Barebone with Black Conveyor Sheets . . . . .	142
230	6.6.2	Version 2: Enclosed with White Conveyor Sheets and Physical Sorter	143
231	6.7	Software Application . . . . .	146
232	6.7.1	Version 1: Progress Bar with Black Conveyor Sheets . . . . .	146
233	6.7.2	Version 2: Improved UI without Progress Bar . . . . .	148
234	6.7.3	Mango Image Sorting . . . . .	149
235	6.7.4	Error Handling . . . . .	149
236	6.7.5	Sample UI Outputs . . . . .	151
237	6.8	Summary . . . . .	152
238	<b>Chapter 7 CONCLUSIONS, RECOMMENDATIONS, AND FUTURE DI-</b>		
239	<b>RECTIVES</b>		<b>156</b>
240	7.1 Concluding Remarks . . . . .		157
241	7.1.1 Objectives Achieved . . . . .		157
242	7.1.1.1 GO: To develop a user-priority-based grading and sorting		
243	system for Carabao mangoes, using machine learning		
244	and computer vision techniques to assess ripeness, size,		
245	and bruises. . . . .		157
246	7.1.1.2 SO1: To make an image acquisition system with a con-		
247	veyor belt for automatic sorting and grading mangoes.		
248	. . . . .		157
249	7.1.1.3 SO2: To get the precision, recall, F1 score, confusion		
250	matrix, and train and test accuracy metrics for classifying		
251	the ripeness and bruises with an accuracy score of at least		
252	90%. . . . .		158
253	7.1.1.4 SO3: To create a microcontroller-based system to operate		
254	the image acquisition system, control the conveyor belt,		
255	and process the mango images through machine learning.		158
256	7.1.1.5 SO4: To grade mangoes based on user priorities for size,		
257	ripeness, and bruises. . . . .		158
258	7.1.1.6 SO5: To classify mango ripeness based on image data		
259	using machine learning algorithms such as kNN, k-mean,		
260	and Naïve Bayes. . . . .		159



# De La Salle University

261	7.1.1.7	SO6: To classify mango size based on image data by getting its length and width using OpenCV, geometry, and image processing techniques. . . . .	159
262	7.1.1.8	SO7: To classify mango bruises based on image data by employing machine learning algorithms. . . . .	159
263	7.2	Contributions . . . . .	159
264	7.3	Recommendations . . . . .	160
265	7.4	Future Prospects . . . . .	160
269	<b>References</b>		<b>162</b>
270	<b>Appendix A STUDENT RESEARCH ETHICS CLEARANCE</b>		<b>166</b>
271	<b>Appendix B REVISIONS TO THE PROPOSAL</b>		<b>168</b>
272	<b>Appendix C REVISION TO THE FINAL</b>		<b>174</b>
273	<b>Appendix D QUESTIONNAIRE TO THE EXPERT</b>		<b>177</b>
274	<b>Appendix E CERTIFICATE FROM FARMERS</b>		<b>184</b>
275	<b>Appendix F DATASET VALIDATION</b>		<b>192</b>



## 276 LIST OF FIGURES

277	1.1	Carabao Mangoes at Different Ripeness Stages (Guillermo et al., 2019) . . . . .	2
278	2.1	Prototype for Grading Mangoes (Adam et al., 2022) . . . . .	15
279	2.2	System Block Diagram (Samaniego Jr. et al., 2023) . . . . .	16
280	2.3	Background Removal of Mango (Tomas et al., 2022) . . . . .	18
281	3.1	Theoretical Framework Diagram. . . . .	24
282	3.2	Conceptual Framework Diagram. . . . .	25
283	4.1	Hardware Schematic . . . . .	34
284	4.2	Prototype Framework . . . . .	36
285	4.3	Prototype Main Flowchart . . . . .	37
286	4.4	Initial 3D Model of the Prototype . . . . .	39
287	4.5	Raspberry Pi 4 Model B . . . . .	40
288	4.6	Raspberry Pi Camera Module Version 2 . . . . .	42
289	4.7	12 Volt DC Gear Motor . . . . .	43
290	4.8	SanDisk Ultra MicroSD Card . . . . .	44
291	4.9	LED Light Strip . . . . .	45
292	4.10	Bench Power Supply . . . . .	47
293	4.11	4 Channel Relay Module . . . . .	48
294	4.12	Power Supply for the RPi . . . . .	49
295	4.13	Single Narrow Mini Conveyor . . . . .	51
296	4.14	Double Narrow Mini Conveyor . . . . .	52
297	5.1	Image Acquisition Dimensions . . . . .	61
298	5.2	Camera Setup . . . . .	67
299	5.3	Carabao Mangoes Image Dataset Collection . . . . .	67
300	5.4	Sample Mango Image . . . . .	68
301	5.5	Collecting Mango on a Farm . . . . .	70
302	5.6	CNN Ripeness 70-15-15 Image Datasplit . . . . .	72
303	5.7	CNN Bruises 70-15-15 Image Datasplit . . . . .	73
304	5.8	Bruises Image Datasplit . . . . .	77
305	5.9	Ripeness Image Datasplit . . . . .	78
306	5.10	Carabao Mango Ripeness Stages (Bureau of Agriculture and Fisheries Product Standards, 2004) . . . . .	81
307	5.11	Different Kinds of Mango Defects (Scott Ledger and Cooke, 2000) . . . . .	82



309	5.12 Length and Width of Mango (Bureau of Agriculture and Fisheries Product Standards, 2006) . . . . .	84
311	5.13 Annotated Mango Image Dataset . . . . .	85
312	6.1 Ripeness Confusion Matrix using Naive Bayes . . . . .	96
313	6.2 Ripeness Confusion Matrix using KMeans . . . . .	97
314	6.3 Ripeness Confusion Matrix using KNN . . . . .	98
315	6.4 EfficientNetV2-B3 Ripeness Confusion Matrix . . . . .	101
316	6.5 EfficientNetV2-B3 Ripeness Accuracy and Loss Graph . . . . .	102
317	6.6 EfficientNetV2-B3 Bruises Confusion Matrix . . . . .	104
318	6.7 EfficientNetV2-B3 Bruises Accuracy and Loss Graph . . . . .	104
319	6.8 Ripeness Training and Testing of EfficientNet-B5 . . . . .	116
320	6.9 Ripeness Training and Testing of EfficientNet-B6 . . . . .	117
321	6.10 Ripeness Training and Testing of EfficientNetV2-B3 . . . . .	119
322	6.11 Bruises Training and Testing of EfficientNet-B2 . . . . .	121
323	6.12 Bruises Training and Testing of EfficientNet-B3 . . . . .	122
324	6.13 Bruises Training and Testing of EfficientNetV2-B3 . . . . .	124
325	6.14 Mango Size with Reflective Material . . . . .	130
326	6.15 Mango Size Best Case . . . . .	131
327	6.16 Mango Top Side with White Conveyor . . . . .	131
328	6.17 Mango Bottom Side with White Conveyor . . . . .	132
329	6.18 Calibration using Faster RCNN and a Philippine one peso coin . . . . .	134
330	6.19 Resulting Bounding Boxes of the Mangoes . . . . .	135
331	6.20 Mangoes Tested for Size Measurement . . . . .	136
332	6.21 Length Comparison in cm . . . . .	136
333	6.22 Width Comparison in cm . . . . .	137
334	6.23 Percent and Absolute Difference between Both Methods . . . . .	137
335	6.24 Only Bruises as a None Zero Value . . . . .	141
336	6.25 Only Ripeness and Bruises as a None Zero Value . . . . .	141
337	6.26 Only Ripeness as a None Zero Value . . . . .	142
338	6.27 Version 1 of the Prototype . . . . .	144
339	6.28 Hardware View . . . . .	145
340	6.29 Version 2: Improved Prototype . . . . .	146
341	6.30 Version 1 of the RPi's User Interface . . . . .	147
342	6.31 Version 2 of the RPi's User Interface . . . . .	148
343	6.32 Mango Image Data Sorting . . . . .	149
344	6.33 Error Messages . . . . .	150
345	6.34 Error message for Letter as Input . . . . .	150
346	6.35 Help Page UI . . . . .	151
347	6.36 Sample Ripeness and Bruises Results . . . . .	152



348

## LIST OF TABLES

349	1.1 Expected Deliverables per Objective . . . . .	7
350	1.1 Expected Deliverables per Objective . . . . .	8
351	1.1 Expected Deliverables per Objective . . . . .	9
352	2.1 Comparison of Existing Studies . . . . .	18
353	2.2 Comparison of Sorting Algorithm Models . . . . .	21
354	5.1 Summary of methods for reaching the objectives . . . . .	57
355	5.2 Confusion Matrix Example . . . . .	78
356	6.1 Summary of methods for achieving the objectives . . . . .	92
357	6.2 Ripeness Classification Report using Naive Bayes . . . . .	95
358	6.3 Ripeness Classification Report using KMeans . . . . .	97
359	6.4 Ripeness Classification Report using KNN . . . . .	98
360	6.5 EfficientNetV2-B3 Ripeness Classification Report with Precision: 0.9848, Recall: 0.9847, F1 Score: 0.9847 . . . . .	101
361	6.6 EfficientNetV2-B3 Bruises Classification Report with Precision: 0.9887, Recall: 0.9886, F1 Score: 0.9886 . . . . .	104
362	6.7 CNN Training Results for GPU . . . . .	105
363	6.8 CNN Bruises Results for CPU . . . . .	106
364	6.9 Accuracy of Different CNN Models . . . . .	106
365	6.10 Test Accuracy of Different EfficientNet Version 1 and 2 . . . . .	107
366	6.11 Expert Classification Results for Mango Phenotypic Traits . . . . .	126
367	6.12 Mango Size Results . . . . .	139
368	6.13 Mango Size Difference to Ground Truth Results . . . . .	140
369	6.14 Mean and Standard Deviation of Size . . . . .	140
370		
371		



## 372 ABBREVIATIONS

373	AC	Alternating Current .....	13
374	CNN	Convolutional Neural Network .....	v
375	CPU	Central Processing Unit .....	40
376	FASTER R-CNN	Faster Region-based Convolutional Neural Network.....	v
377	GPU	Graphics Processing Unit.....	74
378	GUI	Graphical User Interface .....	54
379	KNN	K-Nearest Neighbors .....	25
380	LED	Light Emitting Diode .....	24
381	RESNET	Residual Network .....	105
382	RPI	Raspberry Pi .....	v
383	UI	User Interface .....	54
384	VGGNET	Visual Geometry Group Network.....	74
385	SGD	Stochastic Gradient Descent .....	134



386

## NOTATION

387	$B(P)$	Bruises User Priority/Weight .....	86
388	$b(p)$	Bruises AI Prediction .....	86
389	$R(P)$	Ripeness User Priority/Weight .....	86
390	$r(p)$	Ripeness AI Prediction .....	86
391	$S(P)$	Size User Priority/Weight.....	86
392	$s(p)$	Size AI Prediction .....	86
393	$D(p, d, f)$	Real World Dimension .....	27
394	$p$	Pixel Dimension .....	27
395	$d$	Distance from Camera to Object.....	27
396	$f$	Focal Length .....	27
397	$g$	Green Mango Ripeness.....	125
398	$yg$	Yellow_Green Mango Ripeness.....	125
399	$y$	Yellow Mango Ripeness .....	125
400	$b$	Bruised Mango .....	125
401	$nb$	Non-bruised Mango.....	125



## 402 GLOSSARY

403	Adam	An optimizer that computes adaptive learning rates for each parameter, combining the advantages of two other extensions of stochastic gradient descent.
404	AdamW	A variant of Adam that decouples the weight decay from the gradient update, which often leads to better generalization and more stable convergence.
405	bruises	The darkened black or brown region on the mango's skin resulting from impact, compression, or over-ripening, indicating tissue damage beneath the surface.
406	ripeness	The stage at which a mango has developed its optimal color, texture, flavor, and aroma for consumption.
407	Carabao mango	A popular variety of mango grown in the Philippines, known for its sweet and juicy flesh.
408	accuracy score	A performance metric that measures the overall proportion of correct predictions made by a machine learning model.
409	confusion matrix	A table that summarizes the performance of a classification model, showing the number of true positives, true negatives, false positives, and false negatives.
410	machine learning	A subset of Artificial Intelligence that enables systems to learn and improve from data.
411	computer vision	The use of cameras and algorithms to provide imaging-based inspection and analysis.
412	microcontroller	A small computing device that controls other parts of a system such as sensors.
413	Precision	A performance metric that reflects the percentage of instances classified as positive that are truly positive.
414	recall	A performance metric that measures the proportion of actual positive instances that the model correctly identified.
415	User Priority-Based Grading	A customizable grading system where users can assign weights to grading factors.



416

## LISTINGS

417	5.1 Datasplit Logs . . . . .	89
418	5.2 Calibration of Reference Philippine Coin . . . . .	90
419	6.1 Getting Size through Foreground Masking part 1 . . . . .	133
420	6.2 Getting Size through Foreground Masking part 2 . . . . .	154
421	6.3 Initializing the Calibration Box . . . . .	155
422	6.4 Sorting the Mangoes . . . . .	155



De La Salle University

423

## **Chapter 1**

424

## **INTRODUCTION**



## 425      **1.1 Background of the Study**

426      Carabao mango (*Mangifera indica L.*) is a variety of a mango that is found and cultivated  
427      in the Philippines. It is known for its sweet signature taste that was recognized sweetest in  
428      the world in the Guinness Book of World Records in 1995. The mango was named after  
429      the national animal of the Philippines, a native breed of buffalo. On average, it is 12.5 cm  
430      in length and 8.5 cm in diameter, having a bright yellow color when ripe as seen in Figure  
431      1.1 (Knight et al., 2009). It is often cultivated during late May to early July (Bayogan and  
432      Secretaria, 2019).

433      Likewise, the Philippines produced an estimated 596.34 thousand metric tons of man-  
434      goes during the April to June 2023 quarter, marking an 11.4 percent increase from the  
435      535.43 thousand metric tons harvested in the same three-month period of 2022. Of this total  
436      output, the mango variety accounted for the vast majority at 495.06 thousand metric tons,  
437      or 83.0 percent of the nation's entire mango production (Philippine Statistics Authority,  
438      2023).



Fig. 1.1 Carabao Mangoes at Different Ripeness Stages (Guillermo et al., 2019)

439      This shows that mangoes are a highly valued fruit in the Philippines as it is not only  
440      the country's national fruit but also amongst the leading agricultural exports of the country,



# De La Salle University

441 ranking only third below bananas and pineapples. This gives the country the 9th slot  
442 amongst the leading exporters of Mangoes across the world. Attributed to this ranking is  
443 the country's export of both fresh and dried mangoes, as well as low tariff rates. This allows  
444 the country to export a large quantity of the fruit in countries such as Singapore, Japan, and  
445 the USA as they can enter duty free markets provided by the World Trade Organization and  
446 Japan. Due to this, the mangoes have become a major source of income to an estimated 2.5  
447 million farmers in the country (Centino et al., 2020).

448 Before mangoes are sold in markets, they first undergo multiple post-harvest processes.  
449 This is to ensure that the mangoes that arrive in markets are utmost quality before being  
450 sold to consumers. Moreover, it ensures that mangoes are contained and preserved properly  
451 such that they do not incur damages and/or get spoiled on its transportation to the market .  
452 Processing of the mango involves pre-cooling, cleaning, waxing, classification, grading,  
453 ripening, packaging, preservation, storage, packing, and transportation (Patel et al., 2019).

454 Among the processes that mangoes undergo, classification and grading is important as it  
455 allows the manufacturer to separate mangoes with good qualities versus mangoes with poor  
456 qualities. According to a study by (Lacap et al., 2021), size, length, width, volume, density,  
457 indentation, and grooves are aspects that determine the maturity of mangoes. These traits are  
458 being checked along with the ripeness of the mango, sightings of bruise injury, and cracks  
459 on the fruit as these aspects affect the sellability of the fruit as well as the chances of it  
460 getting spoiled sooner.

461 Previous studies have been made to automate the sortation process of the mangoes.  
462 Among these is a research done by Abbas et al. (2018), which focuses on classification  
463 of mangoes using their texture and shape features. They do this by, first, acquiring an  
464 image of the mango using a digital camera. Then, these images are fed to the MaZda



465 package, which is a software originally developed for magnetic resonance imaging. Within  
466 the MaZda package is the B11 program, which uses Principal Component Analysis, Linear  
467 Discriminant Analysis, Nonlinear Discriminant Analysis, and texture classification to  
468 extract features from the mango, which in this case are the length, width, and texture. This  
469 data is then compared to a database in order to classify any given mango (Abbas et al.,  
470 2018).

471 Another study is done by Rizwan Iqbal and Hakim (2022), which classifies mangoes  
472 based on their color, volume, size, and shape. This is done by making use of Charge  
473 Coupled Devices, Complementary Metal-Oxide Semiconductor sensors, and 3-layer CNN.  
474 To classify the mangoes, images are first captured and preprocessed to be used as a data set  
475 (Rizwan Iqbal and Hakim, 2022). This data set is then augmented to be used as a model  
476 for the 3-layer CNN. After extracting the features of the mango, the 3-layer CNN is used  
477 as a method for their classification as it can mimic the human brain in pattern recognition,  
478 and process data for decision making. This is important as some mangoes have very subtle  
479 differences which make it difficult to differentiate them.

## 480 1.2 Prior Studies

481 A paper written by Amna et al. (2023), designed an automated fruit sorting machine based  
482 on the quality through an image acquisition system and CNN. Furthermore, the results  
483 of the paper show that the image processing detection score was 89% while that of the  
484 tomatoes was 92% while the CNN model had higher validity of 95% for mangoes and  
485 93% for tomatoes. 15%, while the percentage of distinction between the two groups was  
486 reported to be 5% respectively (Amna et al., 2023). Despite the high accuracy score in



487 detecting mango defects, the fruit sorting system only sorts based on the mango defects  
488 and not on ripeness, and weight.

489 Furthermore, the article presented by Guillergan et al. (2024) designed an Automated  
490 Carabao mango classifier, in which the mango image database is used to extract the features  
491 like size, area along with the ratio of the spots for grading using Naïve Bayes Model. For the  
492 results, the Naïve Bayes' model recognized large and rejected mangoes with 95% accuracy  
493 and the large and small/medium difference with a 7% error, suggesting an application for  
494 quality differentiation and sorting in the mango business industry. Despite the high accuracy  
495 of classifying Carabao mangoes, the researchers used a high quality DSLR camera for the  
496 image acquisition system without any microcontroller to control the mangoes (Guillergan  
497 et al., 2024).

### 498 1.3 Problem Statement

499 As mangoes are among the top exports of the Philippines (Centino et al., 2020), assessing  
500 the physical deformities is a necessity. The physical deformities of the mango can determine  
501 the global competitiveness of the country. Having higher quality exports can often lead to  
502 gaining competitive edge, increase in demand, increase export revenues, and becoming less  
503 susceptible to low-wage competition (D'Adamo, 2018). In order to increase the quality  
504 of mango fruit exports, a key post-harvest process is done, which is sorting and grading.  
505 Mango sorting and grading then becomes important to determine which batches are of high  
506 quality and can be sold for a higher price, and which batches are of low quality and can  
507 only be sold for a low price (Tai et al., 2024). Traditionally, fruit sorting and grading is  
508 inefficient as it is done manually by hand. Some tools are used such as porous ruler to



509 determine fruit size and color palette for color grading. However, among the problems  
510 encountered in the process of manually sorting and grading mangoes are susceptibility to  
511 human error and requiring a number of laborers to do the task.

512 With the current advancements in technology, some researchers have already taken  
513 steps to automate the process of sorting and grading mangoes. However, these attempts  
514 would often only consider some of the aspects pertaining to size, ripeness, and bruises  
515 but not dynamically change the method of sorting and grading. Furthermore, most of the  
516 journal articles have a fix static method in grading and sorting the mangoes. This means  
517 that it doesn't take into consideration the user's priority when grading and sorting the  
518 mangoes. Lastly, not all research approaches were able to implement a hardware for their  
519 algorithm, limiting their output to only a software implementation and not an embedded  
520 system. As such the proposed system would assess the quality of the mango based on  
521 all the mentioned mango traits, namely size, bruises, and ripeness while also taking into  
522 consideration being non-destructive and the user's priority when grading and sorting the  
523 mangoes. These aspects are important because, as was previously mentioned, there is a  
524 need to develop a user priority based mango sorter that takes into account all these aspects  
525 at the same time while being non-destructive.

## 526 **1.4 Objectives and Deliverables**

### 527 **1.4.1 General Objective (GO)**

- 528 • GO: To develop a user-priority-based grading and sorting system for Carabao man-  
529 goes, using machine learning and computer vision techniques to assess ripeness, size,  
530 and bruises. ;



### 531      **1.4.2 Specific Objectives (SOs)**

- 532      • SO1: To make an image acquisition system with a conveyor belt for automatic sorting  
533      and grading mangoes. ;
- 534      • SO2: To get the precision, recall, F1 score, confusion matrix, and train and test  
535      accuracy metrics for classifying the ripeness and bruises with an accuracy score of at  
536      least 90%.;
- 537      • SO3: To create a microcontroller-based system to operate the image acquisition  
538      system, control the conveyor belt, and process the mango images through machine  
539      learning. ;
- 540      • SO4: To grade mangoes based on user priorities for size, ripeness, and bruises. ;
- 541      • SO5: To classify mango ripeness based on image data using machine learning  
542      algorithms such as kNN, k-mean, and Naïve Bayes. ;
- 543      • SO6: To classify mango size based on image data by getting its length and width  
544      using OpenCV, geometry, and image processing techniques. ;
- 545      • SO7: To classify mango bruises based on image data by employing machine learning  
546      algorithms.

### 547      **1.4.3 Expected Deliverables**

548      Table 1.1 shows the outputs, products, results, achievements, gains, realizations, and/or  
549      yields of the Thesis.



TABLE 1.1 EXPECTED DELIVERABLES PER OBJECTIVE

Objectives	Expected Deliverables
GO: To develop a user-priority-based grading and sorting system for Carabao mangoes, using machine learning and computer vision techniques to assess ripeness, size, and bruises.	<ul style="list-style-type: none"> <li>• To develop a Carabao mango grading and sorting system.</li> <li>• To grade Carabao mangoes into three categories based on ripeness, size, and bruises using machine learning.</li> <li>• To integrate sensors and actuators to control the conveyor belt and image acquisition system.</li> </ul>
SO1: To make an image acquisition system with a conveyor belt for automatic sorting and grading mangoes.	<ul style="list-style-type: none"> <li>• To make an image acquisition system with a camera and LED light source.</li> <li>• To build a flat belt conveyor for moving the mangoes.</li> </ul>
SO2: To get the precision, recall, F1 score, confusion matrix, and train and test accuracy metrics for classifying the ripeness and bruises with an accuracy score of at least 90%.	<ul style="list-style-type: none"> <li>• To use a publicly available dataset of at least 10,000 mango images for classification of ripeness and bruises.</li> </ul>
SO3: To create a microcontroller-based system to operate the image acquisition system, control the conveyor belt, and process the mango images through machine learning.	<ul style="list-style-type: none"> <li>• To develop an intuitive UI where users can start and stop the system.</li> <li>• To implement a priority-based grading system with sliders for ripeness, bruises, and size.</li> </ul>
SO4: To grade mangoes based on user priorities for size, ripeness, and bruises.	<ul style="list-style-type: none"> <li>• To utilize a linear combination formula as the overall mango score, where each classification level contributes a grade, weighted by the priority assigned to the three properties.</li> <li>• To assign score values for each classification level of the mango.</li> </ul>

*Continued on next page*



TABLE 1.1 EXPECTED DELIVERABLES PER OBJECTIVE

Objectives	Expected Deliverables
SO5: To classify mango ripeness based on image data using machine learning algorithms such as kNN, k-mean, and Naïve Bayes.	<ul style="list-style-type: none"> <li>To train a machine learning model such as kNN, k-means, or Naïve Bayes capable of classifying mango ripeness based on the image color.</li> <li>To gather a dataset of annotated images with ripeness labels.</li> <li>To obtain an evaluation report of performance metrics of the model.</li> </ul>
SO6: To classify mango size based on image data by getting its length and width using OpenCV, geometry, and image processing techniques.	<ul style="list-style-type: none"> <li>To develop an image processing algorithm capable of determining mango size using OpenCV, NumPy, and imutils.</li> <li>To classify mangoes based on size into small, medium, and large based on measurements.</li> </ul>
SO7: To classify mango bruises based on image data by employing machine learning algorithms.	<ul style="list-style-type: none"> <li>To train a machine learning model such as capable of distinguishing bruised and non-bruised mangoes.</li> <li>To train a machine learning model such as kNN, k-means, and Naïve Bayes capable of assessing the extent of bruising on the mangoes if it is significant or partial.</li> <li>To gather a dataset of annotated images based on bruises.</li> <li>To obtain an evaluation report of performance metrics of both CNN and other machine learning models.</li> </ul>

550

## 1.5 Significance of the Study

551

Automating the process of sorting and grading mangoes increases efficiency and productivity for the user which would in effect remove human error in sorting and grading and decrease the human labor and time taken to sort and grade the mangoes. This is especially important for farmers with a large amount of fruit such as mangoes and a lesser labor force.

552

553

554



555 A recent study showed that their automated citrus sorter and grader using computer vision  
556 can reduce the human labor cost and time to sort and grade when comparing the automated  
557 citrus sorter and grader to manual human labor (Chakraborty et al., 2023).

558 Another benefit to automating sorting and grading mangoes is the improvement in  
559 quality control. This implies that compared to human labor, automating sorting and  
560 grading mangoes can uniformly assess the quality of mangoes based on size, color, and  
561 bruises, ensuring that the expected grade and high-quality mangoes reach the consumer.  
562 By accurately identifying substandard mangoes, the system helps in reducing waste and  
563 ensuring that only marketable fruits are processed further.

564 Likewise, the scalability of automating sorting and grading mangoes is simpler, es-  
565 pecially for lower labor force farmers with large volumes of mangoes. Because of the  
566 possibility of large-scale operations by automating sorting and grading mangoes, farmers  
567 can now handle large volumes of mangoes, making them suitable for commercial farms  
568 and processing plants.

### 569 **1.5.1 Technical Benefit**

- 570 1. The development of an automated Carabao mango sorter would increase the quality  
571 control of classifying Carabao mango based on ripeness, size, and bruising.
- 572 2. The accuracy in sorting Carabao mangoes will be significantly improved while  
573 reducing the errors due to human factors in manual sorting.
- 574 3. The automated Carabao mango sorter carefully sorts the mangoes while ensuring  
575 that they remain free from bruising or further damage during the process



576 **1.5.2 Social Impact**

- 577 1. The reduction in manual labor creates opportunities in maintenance and technologies  
578 in the automated Carabao mango sorter.
- 579 2. The automated Carabao mango sorter system improves Carabao mango standards  
580 and enhances the satisfaction of the buyers and the customers through guaranteeing  
581 consistent Carabao mango grade.
- 582 3. Opportunity to increase sales and profit for the farmers through consistent quality  
583 and grade Carabao mangoes while reducing the physical labor to sort it.

584 **1.5.3 Environmental Welfare**

- 585 1. With the utilization of non-destruction methods of classifying Carabao mangoes  
586 together with an accurate sorting system, overall waste from Carabao mangoes is  
587 reduced and the likelihood of improperly sorted mangoes is decreased.
- 588 2. Automation of sorting and grading Carabao mangoes promotes sustainable farming  
589 practices.

590 **1.6 Assumptions, Scope, and Delimitations**

591 **1.6.1 Assumptions**

- 592 1. The Carabao mangoes are from the same source together with the same variation  
593 2. The Carabao mangoes do not have any fruit borer and diseases



- 594        3. All the components do not have any form of defects
- 595        4. The prototype would have access to constant electricity/power source.
- 596        5. The Carabao mangoes to be tested would be in the post-harvesting stage and in the  
597              grading stage.
- 598        6. The image-capturing system would only capture the two sides of the mango which  
599              are the two largest surface areas of the skin.

600        **1.6.2 Scope**

- 601        1. The prototype would be specifically designed to grade and sort Carabao Mangoes  
602              based on only ripeness, size, and visible skin bruises.
- 603        2. The mangoes used as the subject will be solely sourced from markets in the Philip-  
604              pines.
- 605        3. The Carabao mangoes would be graded into three levels.
- 606        4. The prototype will be using a microcontroller-based system locally stored on the  
607              device itself to handle user interaction.
- 608        5. Computer vision algorithms to be used will include image classification.

609        **1.6.3 Delimitations**

- 610        1. The project would only be able to perform sorting and grading on one specific fruit  
611              which is the Carabao mango and will not be able to sort other types of mangoes.



# De La Salle University

- 612        2. Additionally, the project prototype will only be able to capture, sort, and grade one  
613                 mango subject at a time which means the mangoes have to be placed in the conveyor  
614                 belt in a single file line for accurate sorting.
- 615        3. For the bruises, the system will only be able to detect external bruises and may not  
616                 identify the non-visible and internal bruises.
- 617        4. The system does not load the mangoes onto the conveyor belt itself. Assistance is  
618                 required to put mangoes into the conveyor belt to start the sorting process
- 619        5. The prototype will be powered using Alternating Current (AC) power and will be  
620                 plugged into a wall socket which is only suitable for indoor use.



De La Salle University

621

## Chapter 2

622

## LITERATURE REVIEW



## 623      **2.1 Existing Work**

624      Adam et al. (2022) developed a ripeness grader for Carabao mangoes. The Carabao  
625      mango ripeness grade calculated based on object and color detection which were written  
626      in microcontroller. These are the systems designed by the researchers that consists of  
627      Raspberry Pi 4, Arduino Uno, camera, touch screen LCD, MQ3 gas sensor, ventilation  
628      system as seen on Figure 2.1 The proposed system was able to ascertain an overall reliability  
629      of 95% which means that the specified objective of ascertaining the ripeness level of the  
630      mangoes was met with success. However, accuracy and reliability of the software system  
631      are there since the hardware design does not seem to be workable when one must deal  
632      with the scores of mangoes. In addition, the design of the hardware does not integrate any  
633      form of physical automating, say like the conveyor belt. Besides, the hardware system only  
634      works efficiently when deciding the ripeness grade of mangoes separately.



Fig. 2.1 Prototype for Grading Mangoes (Adam et al., 2022)



635 A study done by Samaniego Jr. et al. (2023) supports and has relevant information  
 636 concerning the aforementioned topic. They proposed a fully-perovskite photonic system  
 637 which has the capability to identify and sort or grade mango based on features such as color,  
 638 weight and, conversely, signs of damages. Some of the techniques in image processing  
 639 that the researchers used included image enhancement, image deblurring, edge detection  
 640 using MATLAB and Arduino as well as color image segmentation. Likewise the system  
 641 block diagram containing these equipment used are seen on Figure 2.2. By carrying out  
 642 the multiple trials on the device they achieved a classification speed of 8.132 seconds and  
 643 an accuracy of 91.2%. The proponents' metrics used for the ratings were speed wherein  
 644 the results were rated "excellent" while the accuracy rating given was "good". One of the  
 645 limitations of the paper is that the researchers were only limited to the color, texture, and  
 646 size of the Carabao mango

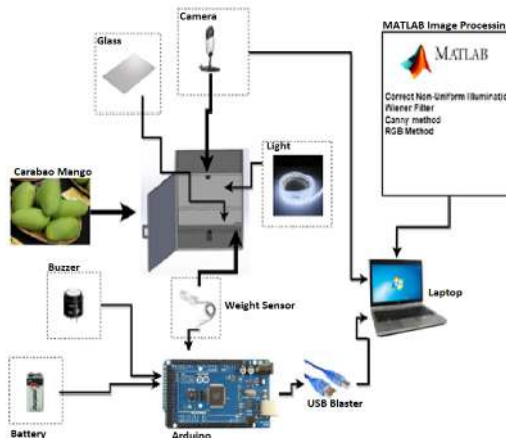


Fig. 2.2 System Block Diagram (Samaniego Jr. et al., 2023)

647 Furthermore, Guillergan et al. (2024) designed an Automated Carabao mango classifier,  
 648 in which the mango image database is used to extract the features like weight, size, area  
 649 along with the ratio of the spots for grading using Naïve Bayes Model. Concerning the



650 quantitative test design, one had to control and experiment with various methods of image  
651 processing that would improve the likelihood of improved classification. Their methodology  
652 entailed sample collection from 300 Carabao mangoes, picture taking using a DSLR camera,  
653 and feature deconstruction for categorization. The system prototype and the software were  
654 designed with the programming language C# with integration of Aforge. NET routines.  
655 The performance of this model was checked with the help of the dataset containing 250  
656 images, precision, recall, F-score key indicators were used. The investigation discovered  
657 that the Naïve Bayes' model recognized large and rejected mangoes with 95% accuracy  
658 and the large and small/medium difference with a 7% error, suggesting an application for  
659 quality differentiation and sorting in the mango business industry. The limitations they  
660 encountered was they were not able to achieve the highest accuracy after using a high  
661 quality DSLR camera and the fact that the researchers were not able to incorporate the use  
662 of microcontrollers.

663 Another study by Tomas et al. (2022) proposed an SVM-based system for classifying  
664 the maturity stages of bananas, mangoes, and calamansi. With the use of 1729 images of  
665 bananas together with 711 mango images and 589 calamansi, the researchers were able to  
666 achieve a high accuracy score of above 90% for all fruits. Some pre-processing techniques  
667 used to get this high accuracy are the change in hue, saturation, and value channels in  
668 the mango image. One of the pre-processing methods (background removal) is shown  
669 on Figure 2.3 To better understand the harvest time of mangoes, the paper by Abu et al.  
670 (2021) examined the association of the harvest season with seasonal heat units, rainfall,  
671 and physical fruit attributes for Haden, Kent, Palmer, and Keitt mango varieties to establish  
672 export and domestic market maturity standards. For the results of the paper, it shows that  
673 temperature, rainfall, and physical characteristics have a reliable, non-destructive indicators



674 for determining mango maturity. This shows that physical characteristics and temperature  
 675 are important when exporting fruits such as mangoes.

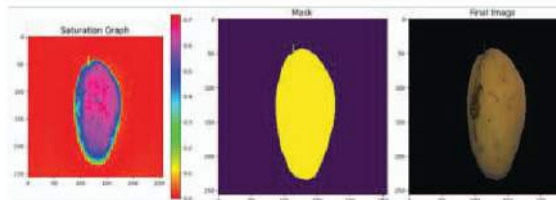


Fig. 2.3 Background Removal of Mango (Tomas et al., 2022)

TABLE 2.1 COMPARISON OF EXISTING STUDIES

Existing Study	Limitations	Accuracy Rating
Adam et al. (2022)	No physical automation, not suitable for large amounts of mangoes, only classifies ripeness and only a sample size of 10 mangoes.	95%
Samaniego Jr. et al. (2023)	Focuses only on color and size.	91.2%
Guillergan et al. (2024)	Relies on high-quality DSLR cameras, and limited automation due to not integrating microcontrollers.	95%
Supekar and Wakode (2020)	No physical automation implemented. Ripeness, size, and shape-based classification achieved 100%, 98.19%, and 99.20% accuracy respectively on their own. However, errors occurred when taking into account all these aspects together for grading mangoes, causing an accuracy rating deduction.	88.88%

676 Previous studies on mango grading have achieved an accuracy rating of up to 95%, as  
 677 shown in Table 2.1. However, these studies either relied on a small sample size, which  
 678 limits statistical significance, or utilized expensive equipment, which may be impractical.  
 679 In light of this, the researchers have set a target accuracy rating of greater than or equal



680 to 90%. This target ensures that the system being developed is comparable to, or better  
681 than, existing studies that used larger sample sizes or assessed multiple mango traits at the  
682 same time. Furthermore, this research aims to distinguish itself by not only maintaining or  
683 exceeding the 90% accuracy rating but also incorporating a graphical user interface (GUI)  
684 for selective priority-based mango classification. The system will integrate both software  
685 and hardware components, and it will evaluate a greater number of mango traits for grading  
686 purposes.

### 687 **2.1.1 Deep Learning Classification Algorithms**

688 Researchers have implemented various artificial intelligence algorithms in order to deter-  
689 mine the optimal and most effective method for sorting mangoes. One of the algorithms that  
690 was used in the classification of mangoes was the CNN or Convolutional Neural Networks.  
691 A study done by Zheng and Huang (2021) explored the effectiveness of CNN, specifically  
692 in classifying mangoes through image processing. The system that the researchers devel-  
693 oped graded mangoes into four groups which was based on the Chinese National Standard.  
694 These mangoes were examined by their shape, color uniformity, and external defects. The  
695 system that was developed had an impressive accuracy of 97.37% in correctly classifying  
696 the mangoes into these grading categories Support Vector Machine was also one of the  
697 classification algorithms that was implemented to detect flaws in mangoes. In that study by  
698 Veling (2019), SVM was used in the classification of diseases from mangoes. The study  
699 used 4 different diseases/defects for testing. The diseases were Anthracnose, Powdery  
700 Mildew, Black Banded, and Red Rust. and provided 90% accuracy for both the leaves and  
701 the fruit

702 In the study done by Schulze et al. (2015), Simple Linear Regression, Multiple Linear



# De La Salle University

703 Regression, and Artificial Neural Network models were all studied and compared for  
704 the purpose of size-mass estimation for mango fruits. The researchers found that the  
705 Artificial Neural Network yielded a high accuracy rating for mass estimation and for mango  
706 classification based on size with a success rate of 96.7%. This is attributed to the Artificial  
707 Neural Network model's ability to learn both linear and nonlinear relationships between  
708 the inputs and the outputs. However, a problem can occur with the use of the model,  
709 which is overfitting. This issue occurs when the model is overtrained with the data set  
710 such that it will start to recognize unnecessary details such as image noise which results in  
711 poor generalization when fed with new data. With this in mind, additional steps will be  
712 necessary to mitigate the issue. Another research article written by Alejandro et al. (2018)  
713 implements a method for sorting and grading Carabao mangoes. This research focuses on  
714 the use of Probabilistic Neural Network, which is another algorithm that is used for pattern  
715 recognition and classification of objects. For this study, the researchers focused on the  
716 area, color, and the black spots of the mango for their Probabilistic Neural Network model.  
717 Their research using the model yielded an accuracy rating of 87.5% for classification of the  
718 mangoes which means it is quite accurate for classifying mangoes within the predefined  
719 categories. However, problems were encountered with the use of the model when trying to  
720 identify mangoes that did not fit the predefined size categories of small, medium, and large.  
721 This means that the PNN model may become challenged when presented with a mango  
722 with outlying traits or traits that were very different from the data set.



TABLE 2.2 COMPARISON OF SORTING ALGORITHM MODELS

Sorting Algorithm Model	Accuracy Rating	Criteria	Problems Encountered
Convolution Neural Network	97.37%	shape, color, defects	Minor blemishes affected the accuracy.
Support Vector Machine	90%	mango defects and diseases	The model is sensitive to noise, which requires intensive image preprocessing.
Artificial Neural Network	96.7%	for mango size and mass	Overfitting
Probabilistic Neural Network	87.5%	for mango area, color, and black spots	Difficulty in identifying mangoes that have outlying features or did not fit the predefined categories

## 2.2 Lacking in the Approaches

The majority of past researchers such as Amna et al. (2023) and Guillermo et al. (2019) were able to implement a fruit and mango sorter together with an accurate AI algorithm to detect the ripeness defects. This means that none of the previous research papers were able to integrate an interchangeable user-priority-based grading together with size, ripeness, and bruises using machine learning for Carabao mango sorter and grader. Our research however would implement an automated Carabao mango sorter in terms of size, ripeness, and bruises with its own UI, conveyor belt, DC motors, and bins for collecting the different ripeness and defect grade of the Carabao mango.



## 2.3 Summary

To reiterate, there is an innovative gap that needs to be filled with regards to the process of sorting and grading Carabao mangoes. The traditional methods for conducting this process manually by hand, by a porous ruler, by a sugar meter, and by a color palette can be prone to human error and expensive costs due to the number of laborers required to do the task. On the other hand, although researchers have already taken steps to automate the process of mango sorting and grading, there is still a need for an implementation that takes into account size, ripeness, and bruises altogether whilst being non-destructive with its own user-priority-based grading and sorting and having its own embedded system. The research articles shown above show the different computer vision and CNN approaches for sorting and classifying mangoes. For example, a system created by Adam et al. (2022) was more focused on ripeness detection. Samaniego Jr. et al. (2023) considered photonic systems for grading mango fruit based on color and weight. On the other hand, Guillermo et al. (2019) implemented the Naïve Bayes classification model on mangoes with high accuracy, which thereby did not include any microcontroller. There was an attempt to study each of those parameters separately and that is why the multifactorial approach was not used. With this in mind, the system being proposed does exactly what was mentioned, to implement a non-destructive and automated sorting and grading system for Carabao mangoes that takes into account size, ripeness, and bruises altogether using machine learning, as well as having its own embedded system. This system will be mainly composed of a conveyor belt, servo motors, a camera, microcontrollers, and an LCD display for the user interface. By doing so, the system should be able to improve the efficiency and productivity of mango sorting and grading, remove the effect of human error and reduce time consumption. The



# De La Salle University

755 studies also provided critical insights regarding the effective algorithms that can be used  
756 in classification stages in image processing. The use of CNN had the most accuracy with  
757 manageable potential challenges. Lastly, by scaling the implementation, the overall export  
758 quality of the Carabao mangoes can be improved.



759

## Chapter 3

760

# THEORETICAL CONSIDERATIONS



### 761 3.1 Introduction

762 Likewise, the purpose of this chapter is to go through the important theories in developing  
 763 the prototype together with training and testing the machine learning model.

### 764 3.2 Relevant Theories and Models

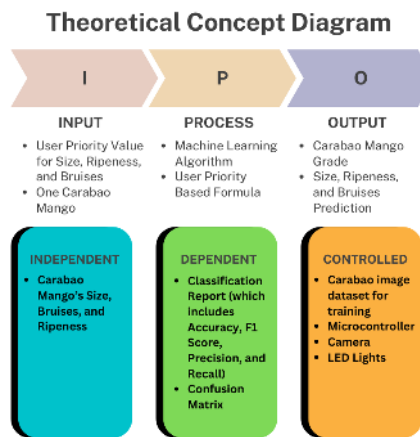


Fig. 3.1 Theoretical Framework Diagram.

765 The theoretical framework seen in figure 3.1 follows the IPO (Input-Process-Output)  
 766 Model for a Carabao Mango Sorting System. The Input section includes user-defined  
 767 priority values for size, ripeness, and bruises, along with a single mango for analysis. The  
 768 Process section highlights the use of a machine learning algorithm and a user-priority-based  
 769 formula to classify the mango. The Output consists of the mango's grade, predicted size,  
 770 ripeness, and bruises. Below the IPO model, the diagram categorizes variables into three  
 771 groups: Independent (mango's size, ripeness, and bruises), Dependent (classification report  
 772 with accuracy, precision, recall, and confusion matrix), and Controlled (image dataset,  
 773 microcontroller, camera, and Light Emitting Diode (LED) lights).



### 774    3.3 Technical Background

775    At its core, the system will be using machine learning concepts pertaining to Convolutional  
 776    Neural Network (CNN) and OpenCV, and may use other algorithms such as Naive Bayes  
 777    and k-Nearest Neighbors (KNN) to supplement the classification tasks, particularly for  
 778    assessing mango ripeness, bruise detection, and size determination. The system will be  
 779    built on an embedded framework, integrating a Raspberry Pi microcontroller to control the  
 780    Raspberry Pi camera, actuators, LED lights, and motors. A user-friendly GUI will also be  
 781    utilized to ensure users can customize the prioritization of the mango sorting system.

### 782    3.4 Conceptual Framework Background

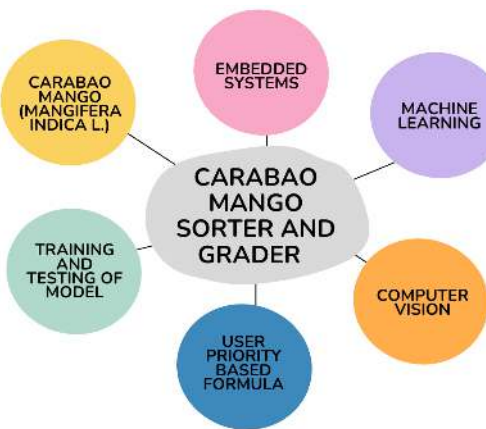


Fig. 3.2 Conceptual Framework Diagram.

783    The conceptual framework seen in figure 3.2 illustrates the key components involved  
 784    in the Carabao Mango Sorter and Grader system. At the center, the system is represented  
 785    as the core element, surrounded by six interconnected components: Carabao Mango  
 786    (*Mangifera indica L.*), Embedded Systems, Machine Learning, Computer Vision, User



787 Priority-Based Formula, and Training and Testing of the Model. These elements represent  
788 the different technologies, methodologies, and considerations required for the development  
789 and operation of the sorter and grader. The diagram provides an overview of how various  
790 disciplines contribute to the project's functionality.

## 791 **3.5 Software Concepts**

### 792 **3.5.1 Thresholding**

793 Thresholding is a computer vision image segmentation technique that is used to separate  
794 objects from their surroundings by converting a grayscale image to binary. The conversion  
795 is done by choosing a certain threshold intensity value. It is usually done by assigning pixels  
796 with an intensity higher than the threshold are mapped to one value (commonly white),  
797 and pixels with an intensity lower than the threshold are mapped to another (commonly  
798 black). The result of this technique is in a high-contrast image that makes it easy to detect  
799 the object's boundary and shape in the image.

800

801 In this project, two types of thresholding were applied:

- 802 • Absolute Difference Thresholding – This method involves computing the absolute  
803 difference between two images. The first image is one of the object, and the other  
804 of the same background without the object. The result isolates only the pixels that  
805 have changed between the two images, thus isolating the mango from its background  
806 successfully.
- 807 • Binary Thresholding – Once the difference image has been created, binary threshold-



808       ing is used. A threshold value is employed to threshold the difference image into a  
 809       binary image. Values greater than the threshold are made white (foreground), and  
 810       values less than that are made black (background). This creates a clear silhouette of  
 811       the mango, which is appropriate for size estimation and contour detection.

812       **3.5.2 Object Size Calculation**

813       Object size calculation is the calculation of a certain object's true size from image data. This  
 814       is essential in computer vision systems to efficiently process object features in real-time.  
 815       In this research, the size of the Carabao mango is estimated through image measurement  
 816       techniques based on geometric principles and camera calibration.

$$\text{Real World Dimension} = \frac{\text{Pixel Dimension} \times \text{Distance from Camera to Object}}{\text{Focal Length}} \quad (3.1)$$

$$D(p, d, f) = \frac{p \cdot d}{f} \quad (3.2)$$

817       where  $D(p, d, f)$  is the real world dimension of the object,  $p$  is the pixel dimension of  
 818       the object,  $d$  is the distance from the camera to the object, and  $f$  is the focal length of the  
 819       camera. This relationship follows from the pinhole camera model, where the real-world  
 820       dimension is proportional to the image dimension and the ratio of distance to focal length  
 821       Badali et al. (2005).

822       After capture and preprocessing of the image, the binary image so obtained is processed  
 823       with contour detection to find the largest object, which is assumed to be the mango. The  
 824       contour is then bounded with a minimum-area bounding box, and pixel-based length and  
 825       width are calculated using Euclidean distance between the corner points.



826        This size estimation method offers a consistent and efficient way of taking the mea-  
827        surements with only standard camera input, providing consistency in classification and  
828        reducing the necessity for physical measuring devices.

### 829        **3.5.3 Convolutional Neural Network**

830        Convolutional Neural Networks are a class of deep learning models is commonly used in  
831        analyzing visual data. CNNs are particularly effective in image classification tasks due to  
832        their ability to automatically extract and effectively learn the spatial hierarchies of features  
833        directly from the pixels of a given image. This makes it highly suitable for functions such  
834        as object detection and, in the case of this study, image classification.

835        CNN usually applies filters to input images. These filters are designed to detect local  
836        patterns such as edges, textures, and color gradients. The network is able to learn more  
837        patterns as the data goes through the layers. This enables it to recognize effectively the  
838        characteristics that it is looking for.

839        The use of CNNs in this study allows for accurate, automated classification of mango  
840        images which contributes to the development of a reliable, non-destructive grading system  
841        that minimizes human error and ensures consistent quality assessment

## 842        **3.6 Hardware Concepts**

### 843        **3.6.1 Camera Module**

844        The camera module serves as the main image acquisition tool in the mango sorter and  
845        grader system. Its role is to capture clear, high-resolution images of each mango as it moves



846 along the conveyor. These images are critical for analyzing physical traits like ripeness,  
847 bruising, and size through computer vision and machine learning techniques.

848 The camera is directly connected to the Raspberry Pi, which manages both image  
849 capture and processing. It is fixed in position to ensure consistent distance and angle for  
850 all images. It is also paired with a lighting system to provide a consistent lighting for the  
851 images. The system captures images of both the top and bottom sides of each mango to  
852 ensure a more accurate grading. The prototype integrates the Raspberry Pi Camera Module  
853 Version 2. This camera is chosen for its 8MP resolution which is critical in capturing  
854 real-time images. Another reason for integrating this camera is because of its compatibility  
855 with the Raspberry Pi 4, and reliability in capturing detailed images needed for accurate  
856 classification. It is also cost effective and lightweight which is important for the prototype.

### 857 **3.6.2 4 Channel Relay**

858 The relay module in this project is used to control the direction and movement of the  
859 motors that operate the conveyor system and mango sorting mechanism. As an electrically  
860 operated switch, the relay allows the low-power signals from the Raspberry Pi to safely  
861 manage the higher voltage and current required by the DC motors.

862 For the prototype, the relay module is responsible for changing the polarity of motor  
863 connections which enables the motors to rotate in both forward and reverse directions.  
864 This will drive the conveyor belt system. This is essential for moving mangoes along the  
865 conveyor, rotating them for the top and bottom image capture, and directing them to the  
866 appropriate bin based on their grade.

**867 3.6.3 Gear Ratio**

868 In this prototype, gear ratios are used to control the rotational speed of the conveyor belts  
869 that move and rotate the mango. A gear ratio of 1:3 was applied, meaning the motor gear  
870 completes one full rotation for every three rotations of the driven gear. This is also done in  
871 order to avoid overspeeding and make sure that the conveyor belt moves in a controlled  
872 manner. This setup slows down one belt relative to the other, creating a differential speed  
873 between the left and right belts. As a result, the mango rotates in place while being moved  
874 forward. This rotation is essential for capturing both the top and bottom views of the mango  
875 for accurate classification and grading.

**876 3.7 Summary**

877 Overall, chapter 3 establishes key concepts and theoretical considerations that form the  
878 foundation of the Carabao mango sorter and grading system. It discusses and connects  
879 each component together, explaining how each component such as the RaspberryPi and  
880 DC motors work together to create a system that utilizes machine learning and computer  
881 vision techniques to classify mangoes based on user priority.



882

## Chapter 4

883

# DESIGN CONSIDERATIONS



## 884 **4.1 Introduction**

885 Likewise, the objective of chapter 4 is to describe the researcher's design consideration  
886 when developing and testing the prototype. For an overview of the design of the prototype,  
887 the researchers considered different computer vision models in classifying the ripeness  
888 and bruises together with other algorithms to determine the size of the mango. Likewise,  
889 the hardware design was also taken into consideration where the physical design of the  
890 conveyor belt was taken into account.

## 891 **4.2 Engineering Standards**

### 892 **4.2.1 Electrical Certifications**

893 The UL Listed certification indicates that the Raspberry Pi power supply has been tested and  
894 approved by Underwriters Laboratories (UL), meeting safety standards for both the United  
895 States and Canada under certification number E330985. This certification ensures that  
896 the power supply complies with established requirements for electrical safety, insulation,  
897 and protection against potential fire hazards. It also carries an Efficiency Level VI rating,  
898 which represents the highest energy efficiency standard set by the U.S. Department of  
899 Energy (DOE) for external power supplies, ensuring minimal energy loss and optimized  
900 performance.

### 901 **4.2.2 Safety of Machinery**

902 The ISO 13850:2015 – Safety of Machinery (Emergency Stop Function, Principles for  
903 Design) standard defines the safety requirements for emergency stop functions in machinery.



904 It specifies that emergency stop devices must be clearly visible, easily accessible, and  
905 capable of quickly and safely halting machine operations in the event of a malfunction or  
906 hazard. For the prototype, the stop button is located at the bench power supply and the RPi.

#### 907 **4.2.3 Safety Requirements for Technology Equipment**

908 The IEC 62368-1:2018 / ISO 62368-1:2018 – Safety Requirements for Audio/Video,  
909 Information, and Communication Technology Equipment standard establishes international  
910 safety guidelines for modern electronic devices and their power supplies. It replaces  
911 older standards (IEC 60065 and 60950) with a hazard-based safety engineering approach,  
912 ensuring that equipment in the prototype like the RPi power supply and bench power supply  
913 are designed to prevent electrical shock, overheating, and fire risks.

#### 914 **4.2.4 Open-source Software Compliance**

915 The ISO/IEC 5230e - Open-source Software Compliance ensures that organizations using  
916 open-source components in their products maintain proper documentation, license trace-  
917 ability, and transparency in software management. For components in the prototype like  
918 the RPi operating system, which rely on open-source ecosystems, compliance with this  
919 standard promotes responsible use and distribution of software, reducing legal and security  
920 risks associated with open-source code.

### 921 **4.3 System Architecture**

922 The system architecture is represented through a block diagram, showcasing modules  
923 such as image acquisition, preprocessing, feature extraction, machine learning model, and



grading output. Each module is described in detail, emphasizing its role in the overall system. For instance, the image acquisition module uses high-resolution cameras to capture mango images, while the preprocessing module enhances image quality for better feature extraction.

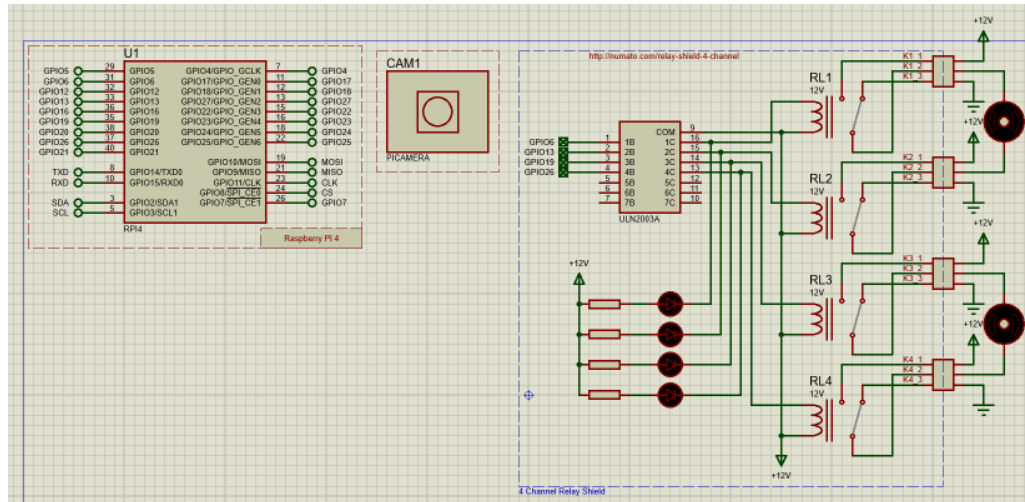


Fig. 4.1 Hardware Schematic

In figure 4.1 presents the electronic circuit diagram, designed using Proteus. The diagram illustrates a system where a Raspberry Pi 4 serves as the central control unit, managing four motors through a relay mechanism. The Raspberry Pi 4, represented by a rectangular box on the left, showcases various pin connections, including GPIO pins, power supply pins (5V and 3V3), ground pins (GND), and communication pins (TXD, RXD, SDA, SCL).

In the center of the diagram, an 18-pin integrated circuit labeled "ULN2803A" is depicted. This component, a Darlington transistor array, likely functions as a buffer, providing the necessary current to drive the relays. Four relays, designated as RL1, RL2, RL3, and RL4, are positioned on the right side of the diagram, each connected to a motor



938 (represented by a circle with an "M" inside) and a +12V power source. Additionally, four  
939 resistors are placed between the ULN2803A and the relays, serving to limit current. The  
940 circuit section containing these resistors is labeled "4 Channel Relay Driver," indicating its  
941 purpose.

942 The camera module is labeled "PICAMERA" is located in the top center of the diagram.  
943 It is represented by a square with a circle inside, symbolizing the camera lens. The camera  
944 module is connected to the Raspberry Pi 4 through the CSI (Camera Serial Interface) pins.  
945 The overall circuit is designed for a 12V system, with the +12V power supply indicated at  
946 various points. The Raspberry Pi 4's GPIO pins are used to control the relays.

## 947 **4.4 Hardware Considerations**

948 The hardware components include high-resolution cameras, lighting systems for consistent  
949 image capture, and microcontrollers like Raspberry Pi or Arduino for system control,  
950 actuators like DC motors to move the mangoes. The choice of hardware is justified based  
951 on cost, performance, and compatibility with the software framework.

### 952 **4.4.1 General Prototype Framework**

953 The Figure 4.2 presents the overall prototype layout of the automated Carabao mango  
954 sorter and grader. The diagram illustrates the flow of operations from mango loading onto  
955 the conveyor belt to sorting them. It illustrates the major elements of the system, that is,  
956 the image acquisition area, lighting system, camera module, Raspberry Pi controller, and  
957 mechanical actuators. The layout illustrates how all the subsystems work together to ensure  
958 mangoes are scanned, processed, sorted based on ripeness, size, and bruises, and eventually

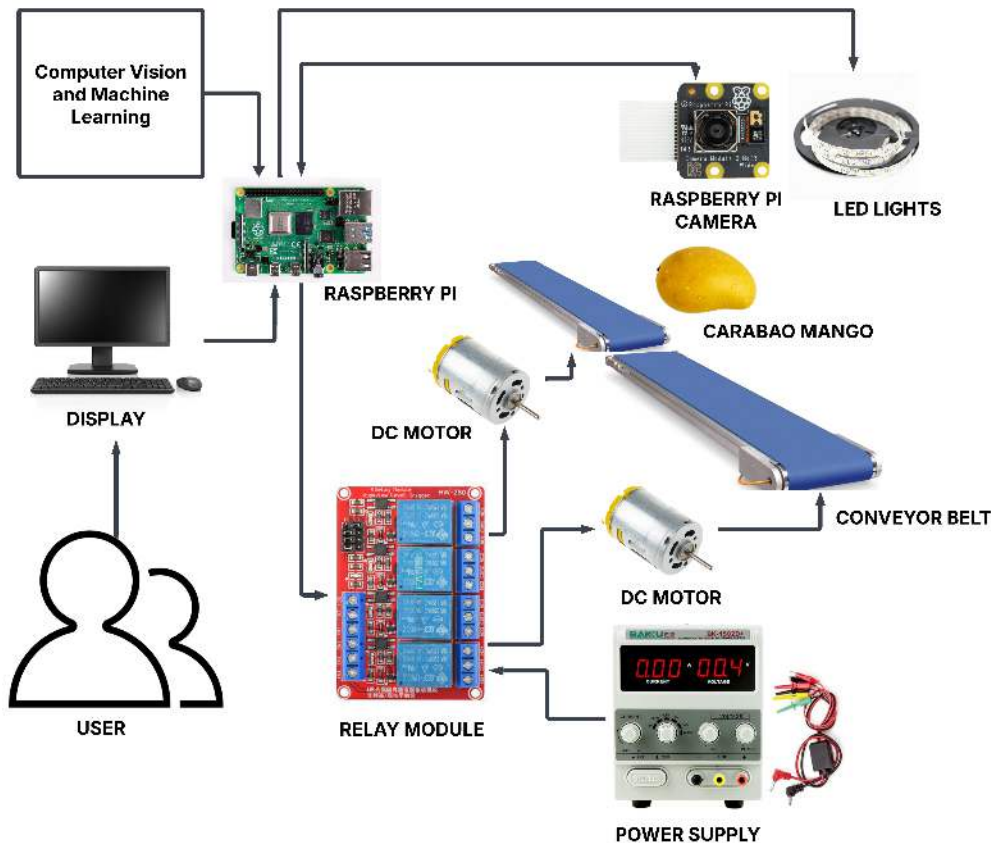


Fig. 4.2 Prototype Framework

sorted based on the calculated priority score. The layout served as the basis for actual prototype development.

#### 4.4.2 Prototype Flowchart

The flowchart in Figure 4.3 represents the overall operational logic of the mango grading and sorting system. The process starts with system initialization, where the camera and lighting modules are switched on and the machine learning algorithms are initialised. The

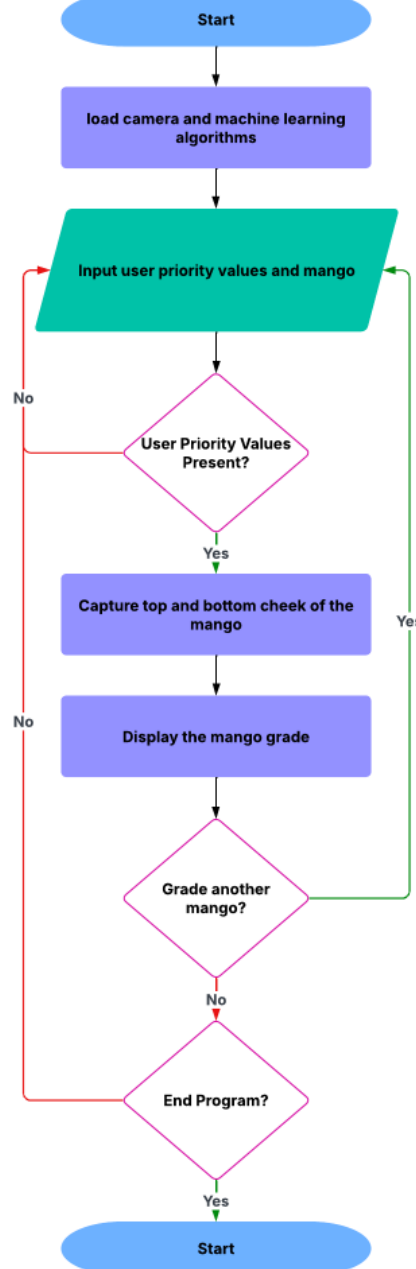


Fig. 4.3 Prototype Main Flowchart



965 input of the user priority values as well as the detection of the mango on the conveyor  
966 belt triggers the capture of both the top and bottom cheek of the mango. The captured  
967 image is processed using machine learning algorithms to determine its ripeness, size, and  
968 bruises. Depending on these classifications along with priority weights given by the user,  
969 the system calculates an overall score. Once this calculation is done, the mango is routed to  
970 the respective bin through the respective actuator. Having this logical sequence is important  
971 to know the system's decision-making and automation process.

#### 972 **4.4.3 Prototype 3D Model**

973 Figure 4.4 shows the first 3D model of the initial physical prototype developed for the  
974 sorting and grading system. This model shows the skeleton of the system and where  
975 the conveyor system is going to be placed strategically in order to flip the mango for  
976 image acquisition. It is useful for where the hardware components would be arranged  
977 and assembled. This 3D model helped the researchers visualize the spacing, alignment,  
978 and where to mount parts before assembling the prototype making sure all electronic and  
979 mechanical components are effectively integrated.

#### 980 **4.4.4 Hardware Specifications**

##### 981 **4.4.4.1 Raspberry Pi**

982 The Raspberry Pi 4 Model B serves as the central processing unit of the prototype, chosen  
983 for its compact form factor, affordability, and substantial computational capability required  
984 for image processing and machine learning tasks. The board's essential features include  
985 GPIO pins for connecting sensors, actuators, and relays, along with USB and HDMI ports



De La Salle University



Fig. 4.4 Initial 3D Model of the Prototype



Fig. 4.5 Raspberry Pi 4 Model B

986 for peripheral integration. Its support for a full operating system enables it to efficiently  
987 manage both the user interface and the core control logic of the mango grading system.

988 **Specifications:**

- 989 • SoC: Broadcom BCM2711  
990 • Central Processing Unit (CPU): Quad-core ARM Cortex-A72 (64-bit)  
991 • Clock Speed: 1.5 GHz (base, overclockable)  
992 • RAM: 8GB LPDDR4-3200 SDRAM  
993 • Wireless: Dual-band 2.4 GHz / 5 GHz Wi-Fi (802.11ac)  
994 • Bluetooth: Bluetooth 5.0 (BLE support)  
995 • Ethernet: Gigabit Ethernet (full throughput)



- 996     • USB: 2 x USB 3.0 ports and 2 x USB 2.0 ports
- 997     • Video Output: 2 x micro-HDMI ports (supports 4K @ 60Hz, dual 4K display capability)
- 998     • Audio: 3.5mm audio/video composite jack
- 1000    • Storage: MicroSD card slot (supports booting via SD card or USB)
- 1001    • GPIO: 40-pin GPIO header (backward-compatible with older models)
- 1002    • Camera/Display: CSI (camera) and DSI (display) ports
- 1003    • Power Input: USB-C (5V/3A recommended)
- 1004    • Power Consumption: 3W idle, up to 7.5W under load

#### 4.4.4.2 Raspberry Pi Camera

This high-quality camera module is specifically engineered for the Raspberry Pi platform, offering 8-megapixel still image capture and video recording capabilities at 1080p (30fps), 720p (60fps), and 480p (90fps). It incorporates a fixed-focus lens with a 62.2-degree diagonal field of view and a 1/4-inch optical format. Compatibility with Python libraries like Picamera and OpenCV facilitates seamless image capture and processing. Its selection was driven by its small size, straightforward integration, and capacity for high-resolution imaging.

##### Specifications:

- 1014    • Sensor: Sony IMX219PQ 8-megapixel CMOS sensor.
- 1015    • Still Images Resolution: 8 MP (3280 x 2464 pixels).

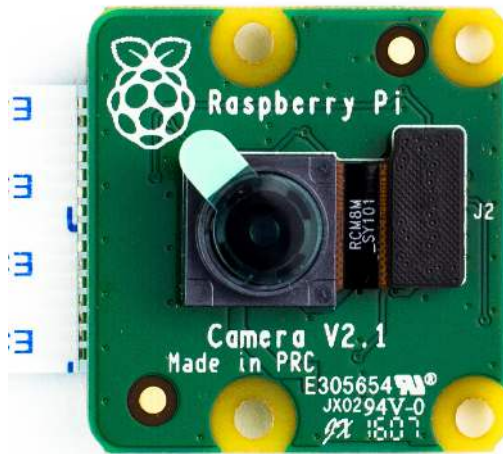


Fig. 4.6 Raspberry Pi Camera Module Version 2

- 1016 • Video Resolution: Supports up to 1080p @ 30fps, 720p @ 60fps, and 480p @ 90fps.
- 1017 • Focus: Fixed-focus lens (manual focus adjustment not supported without physical  
1018 modification).
- 1019 • Lens Size: 1/4-inch optical format.
- 1020 • Field of View (FoV): Diagonal 62.2 degrees.
- 1021 • Interface: Connected via 15-pin ribbon cable to the Raspberry Pi's CSI (Camera  
1022 Serial Interface) port.
- 1023 • APIs/Libraries: Supports Python libraries such as Picamera and OpenCV for image  
1024 capture and processing.
- 1025 • Dimensions: 25 mm x 24 mm x 9 mm.



1026

#### 4.4.4.3 DC Motor



Fig. 4.7 12 Volt DC Gear Motor

1027

This compact 12V DC gear motor delivers high torque and operates quietly, making it suitable for robotics, automation, and industrial control systems. Its spur gear design ensures a high reduction ratio for enhanced torque. Engineered for continuous duty, it maintains low power consumption during standard operation and offers reliability under high-temperature conditions.

1032

**Specifications:**

1033

- Gearbox Type: Spur gear design

1034

- Operating Voltage: 12V (operational range: 6-12V)

1035

- No-load Current Consumption: 0.8A

1036

- Rated Current Draw: 3A (under standard load)



- 1037     • No-load Speed: 282 RPM (maximum)
- 1038     • Operating Speed: 248 RPM (under rated load)
- 1039     • Torque Output: 18 kg-cm (rated)
- 1040     • Stall Torque: 60 kg-cm (maximum)
- 1041     • Power Rating: 50W (maximum)
- 1042     • Unit Weight: 350 grams

1043     **4.4.4.4 MicroSD Card**



Fig. 4.8 SanDisk Ultra MicroSD Card

1044     This compact, high-capacity SanDisk Ultra MicroSD card provides secure digital  
1045     storage for devices like digital cameras, smartphones, and tablets. Its high-speed data  
1046     transfer rate is optimal for handling large files such as images and videos. The card was



# De La Salle University

1047 chosen for the prototype's storage system due to its substantial capacity, reliable data  
1048 protection, and user-friendly design.

1049 **Specifications:**

- 1050 • Capacity: 256GB  
1051 • Type: MicroSDXC (Secure Digital eXtended Capacity)  
1052 • Form Factor: MicroSD (11mm x 15mm x 1mm)  
1053 • File System: Pre-formatted exFAT

1054 **4.4.4.5 LED Lights**



Fig. 4.9 LED Light Strip

1055 The LED strips were implemented to deliver uniform illumination for image capture,  
1056 which is crucial for precise color representation and feature extraction. Their selection was



# De La Salle University

1057 based on exceptional energy efficiency, extended operational lifespan, and consistent light  
1058 output quality.

1059 **Specifications:**

- 1060 • Power Input: 5V DC (USB-powered, compatible with laptops, power banks, or USB  
1061 adapters).
- 1062 • Waterproof Design: Suitable for indoor/outdoor use.
- 1063 • LED Type: SMD 2835 (surface-mount diodes for high brightness and efficiency).
- 1064 • Color Type: White (cool white)
- 1065 • Length: 1m
- 1066 • Beam Angle: 120°
- 1067 • Operating Temperature: -25°C to 60°C.
- 1068 • Storage Temperature: -40°C to 80°C.

1069 **4.4.4.6 Power Supply**

1070 This bench power supply is an adaptable and regulated source that delivers stable voltage  
1071 and current for diverse electronic projects. Designed for testing purposes, it enables precise  
1072 setting of voltage and current parameters. Its versatility, user-friendly operation, and  
1073 accurate control capabilities led to its selection.

1074 **Specifications:**

- 1075 • Type: SMPS (Switch-Mode Power Supply)



Fig. 4.10 Bench Power Supply

- 1076 • Input: 110V AC, 50/60Hz (U.S. Standard)
- 1077 • Output Range: 0-30V DC / 0-5A DC
- 1078 • Voltage Precision:  $\pm 0.010V$  (10 mV) resolution
- 1079 • Current Precision:  $\pm 0.001A$  (1 mA) resolution
- 1080 • Power Precision:  $\pm 0.1W$  resolution
- 1081 • Weight: 5 lbs (2.27 kg)
- 1082 • Dimensions: 11.1" x 4.92" x 6.14" (28.2 cm x 12.5 cm x 15.6 cm)
- 1083 • Maximum Power: 195W
- 1084 • Power Source: AC input only



1085

#### 4.4.4.7 4 Channel Relay Module



Fig. 4.11 4 Channel Relay Module

1086

This compact and versatile relay board enables control of multiple devices through a single microcontroller. It was chosen for its small footprint, operational simplicity, and capacity to manage several devices concurrently. Designed for compatibility with microcontrollers like Arduino and Raspberry Pi, it integrates smoothly into the prototype.

1090

##### Specifications:

1091

- Operating Voltage: 5V DC (compatible with Arduino, Raspberry Pi, and other microcontrollers).

1093

- Number of Relays: 4 independent channels.

1094

- Relay Type: Electromechanical (mechanical switching).

1095

- Max AC Load: 10A @ 250V AC (resistive).



- 1096     • Max DC Load: 10A @ 30V DC (resistive).
- 1097     • Contact Type: SPDT (Single Pole Double Throw) - NO (Normally Open), NC  
1098                 (Normally Closed), COM (Common).
- 1099     • Dimensions: 50mm x 70mm x 20mm
- 1100     • Weight: 50-80 grams.
- 1101     • Status LEDs: Individual LEDs for each relay (indicates ON/OFF state).
- 1102     • Input Pins: 4 digital control pins (one per relay).
- 1103     • Output Terminals: Screw terminals for connecting loads (NO/NC/COM).

1104     **4.4.4.8 RPi Power Supply**



Fig. 4.12 Power Supply for the RPi

1105     This official Raspberry Pi power supply is optimally designed for the Raspberry Pi 4  
1106     Model B, compatible with all its memory variants. Delivering 5.1V at 3A via a USB-C  
1107     connector, it ensures reliable performance. The OKdo-branded unit provides stable power



# De La Salle University

1108 suitable for the Raspberry Pi 4, other single-board computers, and mobile devices, and  
1109 includes comprehensive over-temperature protection with global plug compatibility.

1110 **Features:**

- 1111 • Compatible with Raspberry Pi 4 Model B
- 1112 • Color: Black
- 1113 • USB-C connector
- 1114 • US Plug
- 1115 • Over temperature protection
- 1116 • Short circuit protection
- 1117 • Over current protection
- 1118 • Over voltage protection

1119 **Specifications:**

- 1120 • Input Voltage: 100-264V AC
- 1121 • Input Frequency Range: 47-63Hz
- 1122 • Input Current: 600mA Max
- 1123 • Output Voltage: 5.1V DC
- 1124 • Output Current: 3A
- 1125 • Power Rating: 15.3W



- 1126 • Output Connector: USB Type C

- 1127 • Output Cable Length: 1.5M

- 1128 • Number of Outputs: 1

- 1129 • Unload Standby Power: 0.1W

- 1130 • Max Ripple Noise: 50-240mVp-p

1131 **4.4.4.9 Mini Conveyor Single Narrow**



Fig. 4.13 Single Narrow Mini Conveyor

1132 This miniature conveyor system facilitates the creation of compact factory setups for  
1133 presentations and prototyping. The single narrow configuration is particularly suited for  
1134 small-scale automation tasks and experimental applications.

1135 **Specifications:**

- 1136 • Belt Dimensions: 43.4 x 9 x 9 cm (L x W x H)

- 1137 • Chassis Dimensions: 46 x 10.5 x 11 cm (L x W x H)



- 1138 • Type: Single narrow conveyor
- 1139 • Application: Prototyping and miniature factory setups

1140 **4.4.4.10 Mini Conveyor Double Narrow**



Fig. 4.14 Double Narrow Mini Conveyor

1141 This miniature conveyor system enables the development of small-scale factory environments for demonstrations and prototyping. The double narrow version offers increased length to accommodate more sophisticated automation processes and continuous operation requirements.

1145 **Specifications:**

- 1146 • Belt Dimensions: 85.5 x 9 x 9 cm (L x W x H)
- 1147 • Chassis Dimensions: 88 x 10.5 x 11 cm (L x W x H)
- 1148 • Type: Double narrow conveyor
- 1149 • Application: Extended prototyping and miniature factory setups



## 4.5 Software Considerations

The software stack includes Python for programming PyTorch for machine learning and OpenCV for image processing. These tools are selected for their robustness, ease of use, and extensive community support, ensuring efficient system development.

### 4.5.1 PyTorch

PyTorch is an open-source deep-learning framework used in this project for implementing and running the convolutional neural networks responsible for classifying mango ripeness and detecting bruises. Its dynamic computational graph and GPU acceleration support made it an ideal choice for real-time image classification. Its simplicity and flexibility also allowed for easy integration with the Raspberry Pi which is important as it is the main processing unit for the system.

### 4.5.2 OpenCV

Open Source Computer Vision Library or OpenCV is utilized in the system for all image processing tasks, particularly in preprocessing steps such as background subtraction, thresholding, edge detection, and contour analysis. These operations are essential for calculating the real-world dimensions of the mango. OpenCV was utilized primarily because of its diverse set of functions, performance optimization, and ease of use making it a core tool for enabling accurate and fast computer vision processing within the prototype.



### 1168    **4.5.3 CustomTkinter**

1169    CustomTkinter is a modern alternative to the standard Tkinter library, and is used to  
1170    build the graphical user interface (GUI) of the system. It provides a more polished and  
1171    customizable visual appearance while retaining the simplicity of Tkinter. With features  
1172    such as styled buttons, frames, and labels, CustomTkinter allowed for the creation of  
1173    a user-friendly interface that supports real-time display of classification results, priority  
1174    scoring inputs, and system status updates.

## 1175    **4.6 User Interface**

1176    A User Interface (UI) is designed to display grading results, system status. Wireframes  
1177    illustrate the layout, ensuring usability and accessibility for operators. Likewise, a Graphical  
1178    User Interface (GUI) is also used to allow users to customize the system's grading priorities.

## 1179    **4.7 Summary**

1180    This chapter outlines the foundational design and engineering decisions for the automated  
1181    mango grading system. The design process prioritized creating a scalable, efficient, and  
1182    user-friendly system, guided by established engineering standards for safety and compliance.  
1183    These standards include UL Listing for the power supply, ISO 13850 for the emergency  
1184    stop function, and IEC 62368-1 for the safety of the technology equipment.

1185    The system architecture is built around a RPi 4 Model B as the central controller, which  
1186    manages a network of hardware components. The core hardware includes a RPi Camera  
1187    for image acquisition, 12V DC gear motors to drive the conveyor belts, a 4-channel relay



# De La Salle University

1188 module for motor control, and LED strips to ensure consistent lighting. A detailed hardware  
1189 schematic and a 3D model were created to plan the integration of these electronic and  
1190 mechanical parts effectively.

1191 On the software side, the system leverages a robust stack including PyTorch for running  
1192 the deep learning models, OpenCV for image processing tasks like size determination,  
1193 and CustomTkinter to build an intuitive GUI. This GUI allows operators to input grading  
1194 priorities and view results. The overall operational logic, from mango detection and image  
1195 capture to classification and sorting, is defined by a clear system flowchart. In summary,  
1196 this chapter details the careful selection and integration of both hardware and software  
1197 components to form a coherent, safe, and functional prototype.



1198

## **Chapter 5**

1199

# **METHODOLOGY**



TABLE 5.1 SUMMARY OF METHODS FOR REACHING THE OBJECTIVES

Objectives	Methods	Locations
GO: To develop a user-priority-based grading and sorting system for Carabao mangoes, using machine learning and computer vision techniques to assess ripeness, size, and bruises.	<ol style="list-style-type: none"> <li>1. Hardware design: Build an image acquisition system with a conveyor belt, LED lights, and Raspberry Pi Camera</li> <li>2. Software design: Coded a Raspberry Pi application to grade and sort the Carabao mangoes</li> </ol>	Sec. 5.2 on p. 59
SO1: To make an image acquisition system with a conveyor belt for automatic sorting and grading mangoes.	<ol style="list-style-type: none"> <li>1. Hardware implementation: Design and build an image acquisition system prototype</li> </ol>	Sec. 5.3 on p. 59
SO2: To get the precision, recall, F1 score, confusion matrix, and train and test accuracy metrics for classifying the ripeness and bruises with an accuracy score of at least 90%.	<ol style="list-style-type: none"> <li>1. Performance testing: Train and test the machine learning algorithm for classifying bruises and ripeness</li> <li>2. Data collection: Gather our own Carabao mango dataset together with an online dataset</li> </ol>	Sec. 5.5 on p. 69

*Continued on next page*



*Continued from previous page*

Objectives	Methods	Locations
SO3: To create a microcontroller-based system to operate the image acquisition system, control the conveyor belt, and process the mango images through machine learning.	<ol style="list-style-type: none"> <li>1. Algorithm development: To develop a code for the image acquisition system</li> <li>2. Hardware design: To design a schematic for the microcontroller based system</li> </ol>	Sec. 5.3 on p. 59
SO4: To grade mangoes based on user priorities for size, ripeness, and bruises.	<ol style="list-style-type: none"> <li>1. Formula development: Formulated an equation based on the inputted user priority and the predicted mango classification</li> </ol>	Sec. 5.7 on p. 86
SO5: To classify mango ripeness based on image data using machine learning algorithms such as kNN, k-mean, and Naïve Bayes.	<ol style="list-style-type: none"> <li>1. Performance testing: Train and test the machine learning algorithm for classifying bruises</li> </ol>	Sec. 5.6.6 on p. 82
SO6: To classify mango size based on image data by getting its length and width using OpenCV, geometry, and image processing techniques.	<ol style="list-style-type: none"> <li>1. Performance testing: Train and test the machine learning algorithm for classifying ripeness</li> </ol>	Sec. 5.6.5 on p. 80
SO7: To classify mango bruises based on image data by employing machine learning algorithms.	<ol style="list-style-type: none"> <li>1. Accuracy testing: Get the percent accuracy testing for getting the length and width of the Carabao mango</li> </ol>	Sec. 5.6.7 on p. 84



## 1200 5.1 Introduction

1201 The methodology for this research outlines the development of the Carabao Mango sorter  
1202 using machine learning and computer vision. The sorting system uses a conveyor belt  
1203 system which delivers the mangoes into the image acquisition system. This system captures  
1204 the image of the mangoes which will then be going through the various stages of image  
1205 processing and classification into grades which will depend on the priority of the user.  
1206 This methodology ensures that the grading of the mangoes will be accurate while being  
1207 non-destructive.

## 1208 5.2 Research Approach

1209 This study applies the experimental approach for research in order to develop and properly  
1210 test the proposed system. The experimental approach of the methodology will allow the  
1211 researchers to fine-tune the parameters and other factors in the classification of mangoes in  
1212 order to get optimal results with high accuracy scores while maintaining the quality of the  
1213 mangoes. This approach will also allow for real-time data processing and classification  
1214 which will improve the previous static grading systems. To efficiently design and build  
1215 the prototype, the researchers employed a Scrum agile methodology for managing the two  
1216 main clusters of the prototype which are the software and hardware design.

## 1217 5.3 Hardware Design

1218 The prototype consists of hardware and software components for automated mango sorting  
1219 and grading purposes. The hardware includes the conveyor belt system used to transfer



1220 mangoes from scanning to sorting smoothly. A camera and lighting system are able  
1221 to collect high-resolution images for analysis. The DC motors and stepper motors are  
1222 responsible for driving the conveyor belt and sorting actuators. The entire system is  
1223 controlled by a microcontroller RPi, coordinating actions of all components. Sorting  
1224 actuators then direct mangoes into selected bins based on their classification to make  
1225 sorting efficient.

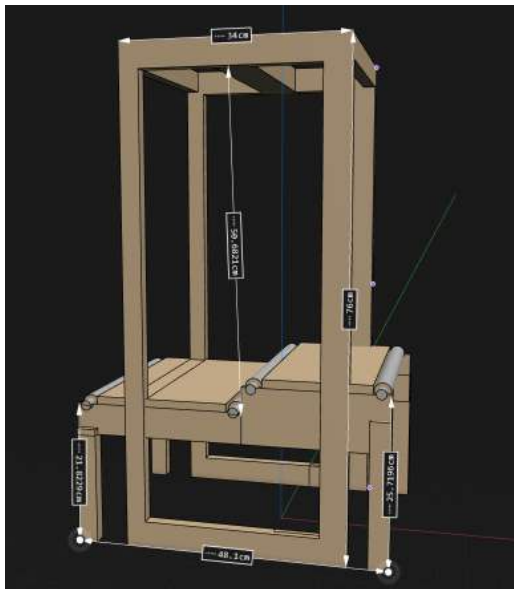
## 1226 **5.4 Software Design**

1227 For the programming language used for the prototype and training and testing the CNN  
1228 model, Python was used for training and testing the CNN model and it was also used in the  
1229 microcontroller to run the application containing the UI and CNN model. PyTorch was the  
1230 main library used in using the EfficientNet model that is used in classifying the ripeness  
1231 and bruises of the mango. Likewise, tkinter is the used library when designing the UI in  
1232 Python.

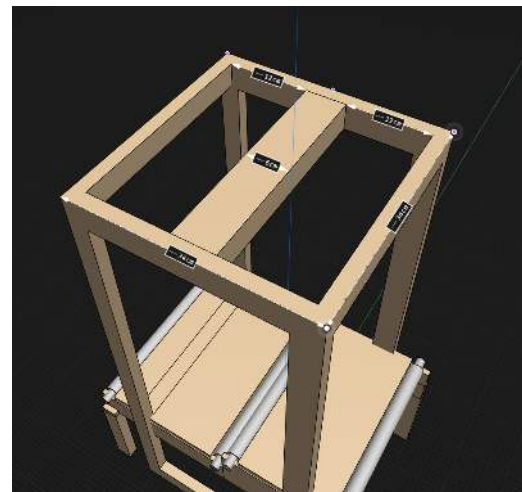
1233 Furthermore, the rest of the software components are of utmost importance to mango  
1234 classification. Image processing algorithms in OpenCV and CNN models extract features  
1235 such as color, size, and bruises that are known to determine quality parameters of mangoes.  
1236 Mangoes are classified based on ripeness and defects by using machine learning algorithms,  
1237 which further enhances accuracy using deep learning techniques. A user interface (UI) is  
1238 designed for users to control and observe the system in real time. Finally, the interface  
1239 programming of the microcontroller provides the necessary synchronization between  
1240 sensors, actuators, and motors throughout the sorting operation scenario.



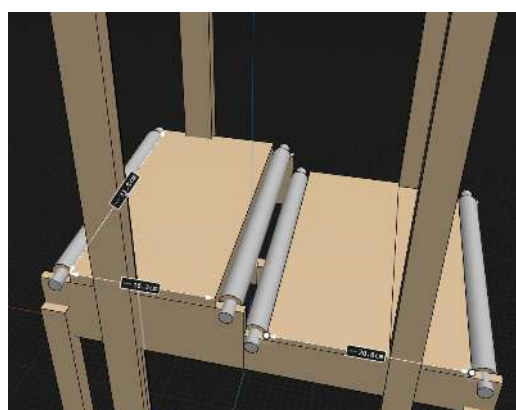
De La Salle University



(a) Left View



(b) Top View



(c) Right View

Fig. 5.1 Image Acquisition Dimensions



### 1241    **5.4.1 Machine Learning Methods**

1242    The processed dataset is to be then used to create models using a variety of machine learning  
1243    methods. For a comprehensive evaluation, the processed dataset was used to train and  
1244    test a variety of machine learning models. The training included Convolutional Neural  
1245    Network (CNN), k-Nearest Neighbors (k-NN), Naive Bayes, and k-Mean clustering and  
1246    various Efficientnet models. This comparative analysis was conducted to benchmark the  
1247    performance of the deep learning approach against traditional machine learning algorithms.

### 1248    **5.4.2 Optimizer**

1249    Choosing the correct optimizer critically impacts both the convergence speed and the  
1250    generalization ability of deep neural networks. The widely used Adam optimizer employs  
1251    adaptive learning rates for each parameter, adjusting them according to the first- and  
1252    second-order moments of gradients. However, Adam implements weight decay as a part of  
1253    gradient updates, which couples regularization and optimization in a way that can hamper  
1254    generalization. AdamW was developed to decouple weight decay from the adaptive gradient  
1255    update. Specifically, in AdamW, weight decay is applied directly to the parameters after  
1256    the Adam update, leading to improved generalization and often more robust performance  
1257    in large-scale tasks. Extensive benchmark comparisons reveal that AdamW outperforms  
1258    standard Adam, especially when it comes to image classification or language modeling  
1259    tasks with deep architectures (Loshchilov and Hutter, 2017).



### 1260    5.4.3 Data Loading Optimization

1261    Efficient data loading is a vital but often underestimated aspect of deep learning. In  
1262    frameworks like PyTorch, the num\_workers parameter of the DataLoader determines how  
1263    many subprocesses are used to fetch batches of data in parallel. Setting num\_workers >0  
1264    enables multiprocessing, which prefetches batches and keeps the GPU occupied without  
1265    idling, especially for large datasets or CPU-intensive augmentations. When misconfigured,  
1266    however, the CPU can become a bottleneck, or resource contention may lead to unexpected  
1267    slowdowns. The ideal number of workers depends on many factors: CPU and memory  
1268    resources, dataset I/O demands, and the complexity of any required preprocessing. Practi-  
1269    cally, practitioners start with a low value for num\_workers, gradually increasing while  
1270    monitoring CPU utilization and GPU occupancy, always balancing throughput gains against  
1271    system constraints (Migacz, 2020).

### 1272    5.4.4 Data Transfer Optimization

1273    Data transfer from host (CPU) to device (GPU) is a significant performance consideration  
1274    during training, particularly as model and batch sizes grow. PyTorch and similar frameworks  
1275    provide pin\_memory and non\_blocking options to optimize these transfers. When data  
1276    is loaded with pin\_memory=True, it is allocated in page-locked (pinned) memory, which  
1277    prevents the operating system from swapping it to disk and enables direct memory access  
1278    (DMA) from the GPU, reducing latency. Setting non\_blocking=True in transfer calls further  
1279    allows these memory copies to be overlapped with computation, eliminating host-thread  
1280    blocking and enabling concurrent initiation of multiple transfers. Together, these settings  
1281    can cut data transfer times and better exploit GPU concurrency. However, misuse, such as



1282 excessive pinned memory allocation, can reduce overall system stability due to increased  
1283 physical memory pressure (Moens, 2024).

1284 **5.4.5 Mixed Precision Training**

1285 Mixed precision training is now a near-standard approach for accelerating deep learning,  
1286 especially on modern GPUs equipped with specialized compute units, such as NVIDIA  
1287 Tensor Cores, that can handle reduced numerical precision efficiently. By employing 16-bit  
1288 floating point (FP16 or BF16) arithmetic for most operations and retaining 32-bit (FP32)  
1289 precision for critical accumulations and weight updates, mixed precision training achieves  
1290 two main benefits: faster computation throughput and decreased memory footprint. This  
1291 allows for increased model or batch sizes and faster experimentation cycles, while, with  
1292 proper loss scaling, preserving model convergence and final accuracy (Markidis and et al.,  
1293 2018).

1294 **5.4.6 Adaptive learning Rate Schedulers**

1295 Adaptive learning rate schedules can profoundly affect both convergence speed and the  
1296 ability of a model to generalize. The cosine annealing schedule cyclically adjusts the  
1297 learning rate from a maximum to a minimum according to a cosine function, periodically  
1298 “restarting” back to the initial value. This warm restart strategy prevents the learning rate  
1299 from decaying to zero too rapidly and encourages exploration of flatter minima in the  
1300 loss surface, thereby enhancing generalization. Cosine annealing with restarts is widely  
1301 cited as a simple but effective modification over static or monotonic decay schedules,  
1302 giving superior performance across various deep learning domains from computer vision to



1303 language modeling (Loshchilov and Hutter, 2016).

#### 1304 **5.4.7 CrossEntropy Loss with Label Smoothing**

1305 Using CrossEntropy loss with label smoothing addressed the issue of overconfidence  
1306 in predictions. Standard CrossEntropy encourages the model to assign near-absolute  
1307 probability to the correct class, which can lead to poor generalization, especially when  
1308 classes are ambiguous or noisy. Label smoothing redistributes a small fraction of probability  
1309 mass to incorrect classes, effectively softening the target distribution. This discourages  
1310 the model from becoming overly confident, reduces variance in predictions, and improves  
1311 robustness against mislabeled or borderline samples (Guo and et al., 2024; Szegedy et al.,  
1312 2016)

#### 1313 **5.4.8 Early Stopping and Checkpointing**

1314 Overfitting is a major concern in deep learning, as models with high capacity can easily  
1315 memorize the training data without learning to generalize to new inputs. Early stopping is a  
1316 widespread technique wherein training is halted when performance on a held-out validation  
1317 set ceases to improve, rather than after a fixed number of epochs. This prevents the model  
1318 from entering the overfitting regime. Model checkpointing complements early stopping  
1319 by routinely saving the model's parameters and, optionally, optimizer states, ensuring  
1320 recoverability in the event of hardware failure and enabling the best-performing model on  
1321 validation metrics to be retained, rather than simply the last epoch's snapshot (Hussein and  
1322 Shareef, 2024; Lee et al., 2024).



### 1323    5.4.9 Input Resolution

1324    The spatial resolution of input images materially affects both computational cost and  
1325    prediction accuracy in deep learning, especially for vision tasks. Higher input resolutions  
1326    can theoretically yield better performance, as more visual detail is made available to  
1327    the model, but this often comes at the expense of increased memory and higher training  
1328    times, sometimes forcing smaller batch sizes and less efficient optimization. Conversely,  
1329    reducing input resolution can dramatically decrease resource requirements, permitting  
1330    faster development and larger batch sizes, but at a potential loss of accuracy, especially for  
1331    tasks that demand fine-grained spatial detail (Richter et al., 2020).

### 1332    5.4.10 Regularization

1333    Regularization techniques combat overfitting, and two of the most prominent in deep  
1334    learning are dropout and drop path, also called “stochastic depth”. Dropout randomly  
1335    deactivates a subset of neurons or weights during each training iteration, preventing any  
1336    single unit from becoming indispensable and encouraging redundancy in representation.  
1337    Drop path extends this principle by stochastically skipping entire layers or blocks during  
1338    training, particularly in architectures with skip connections such as ResNet. This approach  
1339    reduces the effective depth of the model during training while maintaining full depth at  
1340    inference, acting as an implicit model ensemble and further strengthening generalization  
1341    (Huang et al., 2016).



## 5.5 Data Collection Methods

For data collection, publicly available datasets were used along with our own gathered dataset. to gather the images of the mangoes the setup seen in Figure 5.2 was used to film the mangoes for about 5 seconds each side. Using a python script every 20th frame per second was extracted. The collected images were then sorted into the following directories for use in training the model: non-bruised, bruised, green, yellow-green, and yellow.



Fig. 5.2 Camera Setup

For the setup of the captured Carabao mangoes, the height of the camera to the white flat surface is 26 cm which can be seen on Figure 5.2. Furthermore, the Samsung S24's camera is used for capturing both cheeks of the Carabao mango. Initially, the Carabao mangoes would be unripe and green and each day the Carabao mangoes would be pictured until they are yellow ripe. Likewise, Figure 5.3 shows the 8 kilogram green Carabao mangoes from the Bicol region. The same mangoes from Bicol are seen on the Figure 5.3. Note that the mangoes were individually captured one at a time at both cheek sides as a video format



(a) Boxes of Carabao Mangoes



(b) Table of Carabao Mangoes

Fig. 5.3 Carabao Mangoes Image Dataset Collection

1355 which can be seen on Figure 5.4.

1356 For the farm one of our members went to interview the head farmer (Jerry Bravante) as  
1357 seen on Figure 5.5, it is located at Ibaan, Batangas. He has 50 years of experience being a  
1358 farmer and 20 years of experience in quality standards of different mango fruit variations  
1359 such as Carabao, Pico, Indian, and Apple. Additionally, the farm has a total of 4 hectares.

## 1360 5.6 Testing and Evaluation Methods

1361 In a bid to ensure the mango sorting and grading system is accurate and reliable, there is  
1362 intensive testing conducted at different levels. Unit testing is initially conducted on each



Fig. 5.4 Sample Mango Image

1363 component separately, for instance, the conveyor belt, sensors, and cameras, to ensure that  
1364 each of the components works as expected when operating separately. After component  
1365 testing on an individual basis, integration testing is conducted to ensure communication  
1366 between hardware and software is correct to ensure the image processing system, motors,  
1367 and sorting actuators work in concert as required. System testing is conducted to con-  
1368 duct overall system performance testing in real-world conditions to ensure mangoes are  
1369 accurately and efficiently sorted and graded.



(a) Collecting Carabao Mangoes



(b) Carabao Mango Tree



(c) Sack of Carabao Mangoes

Fig. 5.5 Collecting Mango on a Farm



1370 For the training, everything was done on a laptop, specifically the Acer Predator Helios  
1371 16 (PH16-71, 2023 model). The technical specifications of this unit are: Intel Core i9-  
1372 13900HX processor, NVIDIA RTX 4070 GPU with 8GB VRAM, and 32GB DDR5 RAM  
1373 running at 5600MHz.

1374 **5.6.1 Data Augmentation and Splitting**

1375 For the used methods to increase the Carabao mango image dataset, data augmentation  
1376 techniques such as rotation, flipping, Gaussian blur, brightness adjustment, noise, crop, and  
1377 resizing of the images were done. Note that the split ratio of the dataset is 70-15-15 where  
1378 it refers to the training, testing, and validation as seen on the Listing 5.1.

1379 The dataset for mango classification was organized into five categories: bruised, not  
1380 bruised, green, yellow-green, and yellow. To ensure robust model training and evaluation,  
1381 the dataset was initially split into training (70%), validation (15%), and test (15%) sets  
1382 using PyTorch's automated splitting functions. Following standard practice in deep learning  
1383 (Perez, Wang, 2017), only the training set was augmented to increase sample diversity and  
1384 improve generalization, while the validation and test sets remained unaltered to preserve  
1385 their role as unbiased evaluation benchmarks.

1386 The validation set contains a balanced representation of the five mango classes. In the  
1387 bruise-based categories shown on Table 5.6, the distribution shows slightly more bruised  
1388 samples (~260) compared to not bruised (~240). On the other hand, for the ripeness-  
1389 based categories as shown in Tables 5.7, green has the highest count (~250), followed by  
1390 yellow-green (~175), and yellow (~125). This distribution ensures that the validation set  
1391 provides a fair assessment of the model's performance across both damage-related and  
1392 ripeness-related classifications.

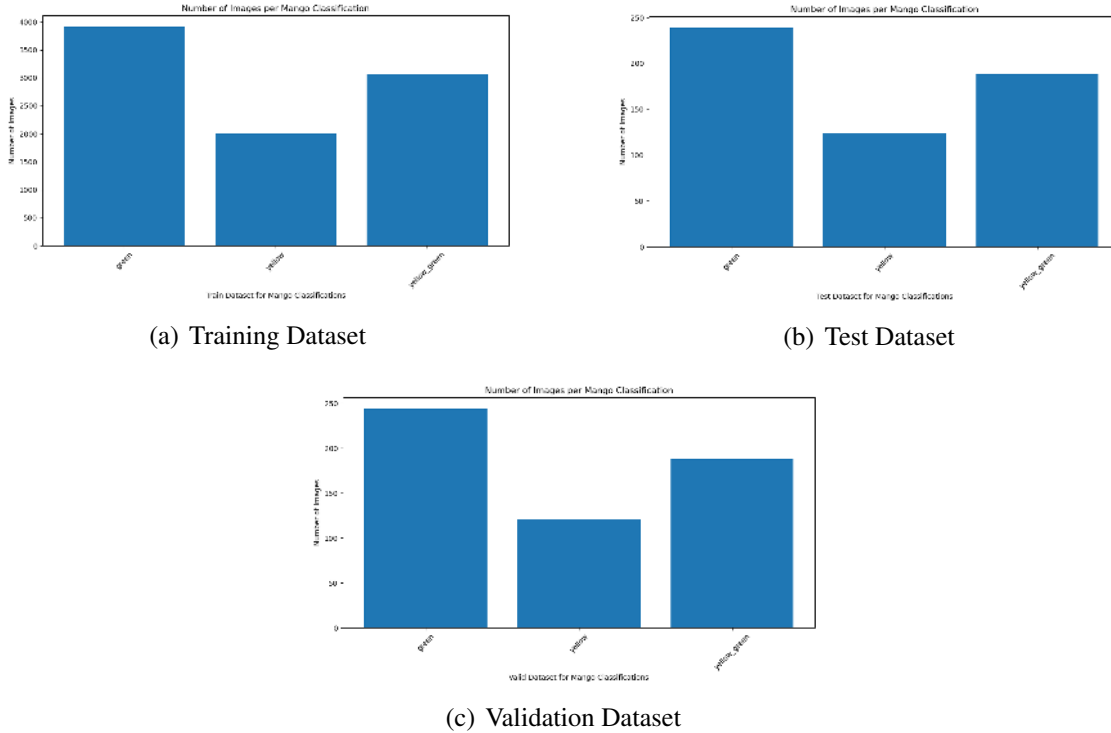


Fig. 5.6 CNN Ripeness 70-15-15 Image Datasplit

The test set mirrors the validation set in structure, maintaining proportional representation across classes. Approximately 260 bruised samples and (~240) not bruised samples are included as seen in Table 5.6. For the ripeness categories seen in Table 5.7, green (~225), yellow-green (~175), and yellow (~125) are represented. This balanced distribution allows for reliable final evaluation of the trained CNN model, ensuring that results are not biased toward any single class.

The training set underwent augmentation to artificially expand the dataset and introduce variability. Augmentation techniques included transformations such as rotation, flipping, scaling, and brightness adjustments. After augmentation, the dataset contained approximately 5,100 bruised and 4,900 not bruised samples as seen in Table 5.7. For the

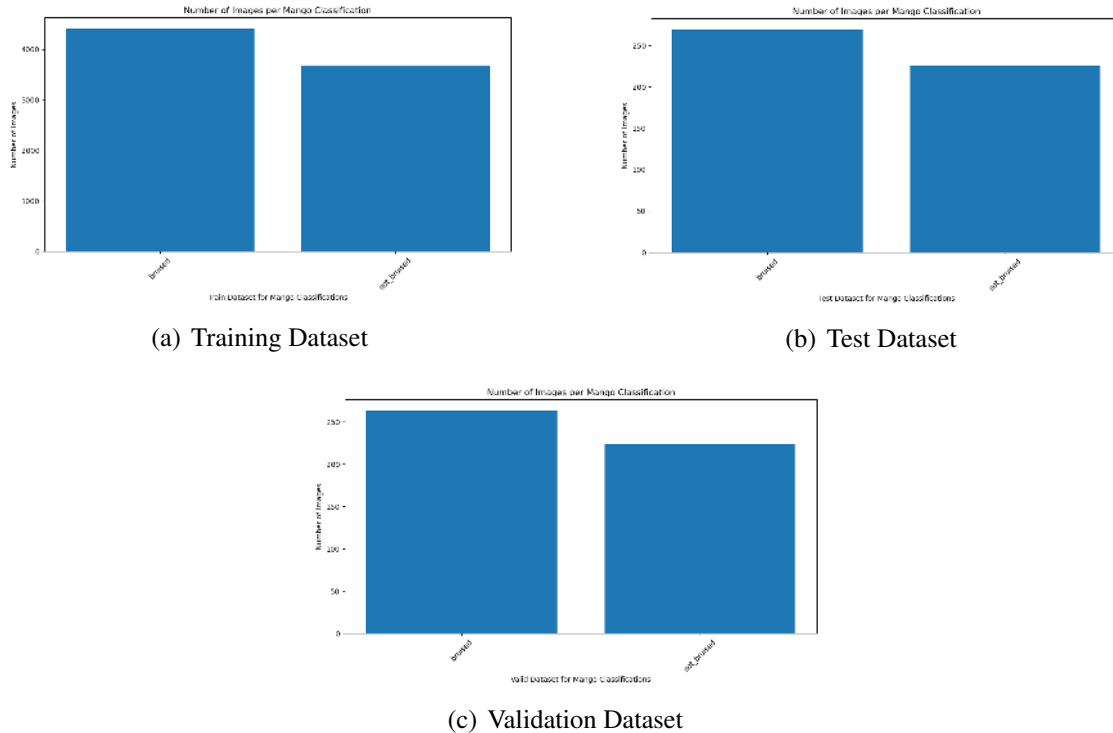


Fig. 5.7 CNN Bruises 70-15-15 Image Datasplit

1403 ripeness categories, green had the highest representation ( $\sim 4,200$ ), followed by yellow-  
 1404 green ( $\sim 3,400$ ), and yellow ( $\sim 2,600$ ) as seen in Table 5.6. This augmentation step increased  
 1405 the training set size substantially, shifting the dataset distribution from 70-15-15 to ap-  
 1406 proximately 90-5-5. Such a shift is expected, as augmentation only affects the training set,  
 1407 thereby increasing its relative proportion.

1408 Augmenting only the training set is a widely accepted best practice in deep learning.  
 1409 According to Shorten and Khoshgoftaar (2019), data augmentation enhances model robust-  
 1410 ness by simulating real-world variability, but applying it to validation or test sets would  
 1411 artificially inflate accuracy by exposing the model to transformed versions of already-seen  
 1412 data. Similarly, Goodfellow et al. (2016) emphasize that evaluation datasets must remain



1413 unseen, original, and unaltered to provide a true measure of generalization. Perez and Wang  
1414 (2017) further demonstrate that augmentation is most effective when applied exclusively to  
1415 training data, as it improves performance without compromising the integrity of evaluation.  
1416 The dataset preparation process therefore ensures that the CNN model is trained on a  
1417 large, diverse, and augmented training set, while validation and test sets remain unaltered  
1418 and representative. This methodology aligns with established best practices in computer vi-  
1419 sion research, supporting both robust training and fair evaluation of the mango classification  
1420 model

### 1421 **5.6.2 Comparative Test of CNN Models**

1422 To identify the most suitable CNN architecture for grading Carabao mangoes, multiple  
1423 CNN models were evaluated under fixed experimental parameters. Each model was  
1424 trained for 15 epochs with an input image size of  $224 \times 224$  pixels, a batch size of 32,  
1425 and the Adam optimizer set at a learning rate of 0.001. Data preprocessing included  
1426 resizing, normalization using ImageNet mean and standard deviation, and augmentation  
1427 techniques such as random horizontal and vertical flips, random rotations, and Gaussian  
1428 blur, which were applied exclusively to the training set. The validation and test sets  
1429 remained unaugmented to ensure unbiased evaluation.

1430 The performance of several CNN architectures, including EfficientNetV1, Efficient-  
1431 NetV2, Visual Geometry Group Network (VGGNet), AlexNet, ResNet50, GoogleNet,  
1432 MobileNetV2, and DenseNet121 was first compared. Based on these results, a more de-  
1433 tailed comparison was then conducted within the EfficientNet family, versions V1 and V2,  
1434 to determine the most effective variant for the task.

1435 No advanced optimization techniques such as early stopping, learning rate schedulers, or



1436 mixed precision training were employed. This decision was intentional to maintain fairness  
1437 across all experiments and to ensure that the only variable factor influencing performance  
1438 was the network architecture itself. Ripeness classification models were trained using a  
1439 Graphics Processing Unit (GPU), while bruise classification models were trained on a  
1440 CPU to compare training times and assess the impact of hardware constraints on accuracy.  
1441 Model performance was evaluated using precision, recall, F1-score, accuracy, resource  
1442 utilization, and elapsed training time.

### 1443 **5.6.3 Benchmarking Best CNN Model on +10k Mango Dataset**

1444 As one of the improvements for the final CNN models, the dataset for mango classification  
1445 was refined and expanded to improve model robustness and reliability across both ripeness  
1446 and bruise detection tasks for the training of the final CNN model where EfficientNetV2-B3  
1447 was used. The data was initially split into training (70%), validation (15%), and test (15%)  
1448 sets, with augmentation applied only to the training set. However, after augmentation, the  
1449 effective distribution shifted to 90% training, 5% validation, and 5% test. In addition, new  
1450 Carabao mango images were incorporated across all classes to strengthen representation  
1451 and improve generalization. As such, to train the final CNN models, the training set for  
1452 ripeness category in Table 5.9b contained 4,900 images of green mangoes, 3,700 images of  
1453 yellow mangoes, and 5,000 images of yellow\_green mangoes. For validation in Table 5.9c,  
1454 the set included 200 green mango images, 175 yellow mango images, and 210 yellow\_green  
1455 images. The test set in Table 5.9a consisted of 200 green mango images, 160 yellow mango  
1456 images, and 220 yellow\_green images. For the bruises category, the training set Table 5.8b  
1457 contained 6,000 images of bruised mangoes and 7,000 images of not\_bruised mangoes  
1458 after augmentation. The validation set in Table 5.8c included 200 bruised mango images



# De La Salle University

1459 and 225 not\_bruised mango images, while the test set as seen in Table 5.8a contained 200  
1460 bruised mango images and 225 not\_bruised mango images. This setup provided a balanced  
1461 evaluation framework for the binary classification task, ensuring that both classes were  
1462 consistently represented across training, validation, and testing.

1463 The dataset was also cleaned to remove sources of noise and ambiguity. Images with  
1464 mixed ripeness features, such as mangoes with both large yellow and green portions, were  
1465 placed under yellow\_green instead, while ambiguous samples, such as yellow mangoes  
1466 with residual greenish portions, were excluded to avoid confusing the model. Empty areas  
1467 present in images were also removed to ensure that only the fruit itself was used for training.

1468 Augmentation strategies were further refined to preserve class-defining features. For  
1469 bruise classification, Gaussian blur was removed since it obscured critical bruise details. For  
1470 ripeness classification, brightness and contrast adjustments were excluded, as these could  
1471 shift mango colors between adjacent classes, such as yellow\_green to yellow, introducing  
1472 artificial mislabels. Other augmentations, such as rotation, flipping, scaling, and minor  
1473 perspective transform, were retained to maintain variability without compromising class  
1474 integrity.

1475 Through these improvements, expanded augmentation, inclusion of new Carabao mango  
1476 samples, dataset cleaning, and task-specific augmentation refinements, the final dataset  
1477 ensured that both CNN models were trained on high-quality, representative, and diverse data.  
1478 This preparation supports fair evaluation on the validation and test sets while maximizing  
1479 the models' ability to generalize to real-world mango classification scenarios.

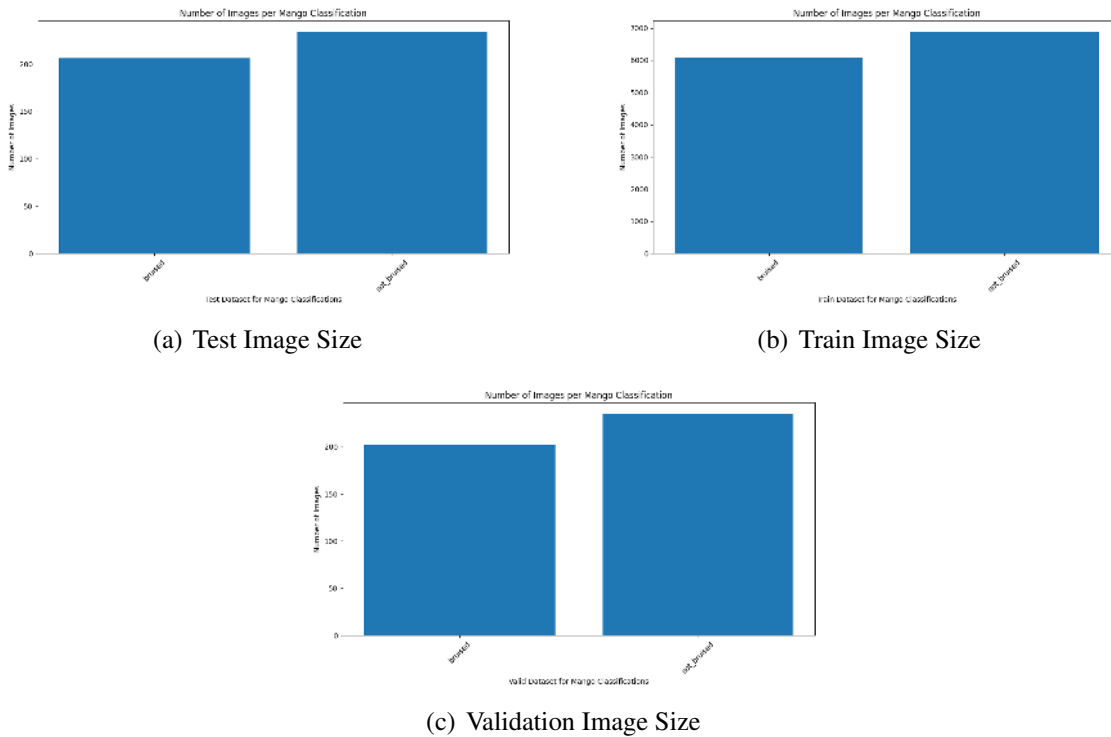


Fig. 5.8 Bruises Image Datasplit

#### 5.6.4 Classification Report

The classification report provides a detailed summary of the model's performance across all output classes by presenting key evaluation metrics such as precision, recall, F1-score, and support. Precision measures the accuracy of positive predictions, recall assesses the model's ability to identify all relevant instances, and the F1-score represents their harmonic mean, offering a balanced measure of performance. In this system, the classification report was used to evaluate how effectively the CNN models identified each mango category—both in ripeness and bruise detection. By analyzing these metrics, the report helps determine which class predictions are most accurate and where the model may require further improvement, ensuring a reliable and interpretable performance assessment for real-world

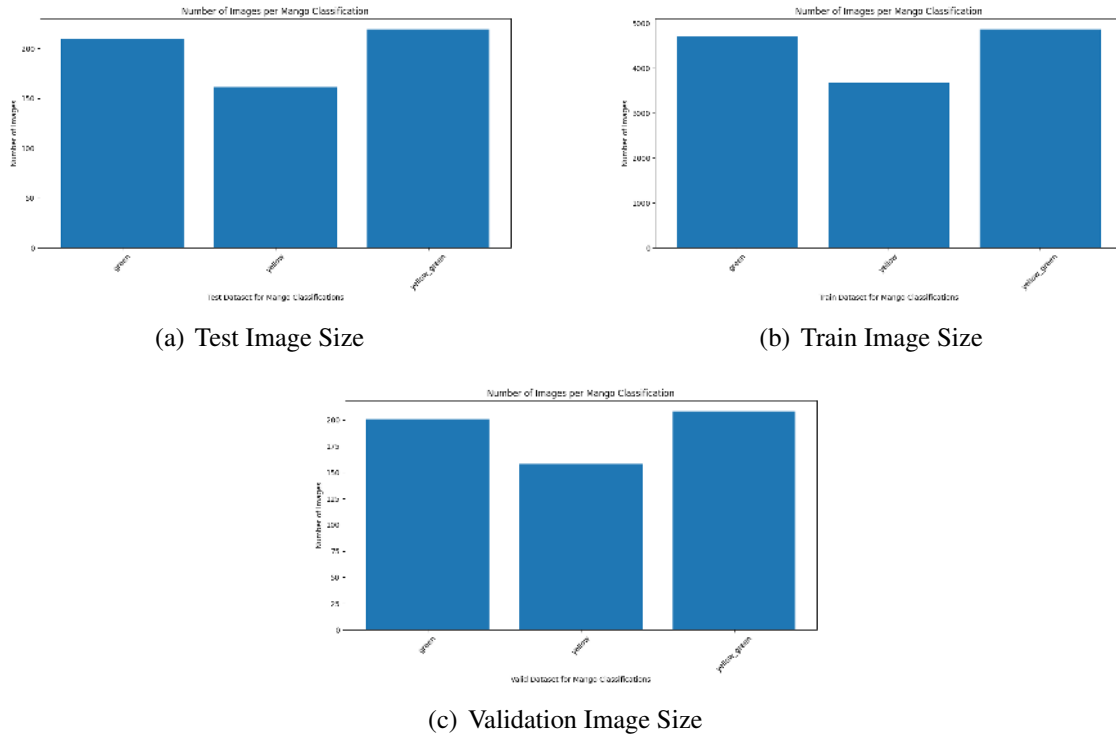


Fig. 5.9 Ripeness Image Datasplit

1490 mango classification.

#### 1491 5.6.4.1 Confusion Matrix

1492 A confusion matrix is a table that visualizes the performance of a classification model. For  
1493 a binary classification problem, it has four components:

	Predicted Positive	Predicted Negative
Actual Positive	TP	FN
Actual Negative	FP	TN

TABLE 5.2 CONFUSION MATRIX EXAMPLE



- 1495     • True Positives (TP): Cases correctly predicted as positive
- 1496     • True Negatives (TN): Cases correctly predicted as negative
- 1497     • False Positives (FP): Cases incorrectly predicted as positive. (Type I error)
- 1498     • False Negatives (FN): Cases incorrectly predicted as negative (Type II error)

#### 1499     **5.6.4.2 Precision**

$$\text{Precision} = \frac{TP}{TP + FP} \quad (5.1)$$

1500     Precision measures how many of the predicted positives are actually positive. It answers  
 1501     the question: "When the model predicts the positive class, how often is it correct?" High  
 1502     precision means low false positives.

#### 1503     **5.6.4.3 Recall**

$$\text{Recall} = \frac{TP}{TP + FN} \quad (5.2)$$

1504     Recall, which is also called sensitivity, measures how many of the actual positives were  
 1505     correctly identified. It answers the question: "Of all the actual positive cases, how many  
 1506     did the model catch?" High recall means low false negatives.

#### 1507     **5.6.4.4 F1 Score**

$$F_1 = 2 \times \frac{\text{Precision} \times \text{Recall}}{\text{Precision} + \text{Recall}} \quad (5.3)$$

1508     The F1 score is the harmonic mean of precision and recall. It provides a single metric  
 1509     that balances both concerns. This is particularly useful when you need to find a balance  
 1510     between precision and recall, as optimizing for one often decreases the other.



1511    **5.6.4.5 Accuracy**

$$\text{Accuracy} = \frac{TP + TN}{TP + TN + FP + FN} \quad (5.4)$$

1512    Accuracy measures the proportion of correct predictions (both true positives and true  
 1513    negatives) among the total cases. While intuitive, accuracy can be misleading with imbal-  
 1514    anced datasets.

1515    To test system performance, various measures of performance are used to evaluate.  
 1516    As seen on equation 5.4, accuracy score is used to measure the percentage of correctly  
 1517    classified mangoes to ensure the system maintains high precision levels. Precision as seen  
 1518    on equation 5.1 and recall as seen on equation 5.2 are used to measure consistency of  
 1519    classification to determine if the system classifies different ripeness levels and defects  
 1520    correctly. Furthermore, the F1 score formula as seen on equation 5.3 is used to evaluate the  
 1521    performance of the model's classification.

1522    A confusion matrix is used to measure correct and incorrect classification to ensure the  
 1523    machine learning model is optimized and that minimum errors are achieved. Throughput  
 1524    analysis is also used to determine the rate and efficiency of sorting to ensure that the  
 1525    system maintains high capacity without bottlenecks to sort mangoes. Using these methods  
 1526    of testing, the system is constantly optimized to ensure high-quality and reliable mango  
 1527    classification.

1528    **5.6.5 Ripeness Training and Testing**

1529    For the testing of the ripeness classification, the Carabao mangoes are classified into three  
 1530    ripeness stages which are Green, green yellow, and yellow. Likewise, The green would  
 1531    represent the underripe mangoes while the green yellow would represent the semi ripe



1532 while the yellow would represent the ripe mangoes. In other words green is underripe,  
 1533 yellow is ripe, and yellow green is semi ripe mangoes. As reference, Figure 5.10 shows the  
 1534 different ripeness stages for Carabao/Pico mangoes Bureau of Agriculture and Fisheries  
 1535 Product Standards (2004).

#### Annex A

##### Stages of ripeness of 'carabao' and 'pico' mango fruits

Stage of ripeness	Peel color	Flesh color
Green	Completely light green	Yellowish white or light yellow green
Breaker	Traces of yellow	Middle area and fruit outline yellowish; other areas, white to yellowish white
Turning	More green than yellow	More yellow than white
Semi-ripe	More yellow than green	Yellow for 'carabao'; yellow orange for 'pico'
Ripe	80-100% yellow ('carabao') or yellow orange ('pico')	Middle area yellow for 'carabao'; yellow orange for 'pico'
Overripe	Yellow for 'carabao'; yellow orange for 'pico'	100% yellow for 'carabao' and yellow orange for 'pico'

Fig. 5.10 Carabao Mango Ripeness Stages (Bureau of Agriculture and Fisheries Product Standards, 2004)

#### 5.6.5.1 Green

The first classification the researchers selected is the Green stage where the mango's skin and cheek color is completely light green with no traces of yellow.

#### 5.6.5.2 Yellow\_Green

The second classification is the Yellow\_Green or Green\_Yellow. The main characteristics of this is that it follows the breaker, turning, and semi-ripe stage of the carabao mango. This



1542 means that if there is a trace of yellow and green on the skin and cheek of the mango then  
 1543 it is classified as Yellow\_Green or Green\_Yellow.

1544 **5.6.5.3 Yellow**

1545 The third and last classification is the Yellow stage where the mango is 80% to 100% yellow  
 1546 on the skin and cheek of the mango. Note that if the mango is overripe then it would be  
 1547 classified to be Yellow for ripeness.

1548 **5.6.6 Bruises Training and Testing**

1549 For the testing of the bruise classification of the Carabao mangoes, it would classified into  
 1550 two categories which are bruised and not bruised. To define what bruise and not bruise  
 1551 mangoes looked like Figure 5.11 is used as reference to categorize which mangoes are  
 1552 bruised and not bruised. This means that if the mango has any of these features are shown  
 on the mango then it is considered as bruised.

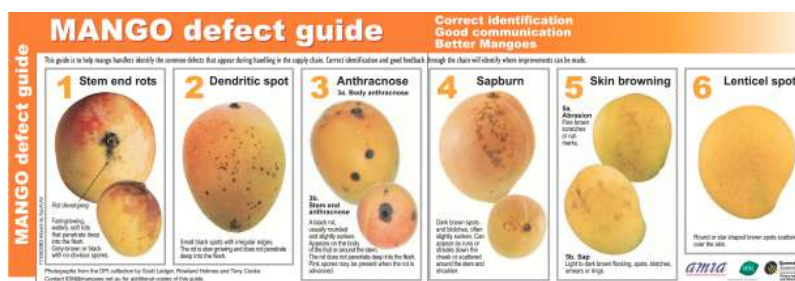


Fig. 5.11 Different Kinds of Mango Defects (Scott Ledger and Cooke, 2000)

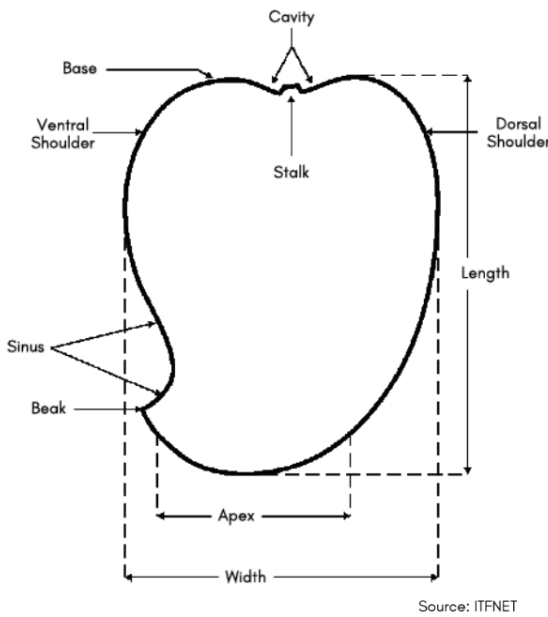
1553



1554	<b>5.6.6.1 Stem End Rots</b>
1555	They are characterized by fast-growing, watery, soft rots that penetrate deeply into the flesh.
1556	Likewise, they usually appear as grey-brown or black rots starting from the stem end,
1557	often without obvious spores, that can spread rapidly into the mango (de Souza-Pollo and
1558	de Goes, 2009; Kadam et al., 2002).
1559	<b>5.6.6.2 Dendritic Spot</b>
1560	They are small black spots with irregular edges scattered across the skin. Furthermore, they
1561	grow slowly and do not penetrate into the flesh, remaining largely superficial (Ltd, 2007).
1562	<b>5.6.6.3 Anthracnose</b>
1563	It appears in two forms. First form is body anthracnose. Body anthracnose presents as black
1564	rots on the fruit surface that are usually round, slightly sunken, and located on different
1565	parts of the mango. Likewise, the second form is stem end anthracnose, occurring around
1566	the stem and also presenting as black rots. While these rots do not penetrate deeply into the
1567	flesh, advanced cases may show pink spores (de Souza-Pollo and de Goes, 2009; Kadam
1568	et al., 2002).
1569	<b>5.6.6.4 Sapburn</b>
1570	They appear as dark brown spots or blotches that are often slightly sunken. Likewise,
1571	damage can occur as runs or streaks down the cheek or as scattered marks around the stem
1572	and shoulder, resulting from sap exposure (Paul, 1993).



1573	<b>5.6.6.5 Skin Browning</b>
1574	It may take two forms. The first form is abrasion while the second form is sap browning.
1575	Abrasions are recognized as fine brown scratches or rub marks, while sap-related browning
1576	appears as light to dark brown flecking, spots, blotches, smears, or rings. These types of
1577	browning are generally limited to the skin and do not penetrate deeply (Paul, 1993).
1578	<b>5.6.6.6 Lenticel Spot</b>
1579	They are another common defect, appearing as round or star-shaped brown spots scattered
1580	across the skin surface. Furthermore, these defects are usually cosmetic in nature and do
1581	not significantly affect the flesh (Nguyen, 2015).
1582	<b>5.6.7 Size Determination</b>
1583	To get the size of the mango, computer vision techniques such as Gaussian Blur and
1584	Thresholding are used to get the length and width of the mangoes. Refer to Figure 5.12 for
1585	the location of the length and width of mango.
1586	<b>5.6.7.1 Real World Dimensions</b>
1587	For the real world dimensions method of getting the length and width of the mango a
1588	foreground masking is generated by getting absolute difference between the foreground,
1589	that is the mango, and the background. Furthermore, image augmentation techniques such
1590	as Gaussian blur, grayscale, and Canny edge detection are used. After that, the largest
1591	contour on the foreground masking image is used. Once the largest contour is found then
1592	the length and width is calculated using Equation 3.2.



Parts of a mango fruit

Fig. 5.12 Length and Width of Mango (Bureau of Agriculture and Fisheries Product Standards, 2006)

### 1593 5.6.7.2 Object Detection

1594 For the object detection method, an annotated Carabao mango dataset containing 488  
1595 images were used. Likewise, the pretrained Faster R-CNN model used is the MobileNetV3.



Fig. 5.13 Annotated Mango Image Dataset



1596     **5.6.7.3 Calibration by Getting the Pixels per cm**

1597     To get the accurate length and width of a mango the pixel-to-centimeter ratio of an image  
 1598     using a reference object, such as a coin, with a known real-world size. As seen on Listing 5.2,  
 1599     it takes the bounding box coordinates of the reference object (which is a Philippine 1 peso  
 1600     coin) and computes its width and height in pixels. Since the reference object may not be  
 1601     perfectly square, the larger of these two values is selected as the effective reference size  
 1602     (of the coin) in pixels. Using the known physical size of the coin in cm, the function then  
 1603     calculates how many pixels correspond to one centimeter. This means that if a coin of  
 1604     known diameter appears in the image, the function determines the relationship between  
 1605     its pixel size and real-world measurement to establish a scale. Once this scale is set, the  
 1606     mango image can be measured accurately by comparing its pixel size to the calibrated ratio.

1607     **5.7 Mango Formula with User Priority**

1608     The linear equation used to calculate the Carabao mango grade is shown below. Likewise,  
 1609     the variables  $B(P)$ ,  $R(P)$ , and  $S(P)$  represent the user-defined priority weightings for  
 1610     bruising, ripeness, and size characteristics in the User Priority-Based Grading system.  
 1611     Additionally,  $b(p)$ ,  $r(p)$ , and  $s(p)$  correspond to the machine learning model's predicted  
 1612     values for the bruising, ripeness, and size attributes of the Carabao mango.

$$\text{Mango Grade} = b(P)B(P) + r(P)R(P) + s(P)S(P) \quad (5.5)$$

1613     The machine learning predictions are assigned the following numerical values:



1614	<b>Ripeness Scores:</b>	$r(\text{yellow}) = 1.0$ (5.6)
		(5.6)
	$r(\text{yellow green}) = 2.0$	(5.7)
		(5.7)
	$r(\text{green}) = 3.0$	(5.8)
1615	<b>Bruises Scores:</b>	$b(\text{bruised}) = 1.0$ (5.9)
		(5.9)
	$b(\text{not bruised}) = 2.0$	(5.10)
1616	<b>Size Scores:</b>	$s(\text{small}) = 1.0$ (5.11)
		(5.11)
	$s(\text{medium}) = 2.0$	(5.12)
	$s(\text{large}) = 3.0$	(5.13)
1617	Note that the scores value for each respective classification cannot be changed by the	
1618	user without changing the code itself. This means that only the weight of either the ripeness,	
1619	bruises, and size can be changed to either low, high, or remove it by setting it to zero.	
1620	Furthermore, only real numbers are allowed to be inputted as a weight. This means that	
1621	negative and imaginary numbers are not considered in Equation 5.5.	
1622	<h2>5.8 Summary</h2>	
1623	This chapter details the methodology for developing an automated Carabao mango grad-	
1624	ing and sorting system integrating machine learning and computer vision. The research	



# De La Salle University

1625 employed an experimental approach managed via Scrum agile methodology to iteratively  
1626 develop and test the hardware and software components. The hardware design features a  
1627 conveyor belt system, an image acquisition setup with controlled lighting, and a RPi micro-  
1628 controller coordinating DC motors and sorting actuators. The software, built with Python  
1629 and PyTorch, utilizes a custom-trained CNN for classification. The core machine learning  
1630 pipeline involved extensive comparative testing of architectures, including EfficientNet,  
1631 VGGNet, and ResNet, with EfficientNetV2-B3 ultimately selected for its optimal balance  
1632 of accuracy and efficiency.

1633 A significant focus was placed on data collection and optimization. A custom dataset  
1634 of Carabao mangoes was created by capturing video of individual fruits and extracting  
1635 frames, which were then sorted into categories for ripeness (green, yellow-green, yellow)  
1636 and bruises (bruised, not bruised). The dataset was split 70-15-15 for training, validation,  
1637 and testing, with aggressive data augmentation (rotation, flipping, blur) applied only to the  
1638 training set to improve model generalization. The training process incorporated several  
1639 advanced optimizations: the AdamW optimizer for better generalization, mixed-precision  
1640 training to accelerate computation, data loading and transfer optimizations to prevent  
1641 bottlenecks, and regularization techniques like dropout and label smoothing to combat  
1642 overfitting. A cosine annealing learning rate scheduler and early stopping were also  
1643 implemented to ensure stable convergence.

1644 For system evaluation, the methodology defined specific testing protocols for each  
1645 attribute. Ripeness was classified into three visually distinct stages, while bruise detection  
1646 was trained to identify defects like stem end rot and anthracnose based on a standard defect  
1647 guide. Two methods for size determination were developed and compared: a traditional  
1648 computer vision approach using foreground masking and thresholding, and a more robust



# De La Salle University

1649 object detection method using a Faster R-CNN model trained on 488 annotated mango  
1650 images. A key innovation is the user-priority formula, a weighted equation that allows users  
1651 to customize the importance of ripeness, bruises, and size in the final grade (A, B, or C).  
1652



Listing 5.1: Datasplit Logs

```

1 Class Mapping:
2 -----
3 green      -> ripeness/green
4 yellow     -> ripeness/yellow
5 yellow_green -> ripeness/yellow_green
6 bruised    -> bruises/bruised
7 unbruised  -> bruises/not_bruised
8 Splitting dataset into hierarchical structure...
9 Processing green -> ripeness/green
10 Train: 1225, Val: 262, Test: 263
11 Processing yellow -> ripeness/yellow
12 Train: 616, Val: 132, Test: 132
13 Processing yellow_green -> ripeness/yellow_green
14 Train: 935, Val: 200, Test: 201
15 Processing bruised -> bruises/bruised
16 Train: 1363, Val: 292, Test: 293
17 Processing unbruised -> bruises/not_bruised
18 Train: 1143, Val: 245, Test: 246
19 Applying massive augmentation to generate 10000 additional images...
20 Total augmentation combinations available: 309
21 Original training images: 6832
22 Total augmented images created: 13664
23 Target was: 10000
24
25 Dataset Statistics:
26 =====
27
28 RIPENESS Category:
29 -----
30 green      - Train: 7830, Val: 488, Test: 478
31 yellow     - Train: 4010, Val: 242, Test: 248
32 yellow_green - Train: 6130, Val: 376, Test: 376
33 Subtotal   - Train: 17970, Val: 1106, Test: 1102
34
35 BRUISES Category:
36 -----
37 bruised    - Train: 8820, Val: 526, Test: 538
38 not_bruised - Train: 7370, Val: 446, Test: 450
39 Subtotal   - Train: 16190, Val: 972, Test: 988
40
41 =====
42 TOTAL      - Train: 34160, Val: 2078, Test: 2090
43 Ratios     - Train: 89.1%, Val: 5.4%, Test: 5.5%
44
45 Dataset processing complete! Output saved to: E:\dir
46
47 =====

```



Listing 5.2: Calibration of Reference Philippine Coin

```
1 def calibrate_with_reference_object(self, image, reference_box,
2     reference_size_cm):
3     x1, y1, x2, y2 = reference_box
4
5     # Calculate reference object dimensions in pixels
6     ref_width_pixels = x2 - x1
7     ref_height_pixels = y2 - y1
8
9     # Use the max dimension for calibration
10    ref_size_pixels = max(ref_width_pixels, ref_height_pixels)
11
12    # Calculate pixels per cm
13    self.pixels_per_cm = ref_size_pixels / reference_size_cm
14    self.reference_object_size_cm = reference_size_cm
15
16    print(f"Reference object: {reference_size_cm} cm")
17    print(f"Reference pixels: {ref_size_pixels:.1f} pixels")
18    print(f"Scale: {self.pixels_per_cm:.2f} pixels/cm")
19
20    return self.pixels_per_cm
```



1653

## Chapter 6

1654

# RESULTS AND DISCUSSIONS



TABLE 6.1 SUMMARY OF METHODS FOR ACHIEVING THE OBJECTIVES

Objectives	Methods	Locations
GO: To develop a user-priority-based grading and sorting system for Carabao mangoes, using machine learning and computer vision techniques to assess ripeness, size, and bruises.	<p>Results:</p> <ul style="list-style-type: none"> <li>1. Successfully developed a user-priority-based grading and sorting system using machine learning and computer vision which can assess the mangoes' ripeness, size and bruises.</li> </ul>	Sec. 6.8 on p. 152
SO1: To make an image acquisition system with a conveyor belt for automatic sorting and grading mangoes.	<p>Results:</p> <ul style="list-style-type: none"> <li>1. Successfully integrated a conveyor belt with the image acquisition in order to achieve efficient flow of automated sorting and grading of the mangoes.</li> <li>2. Successfully integrated LED strips to provide optimal lighting for image capturing of the mangoes.</li> <li>3. Successfully fixed the hardware components in place</li> </ul>	Sec. 6.6 on p. 142
SO2: To get the precision, recall, F1 score, confusion matrix, and train and test accuracy metrics for classifying the ripeness and bruises with an accuracy score of at least 90%.	<p>Results:</p> <ul style="list-style-type: none"> <li>1. Successfully achieved 98% overall accuracy for ripeness classification of Carabao mangoes</li> <li>2. Successfully achieved 99% overall accuracy for bruises classification of Carabao mangoes</li> </ul>	Sec. 6.1 on p. 94

*Continued on next page*

## 6. Results and Discussions



# De La Salle University

*Continued from previous page*

Objectives	Methods	Locations
SO3: To create a microcontroller-based system to operate the image acquisition system, control the conveyor belt, and process the mango images through machine learning.	<p>Results:</p> <ul style="list-style-type: none"> <li>1. Successfully made a conveyor belt system to move the mangoes through the image acquisition system to the sorting system</li> <li>2. Successfully mounted the image acquisition system on the prototype</li> <li>3. Successfully made the frame for the conveyor belt and image acquisition system to sit on</li> </ul>	Sec. 6.6 on p. 142
SO4: To grade mangoes based on user priorities for size, ripeness, and bruises.	<p>Results:</p> <ul style="list-style-type: none"> <li>1. Successfully grade mangoes based on the user priorities on the physical characteristics of the mango</li> <li>2. Successfully verified with qualified individual the results</li> <li>3. Successfully utilize the weighted equation to evaluate mango grade based on user priorities</li> </ul>	Sec. 6.5 on p. 138
SO5: To classify mango ripeness based on image data using machine learning algorithms such as kNN, k-mean, and Naïve Bayes.	<p>Results:</p> <ul style="list-style-type: none"> <li>1. Successfully trained a CNN model using EfficientNetV2 and Adam Optimizer for ripeness</li> <li>2. Achieved 98% accuracy on performance metrics using EfficientNetV2</li> <li>3. Obtain performance metrics for KNN, K-Mean, and Naive Bayes methods for comparison and show the superior performance of using CNN</li> <li>4. Successfully fine tuned the CNN model to achieve the highest accuracy possible, choosing the best performing model, and testing other CNN hyperparameters</li> </ul>	Sec. 6.1.1 on p. 94

*Continued on next page*



*Continued from previous page*

Objectives	Methods	Locations
SO6: To classify mango size based on image data by getting its length and width using OpenCV, geometry, and image processing techniques.	<p>Results:</p> <ul style="list-style-type: none"> <li>1. Compared and tested two methods, which are the foreground masking then thresholding and Object Detection, to measure the length and width of the Carabao mangoes</li> <li>2. Version 1, which is the foreground masking then thresholding, has a 12.04% and 3.24% percent difference to the ground truth for length and width.</li> <li>3. Version 2, which is the Object Detection, has a 13.57% and 3.24% percent difference to the ground truth for the length and width.</li> </ul>	Sec. 6.4 on p. 129
SO7: To classify mango bruises based on image data by employing machine learning algorithms.	<p>Results:</p> <ul style="list-style-type: none"> <li>1. Successfully trained a CNN model using EfficientNetV2 and Adam Optimizer for bruises</li> <li>2. Achieved 99% accuracy on performance metrics</li> <li>3. Successfully fine tuned the CNN model to achieve the highest accuracy possible, choosing the best performing, and testing other CNN hyperparameters</li> </ul>	Sec. 6.1.2 on p. 102

## 1655 6.1 Training and Testing Results of the Model

### 1656 6.1.1 Ripeness Classification Results

#### 1657 6.1.1.1 Naive Bayes

1658 Based on the evaluation metrics, the Naive Bayes model demonstrates a clear strength in  
 1659 identifying ripe, yellow mangoes but reveals a significant weakness in classifying those in



# De La Salle University

1660 the transitional yellow-green stage. The model's precision scores for the green and yellow  
 1661 classes are reasonably similar at around 79%. However, its performance drops considerably  
 1662 for the yellow-green class, where a precision of just 58% nearly half of its predictions for  
 1663 this category are incorrect. This pattern is reinforced by the recall scores. The model excels  
 1664 at finding true yellow mangoes, capturing 86% of them, which is its highest performance  
 1665 metric. Conversely, it struggles to identify yellow-green mangoes, with a recall of only  
 1666 51%, meaning it misses almost half of all true instances of this class. The F1-score, which  
 1667 balances precision and recall, provides summary of this performance, yielding a strong  
 1668 score of 80% for yellow but a very poor score of 55% for yellow-green. This confirms that  
 1669 the transitional yellow-green stage is the model's primary source of confusion, likely due  
 1670 to its visual ambiguity, sharing features with both the green and ripe yellow classes.

	Precision	Recall	F1	Support
Green	0.78	0.79	0.78	132
Yellow	0.75	0.86	0.80	66
Yellow_Green	0.58	0.51	0.55	101
Accuracy			0.71	299
Macro Avg	0.70	0.72	0.71	299
Weighted Avg	0.71	0.71	0.71	299

TABLE 6.2 RIPENESS CLASSIFICATION REPORT USING NAIVE BAYES

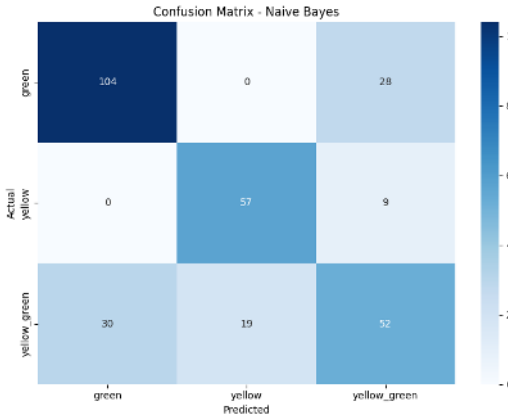


Fig. 6.1 Ripeness Confusion Matrix using Naive Bayes

### 6.1.1.2 KMeans

The KMeans model achieved a weak overall accuracy of 57%, with its performance characterized by a severe precision-recall trade-off across classes and a fundamental failure to identify the transitional stage. The model exhibited high recall for Green with score of 80% but low precision of 57%, which indicates that it captured most green mangoes but also frequently misclassified others as green. It was the opposite for Yellow, where high precision score of 83% and a low recall score of 52%, meaning its yellow predictions were reliable but it missed nearly half of them. Most critically, performance on the Yellow Green class was exceptionally poor with a F1 score of 34%, the model struggled both to correctly label them and to find them at all, this reveals that the clusters formed by KMeans are poorly separated for this specific ripeness classification task.

### 6.1.1.3 KNN

K-Nearest Neighbors (KNN) model demonstrates an improvement in performance, achieving an overall accuracy of 78%. Unlike previous models, KNN shows a strong and



	Precision	Recall	F1	Support
Green	0.57	0.80	0.67	132
Yellow	0.83	0.52	0.64	66
Yellow_Green	0.41	0.30	0.34	101
Accuracy			0.57	299
Macro Avg	0.60	0.54	0.55	299
Weighted Avg	0.57	0.57	0.55	299

TABLE 6.3 RIPENESS CLASSIFICATION REPORT USING KMEANS

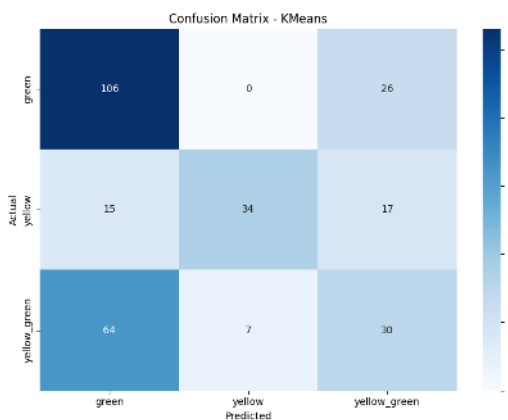


Fig. 6.2 Ripeness Confusion Matrix using KMeans

1685 consistent balance between precision and recall across all three ripeness classes. The  
 1686 model excels at classifying the fully Green and Yellow stages, with high and well-balanced  
 1687 F1-scores of 0.85 and 0.81, respectively, indicating it is more reliable when making a  
 1688 prediction and effective at identifying all instances of these classes than previous models.  
 1689 KNN also shows improvement in handling the yellow-green class, achieving an F1-score  
 1690 of 68%. While this remains the most challenging class, the model's significantly higher  
 1691 scores compared to previous attempts confirm its ability to learn the distinguishing features  
 1692 between the stages.



	Precision	Recall	F1	Support
Green	0.85	0.85	0.85	132
Yellow	0.83	0.79	0.81	66
Yellow_Green	0.67	0.69	0.68	101
Accuracy			0.78	299
Macro Avg	0.78	0.78	0.78	299
Weighted Avg	0.78	0.78	0.78	299

TABLE 6.4 RIPENESS CLASSIFICATION REPORT USING KNN

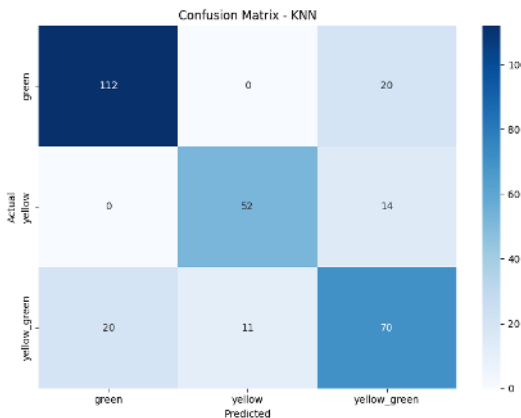


Fig. 6.3 Ripeness Confusion Matrix using KNN

#### 6.1.1.4 CNN

The final CNN model for ripeness and bruise classification utilized EfficientNetV2-B3. Collected experimental data confirmed that it achieved the best performance-to-efficiency ratio. It consistently outperformed other architectures tested during benchmarking and optimization stages. For the final ripeness classification, the complete dataset contained around 14,000 images. The model achieved a test accuracy of 98%, with precision, recall, and F1-score near 0.985. This consistency across metrics demonstrates both high accuracy and class-balanced reliability. It performed uniformly across all ripeness categories without favoring any particular class. Validation accuracy of 98.41% closely matched the test



# De La Salle University

accuracy, confirming excellent generalization. The slightly higher training accuracy of 99.37% indicated minimal overfitting occurrence. The narrow gap between training, validation, and test results reflected stable learning. These findings confirm that dataset refinement and optimization prevented memorization effectively. They also promoted genuine feature learning across ripeness categories and lighting variations.

The confusion matrix in Figure 6.4 further supports these conclusions clearly. Misclassifications were minimal and occurred mostly between adjacent ripeness categories. Errors were concentrated between transitional stages such as yellow-green and yellow mangoes. This pattern matches the biological ambiguity seen during mango ripening transitions. Even human evaluators sometimes disagree on borderline ripeness due to visual overlap. The model's strong accuracy in these ambiguous cases reflects superior discriminative ability. It demonstrates practical reliability for deployment in real-world mango grading systems.

Several major modifications to the training pipeline improved overall model effectiveness significantly. Mixed-precision training using GradScaler and autocast reduced GPU memory consumption substantially. This optimization increased batch size from 32 to 56, enhancing training stability. Larger batch sizes improved gradient estimation and smoothed convergence across training epochs. Input resolution was corrected to 300×300, matching EfficientNetV2-B3's native architecture. This adjustment improved feature extraction and ensured compatibility with pretrained weights. The optimizer was changed from Adam to Adam with Decoupled Weight Decay (AdamW) for stronger regularization. Learning rate was set to 3e-4, and weight decay to 1e-4. These parameters decoupled regularization from gradient updates, ensuring stable convergence behavior. A cosine annealing warm-restart scheduler with T0 = 5 and Tmult = 2 was applied. It included three warm-up epochs to escape sharp minima effectively during training.



# De La Salle University

1726 Additional refinements further improved training robustness and model generaliza-  
1727 tion performance. CrossEntropy loss with label smoothing of 0.05 reduced overconfident  
1728 predictions. This adjustment improved resilience to ambiguous ripeness categories and  
1729 noisy image labels. Early stopping with a patience of five epochs prevented redundant  
1730 computation cycles. Checkpointing saved the best weights once performance improvements  
1731 plateaued consistently. Data loading was optimized with workers set to half of available  
1732 CPU cores. Pin\_memory and non\_blocking transfers accelerated CPU-to-GPU data stream-  
1733 ing throughput. These optimizations minimized data bottlenecks and reduced idle GPU  
1734 computation time. Regularization through dropout = 0.25 and drop-path = 0.15 improved  
1735 network robustness. These techniques prevented neuron co-adaptation and encouraged  
1736 diverse feature representations.

1737 The validation curves in Figure 6.5 confirm stable convergence throughout training. Val-  
1738 iduation accuracy increased steadily before plateauing at a consistently high level. Validation  
1739 loss showed minor oscillations but followed an overall downward trajectory. This inverse  
1740 relationship between loss and accuracy indicates strong discriminative learning ability.  
1741 Accuracy stability despite small loss fluctuations shows resistance to overfitting. These pat-  
1742 terns confirm that optimizations such as label smoothing and annealing worked effectively.  
1743 The model maintained robustness and generalization even in complex visual conditions. Its  
1744 smooth convergence underscores training stability and computational efficiency across all  
1745 epochs.

1746 Lastly, dataset enhancements contributed substantially to achieving these superior  
1747 results overall. The dataset expanded from approximately 6,000 to 14,000 well-curated  
1748 mango images. New Carabao mango samples were added, improving variety and biological  
1749 representativeness. Ambiguous or noisy samples were removed to reduce label uncertainty



# De La Salle University

1750 significantly. Augmentation strategies were refined to introduce meaningful color, rotation,  
 1751 and lighting diversity. These augmentations enhanced robustness by exposing the network to  
 1752 realistic visual variations. As a result, the final model generalized strongly and maintained  
 1753 stable performance. Across all dataset splits, it demonstrated consistent accuracy and  
 1754 balanced classification reliability.

	Precision	Recall	F1	Support
Green	0.98	0.99	0.99	210
Yellow	0.99	0.99	0.99	161
Yellow_Green	0.98	0.98	0.98	219
Accuracy			0.98	590
Macro Avg	0.99	0.99	0.99	590
Weighted Avg	0.98	0.98	0.98	590

TABLE 6.5 EFFICIENTNETV2-B3 RIPENESS CLASSIFICATION REPORT WITH  
 PRECISION: 0.9848, RECALL: 0.9847, F1 SCORE: 0.9847

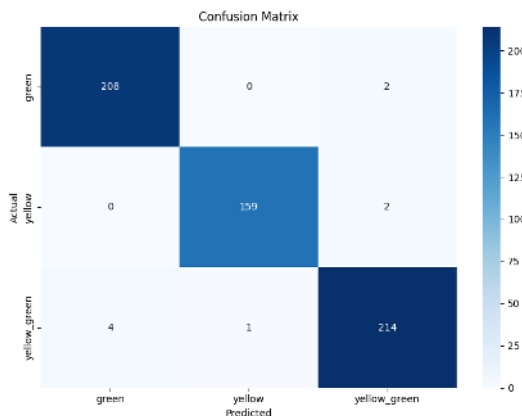


Fig. 6.4 EfficientNetV2-B3 Ripeness Confusion Matrix

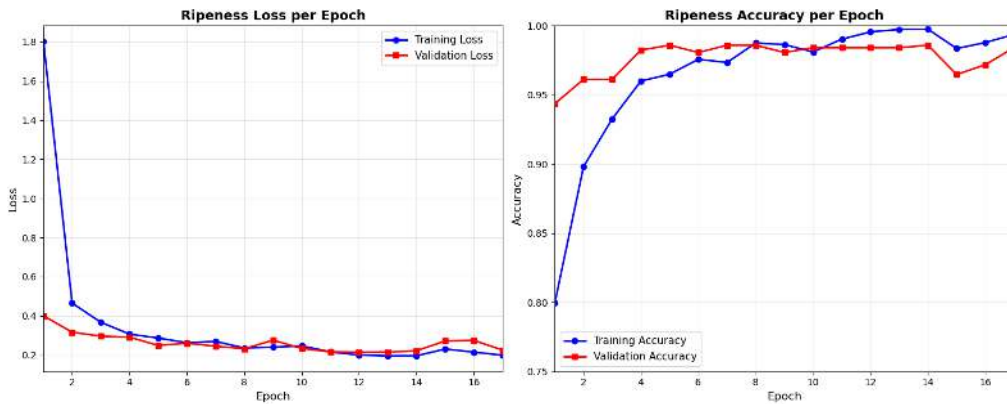


Fig. 6.5 EfficientNetV2-B3 Ripeness Accuracy and Loss Graph

### 6.1.2 Bruises Classification Results

#### 6.1.2.1 CNN

For bruise classification, the final EfficientNetV2-B3 model also performed excellently. It achieved a test accuracy of 99%, with precision, recall, and F1-score near 0.989. The validation accuracy of 99.31% and training accuracy of 99.86% confirmed stability. These results demonstrate exceptional reliability and consistent performance across all dataset splits. The training configuration was refined to improve both computational efficiency and robustness. Batch size was increased to 60, fully utilizing available GPU memory capacity. This adjustment enhanced gradient stability and accelerated convergence across training epochs effectively. Regularization parameters were tuned with a dropout rate of 0.2 overall. A drop-path rate of 0.1 was also applied to further control overfitting. Together, these settings balanced high predictive accuracy with improved model generalization capability. Early stopping with a patience of 10 epochs was employed during training. This ensured meaningful improvement capture while avoiding unnecessary computation after convergence detection.



1770 The confusion matrix in Figure 6.6 reinforces these excellent quantitative results clearly.  
1771 The model correctly identified nearly all samples across both bruise categories tested. Only  
1772 four false negatives and one false positive occurred in total predictions. This minimal error  
1773 distribution illustrates a well-balanced and highly reliable classification profile. The model  
1774 demonstrated strong sensitivity to bruised fruit and high specificity otherwise. Low false  
1775 negatives are particularly important in postharvest quality control applications. Undetected  
1776 bruises pose a major risk to maintaining consistent product quality standards. The low occur-  
1777 rence of such cases underscores the model's robustness and precision. These characteristics  
1778 make EfficientNetV2-B3 ideal for deployment in real-time inspection systems.

1779 The validation curves in Figure 6.7 further illustrate stable training convergence be-  
1780 havior. Validation accuracy rose rapidly during initial epochs and stabilized near 0.99  
1781 overall. Meanwhile, validation loss decreased sharply early on and then gradually leveled  
1782 off. Minor fluctuations in loss reflect typical batch-level variations during optimization cy-  
1783 cles. Despite these oscillations, accuracy remained consistently high and stable throughout  
1784 training. This indicates that the network maintained strong confidence in its classification  
1785 predictions. The inverse correlation between loss and accuracy confirms effective learning  
1786 of features. These patterns demonstrate robust generalization and the absence of significant  
1787 overfitting problems. Together, the curves validate that all applied optimizations improved  
1788 convergence stability efficiently. EfficientNetV2-B3 thus combines exceptional accuracy,  
1789 reliability, and computational efficiency effectively. This performance level establishes it  
1790 as the optimal model for bruise classification. Its predictive precision makes it suitable for  
1791 industrial-grade automated quality control systems.



	Precision	Recall	F1	Support
Bruised	1.00	0.98	0.99	206
Not Bruised	0.98	1.00	0.99	234
Accuracy			0.99	440
Macro Avg	0.99	0.99	0.99	440
Weighted Avg	0.99	0.99	0.99	440

TABLE 6.6 EFFICIENTNETV2-B3 BRUISES CLASSIFICATION REPORT WITH PRECISION: 0.9887, RECALL: 0.9886, F1 SCORE: 0.9886

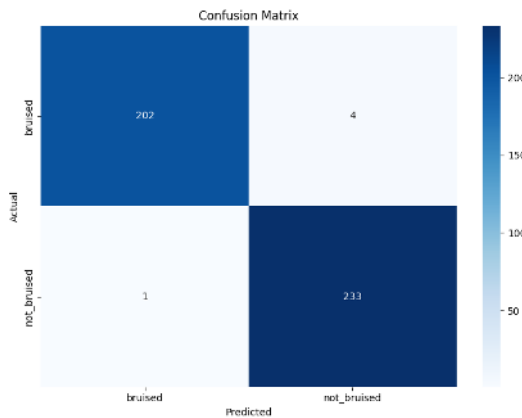


Fig. 6.6 EfficientNetV2-B3 Bruises Confusion Matrix

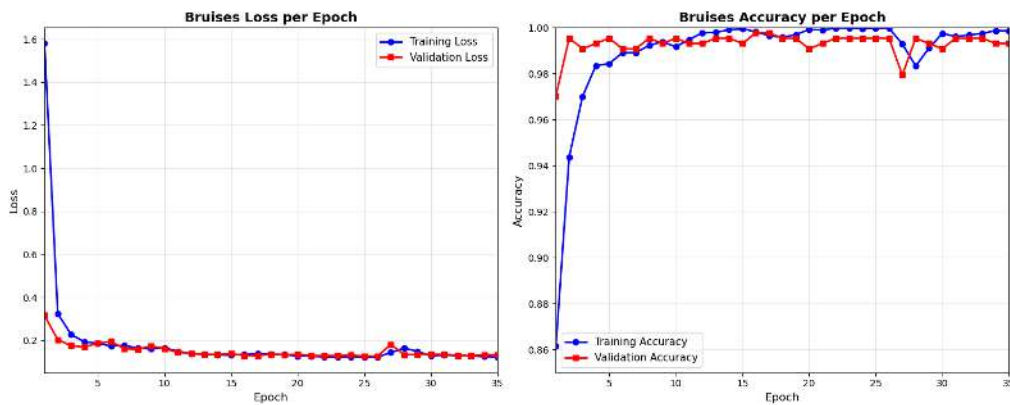


Fig. 6.7 EfficientNetV2-B3 Bruises Accuracy and Loss Graph



1792

## 6.2 Achieving the Highest Accuracy in CNN Models

Network	Prec	Rec	F1	Test Acc	Train Acc	Time	VRAM
VGG16	0.188	0.434	0.263	43	43.57	2h57m	7.0
ALEXNET	0.188	0.434	0.263	43	43.57	4h23m	2.3
RESNET50	0.870	0.869	0.868	87	89.22	7h13m	4.1
GOOGLENET	0.898	0.895	0.892	89	83.58	3h3m	2.9
MOBILENETV2	0.898	0.898	0.897	90	91.13	2h0m	3.6
DENSENET121	0.877	0.877	0.875	88	89.17	2h10m	5.5
EFFNET B0	0.890	0.888	0.887	89	91.24	2h14m	4.1
EFFNET B1	0.916	0.913	0.913	91	89.91	2h25m	5.3
EFFNET B2	0.906	0.902	0.900	90	89.46	2h26m	5.5
EFFNET B3	0.914	0.911	0.909	91	89.72	2h30m	6.8
EFFNET B4	0.899	0.898	0.896	90	92.34	2h50m	8.0
EFFNET B5	0.925	0.924	0.924	92	94.12	5h45m	11.6
EFFNET B6	0.934	0.933	0.933	93	96.03	7h12m	14.5
EFFNET B7	0.883	0.871	0.873	87	90.82	9h9m	18.8
EFFNETV2-B0	0.915	0.913	0.913	91	92.71	1h53m	3.0
EFFNETV2-B1	0.920	0.918	0.919	92	92.65	1h59m	3.7
EFFNETV2-B2	0.920	0.920	0.920	92	92.34	2h0m	3.8
EFFNETV2-B3	0.926	0.926	0.925	93	93.97	2h2m	4.5
EFFNETV2-S	0.894	0.893	0.891	89	90.47	2h17m	6.1
EFFNETV2-M	0.893	0.893	0.892	89	90.02	2h37m	9.9
EFFNETV2-L	0.875	0.871	0.870	87	89.93	13h39m	16.8
<b>AVERAGE</b>	<b>0.835</b>	<b>0.856</b>	<b>0.839</b>	<b>86</b>	<b>85.52</b>	<b>-</b>	<b>7.0</b>

TABLE 6.7 CNN TRAINING RESULTS FOR GPU

1793

““latex

### 6.2.1 Analysis of Table 6.9

1795

For the classification of ripeness, the highest accuracy was obtained with EfficientNetV2-

1796

B0, which achieved 91%. This was followed by MobileNetV2, which achieved 90%,

1797

EfficientNet-B0 and GoogLeNet at 89%, DenseNet121 at 88%, and ResNet50 at 87%. In

## 6. Results and Discussions



# De La Salle University

<b>Network</b>	<b>Prec</b>	<b>Rec</b>	<b>F1</b>	<b>Test Acc</b>	<b>Train Acc</b>	<b>Time</b>	<b>Mem</b>
VGG16	0.297	0.545	0.384	54	54.48	5h38m	6.5
ALEXNET	0.297	0.545	0.384	54	54.48	4h25m	3.3
RESNET50	0.858	0.844	0.844	84	83.92	8h24m	5.4
GOOGLENET	0.843	0.808	0.799	81	57.67	3h14m	4.0
MOBILENETV2	0.859	0.858	0.858	86	85.88	3h44m	4.8
DENSENET121	0.839	0.838	0.838	84	84.7	3h8m	6.7
EFFNET B0	0.873	0.870	0.870	87	90.04	2h37m	5.3
EFFNET B1	0.898	0.897	0.896	90	90.51	2h56m	6.7
EFFNET B2	0.901	0.901	0.901	90	91.21	3h8m	6.7
EFFNET B3	0.913	0.913	0.913	91	90.34	3h27m	8.0
EFFNET B4	0.897	0.897	0.897	90	92.16	4h17m	9.8
EFFNET B5	0.892	0.883	0.881	88	90.53	5h49m	12.2
EFFNET B6	0.884	0.883	0.882	88	90.43	7h51m	14.5
EFFNET B7	0.857	0.856	0.856	86	90.47	10h34m	18.0
EFFNETV2-B0	0.880	0.879	0.878	88	90.69	2h6m	4.4
EFFNETV2-B1	0.893	0.893	0.893	89	91.72	2h32m	5.1
EFFNETV2-B2	0.904	0.889	0.889	89	88.16	2h45m	5.4
EFFNETV2-B3	0.919	0.919	0.919	92	94.46	2h55m	6.2
EFFNETV2-S	0.859	0.858	0.858	86	86.58	2h58m	7.7
EFFNETV2-M	0.856	0.846	0.846	85	84.74	3h30m	9.3
EFFNETV2-L	0.849	0.836	0.836	84	85.05	14h58m	17.9
<b>AVERAGE</b>	<b>0.822</b>	<b>0.841</b>	<b>0.825</b>	<b>84.10</b>	-	-	<b>8.0</b>

TABLE 6.8 CNN BRUISES RESULTS FOR CPU

Model	Accuracy	
	Ripeness	Bruises
EfficientNetB0	89%	87%
EfficientNetB2	92%	90%
VggNet16	43%	54%
AlexNet	43%	54%
Residual Network (ResNet)50	87%	84%
GoogleNet	89%	81%
MobileNetV2	90%	86%
DenseNet121	88%	84%

TABLE 6.9 ACCURACY OF DIFFERENT CNN MODELS



	Test Accuracy	
EfficientNet	Ripeness	Bruises
B0	89%	87%
B1	86%	90%
B2	92%	90%
B3	88%	91%
B4	90%	90%
B5	92%	88%
B6	93%	88%
V2B0	91%	88%
V2B1	92%	89%
V2B2	92%	89%
V2B3	93%	92%
V2-S	89%	86%
V2-M	89%	85%
V2-L	89%	84%

TABLE 6.10 TEST ACCURACY OF DIFFERENT EFFICIENTNET VERSION 1 AND 2

1798 contrast, both VGGNet16 and AlexNet severely underperformed, each reaching only 43%  
 1799 accuracy. A closer inspection of their classification reports revealed that these two models  
 1800 predicted only the green class across all test samples, completely failing to recognize  
 1801 yellow and yellow-green. This explains why their accuracy plateaued at 43%, a value that  
 1802 directly corresponds to the proportion of green samples in the dataset. The collapse into a  
 1803 single-class prediction highlights the limitations of these older architectures: AlexNet and  
 1804 VGGNet16 lack the advanced feature extraction and efficient feature reuse mechanisms  
 1805 present in modern CNNs, making them less capable of capturing the subtle hue and  
 1806 texture variations that distinguish ripeness stages (Krizhevsky et al., 2012) (Simonyan and  
 1807 Zisserman, 2015). AlexNet, while revolutionary in 2012, was designed for large-scale  
 1808 but relatively coarse ImageNet classification and relies on shallow convolutional layers  
 1809 with large receptive fields, which limits its ability to capture fine-grained differences.



# De La Salle University

1810 Similarly, VGGNet16, though deeper, uses very uniform  $3 \times 3$  convolutions without skip  
1811 connections or dense connectivity, leading to redundancy and inefficient feature reuse,  
1812 which modern architectures have since addressed. Furthermore, the training setup and  
1813 hyperparameters, which favored faster convergence in lightweight and well-optimized  
1814 models such as MobileNetV2 and EfficientNet (Howard et al., 2017) (Tan and Le, 2019), did  
1815 not provide the same benefit to AlexNet and VGGNet16 (Huang et al., 2017). Importantly,  
1816 the train accuracy values further reinforce these findings where modern architectures  
1817 such as EfficientNetV2-B3 (93% train, 93% test) and EfficientNet-B6 (96% train, 93%  
1818 test) maintained close alignment between training and test performance, indicating strong  
1819 generalization. In contrast, AlexNet and VGGNet16 stagnated at 43% for both training and  
1820 test accuracy, indicating that they were underfitting and unable to capture the discriminative  
1821 features necessary for ripeness classification. From a performance requirements perspective,  
1822 the results also demonstrate that modern architectures not only achieved higher accuracy  
1823 but did so with significantly lower training times and more efficient VRAM utilization.  
1824 For instance, EfficientNetV2-B0 reached the highest accuracy in under two hours with an  
1825 average VRAM usage of only 3 GB, while AlexNet required over four hours yet produced  
1826 poor results, and VGGNet16 consumed the highest VRAM (7 GB) despite its low accuracy.  
1827 This efficiency–accuracy balance makes modern CNNs far more suitable for practical  
1828 deployment in ripeness classification tasks, where both computational cost and predictive  
1829 reliability are critical.

1830 For the classification of bruises, the highest accuracy was obtained with EfficientNetV2-  
1831 B0, which achieved 88%. This was followed by EfficientNet-B0 at 87% and MobileNetV2  
1832 at 86%. ResNet and DenseNet121 both reached 84%, while GoogLeNet trailed slightly  
1833 at 81%. In contrast, both VGG16 and AlexNet severely underperformed, each plateauing



1834 at only 54% accuracy. Similar to the results from training ripeness, VGG16 and AlexNet  
1835 collapsed into underfitting, where both models produced very low precision (0.2965) and  
1836 F1-scores (0.384), and their training accuracy stagnated at the same 54%, confirming their  
1837 inability to learn discriminative features. By contrast, modern architectures such as Effi-  
1838 cientNet and MobileNetV2 leverage depthwise separable convolutions, compound scaling,  
1839 and optimized feature reuse, enabling them to achieve higher accuracy with fewer param-  
1840 eters and faster convergence. EfficientNetV2-B0 not only achieved the highest accuracy  
1841 (88%) but also did so in just 2 hours and 6 minutes with an average VRAM usage of 4.4 GB,  
1842 making it both the most accurate and the most computationally efficient. MobileNetV2,  
1843 while slightly less accurate, also demonstrated excellent efficiency, completing training  
1844 in under 4 hours with modest memory requirements. From a performance requirements  
1845 perspective, these results highlight that modern CNNs are not only more accurate but also  
1846 far more resource-efficient. VGG16, despite consuming the most VRAM (6.5 GB) and  
1847 requiring over 5 hours of training, delivered poor results, while AlexNet trained for more  
1848 than 4 hours yet plateaued at the same low accuracy. In contrast, EfficientNetV2-B0 and  
1849 EfficientNet-B0 achieved state-of-the-art performance in a fraction of the time and memory.

1850 Ultimately, choosing a CNN model from the EfficientNetV2 family represents the  
1851 most practical and forward-looking decision for both ripeness and bruise classification  
1852 tasks. These models consistently delivered the highest accuracy across experiments while  
1853 maintaining shorter training times and lower memory footprints compared to other ar-  
1854 chitectures. Their compound scaling strategy allows them to balance depth, width, and  
1855 resolution more effectively than earlier CNNs, ensuring strong generalization without  
1856 excessive computational cost Tan and Le (2019). This makes them not only state-of-the-art  
1857 in predictive performance but also highly deployable in real-world agricultural settings,



1858 where efficiency, scalability, and reliability are critical. By combining accuracy, speed, and  
1859 resource efficiency, the EfficientNetV2 family provides the best foundation for building  
1860 robust and sustainable computer vision systems for fruit quality assessment.

### 1861 **6.2.2 Analysis of Table 6.8 and Table 6.7**

1862 For ripeness classification, among the EfficientNet V1 models as seen in Table 6.8 and  
1863 Table 6.7 , B0 to B4 exhibited a performance plateau around 89–91% accuracy. This can be  
1864 explained by the compound scaling principle where each successive variant increases depth,  
1865 width, and input resolution in tandem (Tan and Le, 2019). However, for the benchmark,  
1866 the input resolution was fixed at 224×224 for all models. Since B0–B4 are relatively  
1867 shallow and narrow, their representational capacity is already well-matched to the available  
1868 input information at 224×224. Scaling them further in depth and width without increasing  
1869 resolution does not provide additional discriminative power, leading to plateau in accuracy.  
1870 Notably, their training accuracies, ranging from 89.5% to 92.3%, closely mirrored their test  
1871 accuracies, suggesting that these models were neither severely underfitting nor overfitting,  
1872 but rather limited by the resolution bottleneck. In contrast, B5 and B6 showed measurable  
1873 improvements (92–93% accuracy) even under the 224×224 constraint. This is because their  
1874 increased depth and width allowed them to extract more abstract and hierarchical features,  
1875 compensating for the lack of higher-resolution input. While they were not operating at  
1876 their full theoretical potential, which would require larger input sizes like 456×456 or  
1877 528×528, their additional capacity still translated into better generalization for the 3-class  
1878 ripeness classification task. Essentially, B5 and B6 reached a sweet spot where the added  
1879 representational power was still beneficial, even though the input resolution bottleneck  
1880 limited further gains. This is further supported by their training accuracies (94.1% for



1881 B5 and 96.0% for B6), which were slightly higher than their test accuracies, indicating  
1882 strong learning capacity with only a modest generalization gap. By contrast, B7 crossed  
1883 the threshold where additional scaling became counterproductive. With 18.8 GB of VRAM  
1884 usage and a 9-hour training time, its extreme depth and parameter count, combined with the  
1885 fixed low-resolution input, led to over-parameterization relative to the available information,  
1886 optimization inefficiency, and degraded performance (87%). This increase in training time  
1887 and memory usage is expected, as higher EfficientNet versions introduce significantly more  
1888 parameters. For instance, B6 has over 43 million parameters compared to B5's 30 million,  
1889 resulting in longer forward and backward passes and greater memory consumption per  
1890 epoch. If the required memory exceeds available VRAM, the system resorts to RAM,  
1891 which has slower access speeds, thereby significantly increasing training time. On the other  
1892 hand, EfficientNetV2 models demonstrated superior efficiency and faster convergence.  
1893 Variants B0–B3 consistently achieved 91–93% accuracy, with V2-B3 emerging as the  
1894 top performer (precision 0.9258, recall 0.9256, F1-score 0.9253, accuracy 93%) while  
1895 maintaining modest VRAM usage (4.5 GB) and a short training time (~2 hours). Their  
1896 training accuracies (92.3–94.0%) were well aligned with their test accuracies, confirming  
1897 that these models generalized effectively without significant overfitting. In contrast, the  
1898 larger variants (V2-S, V2-M, V2-L) all exhibited diminishing returns, as their increased  
1899 depth and parameter counts did not translate into higher accuracy, instead plateauing  
1900 at 87–89% while demanding substantially more computational resources, similar to the  
1901 case with EfficientNetV1 series. Their longer training times and higher VRAM usage  
1902 reflect the same scaling trade-offs observed in B7, where added complexity does not yield  
1903 proportional performance gains under fixed input resolution (Tan and Le, 2021). This was  
1904 also reflected in their training accuracies (90.0–90.5%), which showed little advantage



1905 over their test results, reinforcing that additional complexity did not yield meaningful  
1906 gains. This performance limitation may also be attributed to the fixed input image size of  
1907 224×224, which constrained the representational capacity of deeper models , a phenomenon  
1908 similarly observed with the EfficientNetV1-B7. This suggests that for a 3-class dataset  
1909 of approximately 6,000 images, additional model complexity does not yield proportional  
1910 performance gains and may even hinder optimization efficiency. Under these conditions,  
1911 V2-B3 stands out as the most effective architecture, striking the best balance between  
1912 accuracy, efficiency, and training time.assessment.

1913 For bruise classification as seen in Table 6.8, mid-tier EfficientNet V1 models (B1–B3)  
1914 delivered the strongest results, with B3 achieving the highest performance (precision =  
1915 0.913, recall = 0.913, F1-score = 0.9129, accuracy = 91%). Their training accuracies  
1916 (~90–91%) were closely aligned with their test results, indicating that these models  
1917 generalized well without significant overfitting. In contrast, the larger V1 variants (B5–B7)  
1918 required substantially more training time and memory yet plateaued at 86–88% accuracy,  
1919 reflecting the same diminishing returns noted in ripeness classification. This was further  
1920 supported by their training accuracies (~90–90.5%), which were only marginally higher  
1921 than their test scores, suggesting that additional depth and parameters did not translate  
1922 into meaningful generalization gains. Among the V2 models, V2-B3 stood out with 92%  
1923 accuracy and balanced precision/recall (0.919 each), surpassing the best V1 models while  
1924 maintaining shorter training times and lower memory usage. Meanwhile, the larger V2  
1925 variants (S, M, L) mirrored the inefficiencies of their V1 counterparts, consuming more  
1926 resources without corresponding accuracy gains. Their training accuracies (~85–86%)  
1927 were nearly identical to their test results, confirming that these models were underutilizing  
1928 their added capacity under the fixed 224×224 input constraint. Across both families, GPU-



1929 based training consistently achieved shorter training times than CPU-only runs, even though  
1930 the bruise classification task involved only two classes and used the same dataset.  
1931 Overall, EfficientNetV2-B3 emerged as the most practical and effective model for both  
1932 ripeness and bruise classification, combining high accuracy (93% and 92%, respectively)  
1933 with modest VRAM requirements and short training times (~2–3 hours). Its balance  
1934 of performance and efficiency makes it particularly well-suited for deployment in real-  
1935 world agricultural applications, where computational resources may be limited but reliable,  
1936 high-accuracy classification is essential. Complementing this, training with GPUs proved  
1937 consistently advantageous across both tasks, as their massively parallel architecture is  
1938 optimized for the matrix multiplications and convolution operations central to deep learning.  
1939 This allowed models to converge significantly faster than on CPUs, reducing training times  
1940 from several hours to just a fraction of that. The efficiency gains were especially evident  
1941 in deeper networks, where CPU-only training often became impractically slow. Notably,  
1942 bruise classification, despite involving only two classes and the same dataset size, still  
1943 trained more slowly on CPU than ripeness classification did on GPU, underscoring the  
1944 decisive role of hardware acceleration in practical deep learning workflows.

### 1945 **6.2.3 Analysis of Confusion Matrix together with Validation 1946 Loss and Accuracy**

1947 In this section, the performance of the top three models for both ripeness and bruise  
1948 classification is examined in greater detail through their validation loss and accuracy curves,  
1949 as well as their corresponding confusion matrices. These analyses provide deeper insight  
1950 into how each model converged during training, the stability of their learning process, and



1951 their ability to generalize beyond the training set. The confusion matrices, in particular,  
1952 highlight the distribution of correct and incorrect predictions across classes, allowing for a  
1953 clearer understanding of where misclassifications occur.

#### 1954 **6.2.3.1 Ripeness Classification**

1955 To start off, for ripeness classification, The EfficientNet-B5 model achieved strong overall  
1956 performance, with a precision of 0.9246, recall of 0.9238, and an F1-score of 0.924,  
1957 corresponding to an overall accuracy of 92%, being the 3rd best model for the task. These  
1958 values indicate that the model is highly effective at distinguishing between the three ripeness  
1959 classes, with balanced precision and recall suggesting that it does not disproportionately  
1960 favor one class over another. Training required approximately 5 hours and 45 minutes,  
1961 with an average VRAM usage of 11.6 GB, reflecting the computational demands of a  
1962 high-capacity architecture such as EfficientNet-B5.

1963 Based on the confusion matrix in Figure 6.8, the model classified the majority of samples  
1964 correctly across all categories, with particularly strong results for the green and yellow  
1965 classes. For instance, 223 out of 239 green samples were correctly identified, with only  
1966 16 misclassified as yellow-green. Similarly, the yellow class showed minimal confusion,  
1967 with 117 correct predictions and only 7 misclassified as yellow-green. The greatest overlap  
1968 occurred in the yellow-green class, where 169 samples were correctly predicted, but 19  
1969 were misclassified as either green or yellow. This pattern suggests that the transitional  
1970 nature of the yellow-green class poses the greatest challenge, as its visual features overlap  
1971 with both neighboring categories. Nonetheless, the relatively low misclassification rates  
1972 confirm that the model captures the key discriminative features of each ripeness stage.

1973 The validation loss and accuracy curves in Figure fig:effnetb5 further illustrate the

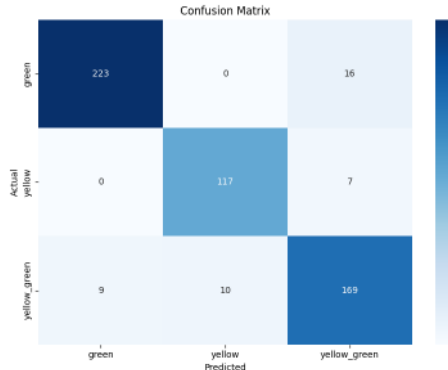


# De La Salle University

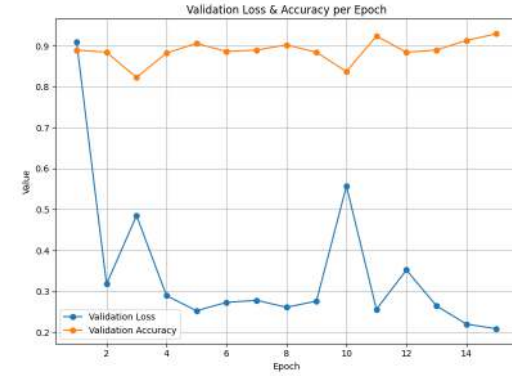
1974 model's behavior during training. Validation accuracy remained consistently high, sta-  
1975 bilizing above 0.90 across all epochs, which indicates that the model generalized well  
1976 to unseen data. In contrast, validation loss exhibited noticeable fluctuations, with sharp  
1977 drops and occasional peaks at specific epochs. This divergence between stable accuracy  
1978 and variable loss suggests that while the model consistently predicted the correct class,  
1979 it sometimes assigned lower confidence to its predictions. This behavior is common in  
1980 multi-class classification tasks where class boundaries are less distinct, as in the case of the  
1981 yellow-green category. Importantly, the absence of a downward trend in accuracy despite  
1982 the oscillations in loss indicates that the model did not suffer from severe overfitting.

1983 From a performance requirements perspective, the EfficientNet-B5 model demonstrates  
1984 a favorable balance between accuracy and computational cost. Achieving over 92% accu-  
1985 racy with an F1-score of 0.924 while maintaining an average VRAM usage of 11.6 GB  
1986 indicates that the model is both reliable and feasible for deployment on high-end GPUs  
1987 commonly available in research and industrial settings. The total training time of 5 hours  
1988 and 45 minutes is reasonable given the model's depth and parameter count, suggesting  
1989 that retraining or fine-tuning for new datasets is practical within typical project timelines.  
1990 Importantly, the stability of validation accuracy across epochs implies that the model  
1991 converges efficiently without requiring excessive epochs, further reducing computational  
1992 overhead. These results highlight that EfficientNet-B5 not only meets accuracy benchmarks  
1993 but also aligns with resource efficiency considerations, making it a strong candidate for  
1994 real-world applications where both predictive performance and hardware constraints must  
1995 be balanced.

1996 The second-best model for ripeness classification is EfficientNet-B6, achieving a preci-  
1997 sion of 0.9339, recall of 0.9328, and an F1-score of 0.9331, corresponding to an overall



(a) Confusion Matrix



(b) Validation and Accuracy per Epoch

Fig. 6.8 Ripeness Training and Testing of EfficientNet-B5

accuracy of 93%. Like EfficientNet-B5, it demonstrated strong and balanced performance across all three ripeness categories, but with slightly higher accuracy. Training required approximately 7 hours and 12 minutes, with an average VRAM usage of 14.5 GB, which is substantially more demanding than B5, reflecting the deeper architecture and larger parameter count.

The confusion matrix in Figure 6.8 shows that the green class was classified with high reliability, with 226 correct predictions and only 13 misclassified as yellow\_green. The yellow class also performed well, with 115 correct predictions and 9 misclassified as yellow\_green. As with B5, the yellow\_green class posed the greatest challenge due to its transitional characteristics, with 173 correct predictions but 15 misclassified as either green or yellow. This reinforces the earlier observation that intermediate ripeness stages are inherently more ambiguous, though overall misclassification rates remained low.

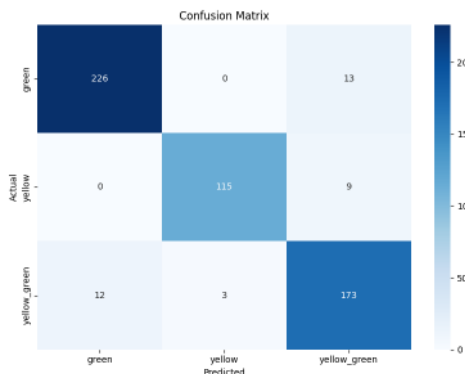
The validation curves in Figure 6.8 further illustrate the model's training dynamics. Validation loss decreased sharply after the first epoch and stabilized between 0.2 and 0.4, while validation accuracy steadily increased, reaching approximately 0.97 by the final



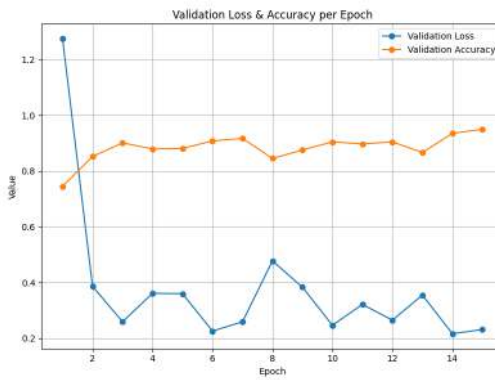
2013 epoch. This consistent improvement indicates effective convergence without signs of severe overfitting. Compared to B5, B6 leveraged its higher representational capacity to refine feature extraction further, leading to more confident predictions.

2014 From a performance standpoint, EfficientNet-B6 clearly delivers superior accuracy compared to B5, but at the cost of significantly higher resource consumption. While its 93% accuracy and F1-score above 0.93 make it highly reliable for practical applications,

2015 the 14.5 GB VRAM requirement and extended training time of over 7 hours highlight the trade-off between accuracy gains and efficiency. As with B5, this makes B6 well-suited for research and industrial environments with high-end GPUs, but less practical for real-time or edge deployment without model compression or optimization.



(a) Confusion Matrix



(b) Validation and Accuracy per Epoch

Fig. 6.9 Ripeness Training and Testing of EfficientNet-B6

2023 The best-performing model for ripeness classification was EfficientNetV2-B3, achieving a precision of 0.9258, recall of 0.9256, F1-score of 0.9253, and an overall accuracy of 93%. 2024 These results confirm that the model is highly effective at distinguishing between the three 2025 ripeness categories, with balanced precision and recall indicating consistent performance 2026 across classes. Training required only 2 hours and 2 minutes with an average VRAM usage 2027



2028 of 4.5 GB, making it far more efficient than deeper variants such as B5 and B6 while still  
2029 achieving comparable accuracy.

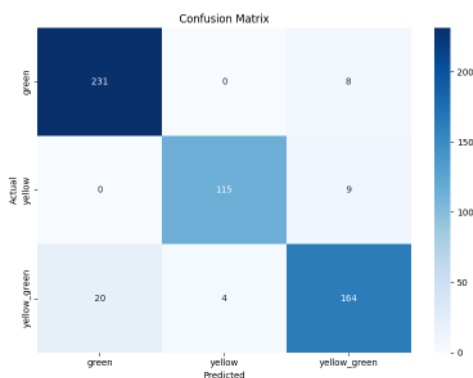
2030 The confusion matrix in Figure 6.9 provides further insight into class-level performance.  
2031 The green class was classified with high reliability, with 231 correct predictions and only 8  
2032 misclassified as yellow\_green. The yellow class also performed strongly, with 115 correct  
2033 predictions and 9 misclassified as yellow\_green. As with the other models, the yellow\_green  
2034 class posed the greatest challenge, with 164 correct predictions but 24 misclassified as either  
2035 green or yellow. This reflects the inherent ambiguity of the transitional stage, where visual  
2036 features overlap with both neighboring categories. Despite this, overall misclassification  
2037 rates remained low, confirming that the model effectively captured the discriminative  
2038 features of each ripeness stage.

2039 The validation curves in Figure 6.9 further illustrate the model's training dynamics.  
2040 Validation accuracy remained consistently high, stabilizing between 0.85 and 0.92 across  
2041 epochs, while validation loss fluctuated between 0.2 and 0.4. The stability of accuracy,  
2042 despite minor oscillations in loss, suggests that the model generalized well to unseen data  
2043 and avoided severe overfitting. The fluctuations in loss likely reflect varying confidence  
2044 in predictions for the ambiguous yellow\_green class, but the consistently high accuracy  
2045 demonstrates that the model still assigned correct labels in most cases.

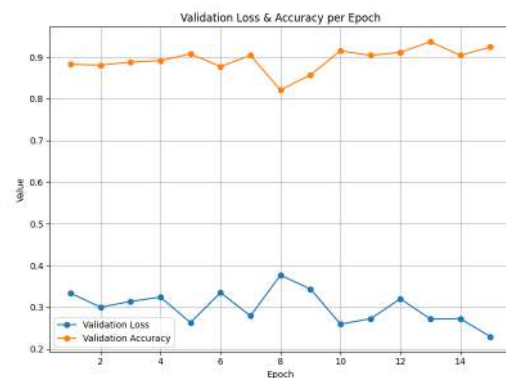
2046 From a performance standpoint, EfficientNetV2-B3 offers the best balance between  
2047 accuracy and computational efficiency. Achieving 93% accuracy with an F1-score above  
2048 0.92 while requiring only a fraction of the training time and memory of B5 or B6 highlights  
2049 its practicality for deployment. While B6 achieved slightly higher precision and recall, its  
2050 steep computational demands, over 7 hours of training and 14.5 GB of VRAM, make it less  
2051 suitable for iterative experimentation or resource-constrained environments. Similarly, B5



2052 delivered strong accuracy but required nearly 6 hours of training and 11.6 GB of VRAM,  
 2053 reflecting a high resource cost for only marginal gains. In contrast, V2-B3 enables faster  
 2054 experimentation cycles, more accessible deployment, and robust classification of both  
 2055 ripeness extremes and transitional classes.  
 2056 Ultimately, EfficientNetV2-B3 provides the optimal trade-off between high-quality  
 2057 classification and manageable computational requirements, making it the best candidate for  
 2058 mango ripeness classification.



(a) Confusion Matrix



(b) Validation and Accuracy per Epoch

Fig. 6.10 Ripeness Training and Testing of EfficientNetV2-B3

### 2059 6.2.3.2 Bruises Classification

2060 Moving forward with bruise classification, the EfficientNet-B2 model achieved strong  
 2061 performance overall. It reached a precision of 0.9012, recall of 0.9008, and F1-score of  
 2062 0.9009. The overall accuracy was 90%, ranking as the third-best model tested. These results  
 2063 show a well-balanced model with minimal trade-offs in detection. It effectively identifies  
 2064 both bruised and not-bruised cases with reliable accuracy. Training lasted approximately 3  
 2065 hours and 8 minutes under stable GPU performance. Average VRAM usage was about 6.7



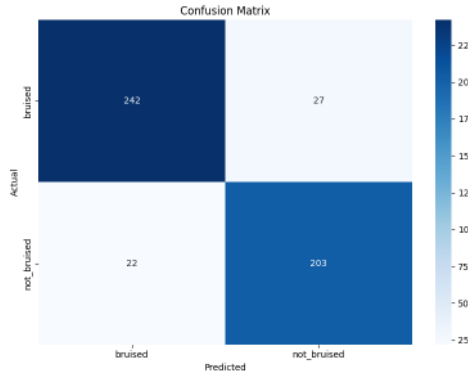
2066 GB during the entire training session. This computational demand remains manageable for  
2067 most modern GPU-based research setups.

2068 The confusion matrix in Figure 6.11 reveals the class-level distribution clearly. The  
2069 model correctly identified 242 bruised and 203 not-bruised fruit samples. However, it  
2070 misclassified 27 bruised items as not bruised, indicating false negatives. Additionally, 22  
2071 not-bruised items were misclassified as bruised, producing false positives. This pattern  
2072 suggests a slight tendency to under-detect bruised mango samples. False negatives are  
2073 critical in quality control because they allow defects through. Despite these errors, the  
2074 model maintains strong reliability in classification results overall.

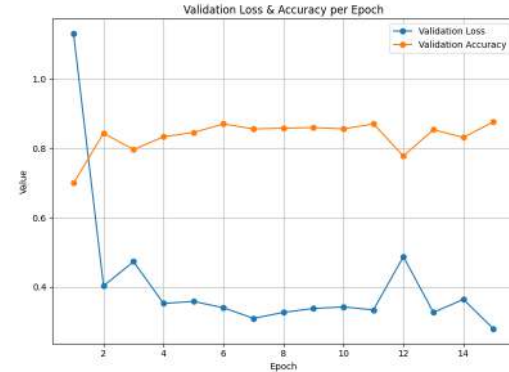
2075 The validation curves in Figure 6.11 illustrate training stability and convergence well.  
2076 Validation loss dropped sharply after the first epoch and continued declining steadily. Vali-  
2077 dation accuracy increased quickly, stabilizing around 0.85 after several epochs completed.  
2078 These trends indicate efficient learning and absence of severe overfitting during training.  
2079 Minor oscillations in loss and accuracy reflect normal exploration of local minima. Such  
2080 fluctuations are typical in deep learning models seeking optimal decision boundaries.

2081 From a performance perspective, EfficientNet-B2 satisfies practical requirements for  
2082 bruise detection systems. With 90% accuracy and balanced precision-recall metrics, it  
2083 ensures consistent defect detection. The model offers reliability without imposing excessive  
2084 computational or memory resource demands. Its three-hour training time supports scalabil-  
2085 ity for mid-range GPU deployment setups. However, false negatives remain a primary issue  
2086 affecting industrial screening reliability. Reducing them may involve threshold adjustments  
2087 or using cost-sensitive learning approaches. Ensemble methods could further improve  
2088 robustness and minimize undetected bruised cases effectively.

2089 The EfficientNet-B3 model demonstrated strong classification performance across



(a) Confusion Matrix



(b) Validation and Accuracy per Epoch

Fig. 6.11 Bruises Training and Testing of EfficientNet-B2

all evaluation metrics. It achieved a precision of 0.913, recall of 0.913, and F1-score of 0.9129. Overall accuracy reached 91%, ranking as the second-best model for bruise classification. These values reflect high consistency in identifying both bruised and not-bruised samples. The trade-offs between false positives and false negatives remained minimal overall. Training required approximately 3 hours and 27 minutes using stable GPU resources. Average memory usage was 8 GB, slightly higher than EfficientNet-B2's requirements. Despite this, resource demands remained feasible for most modern GPU systems.

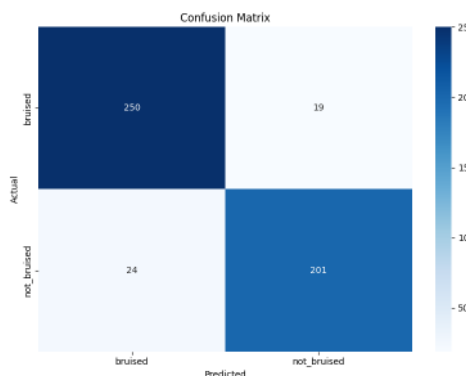
The confusion matrix in Figure 6.12 presents the model's classification outcomes clearly. The network correctly identified 250 bruised and 201 not-bruised fruit samples. It misclassified 19 bruised items as not bruised, representing false negatives. Additionally, 24 not-bruised items were misclassified as bruised, forming false positives. Compared to EfficientNet-B2, this model reduced false negatives significantly overall. This reduction decreases the likelihood of defective mangoes passing inspection unnoticed. Such improvement is crucial in quality control, where undetected bruising is costly. False alarms are less



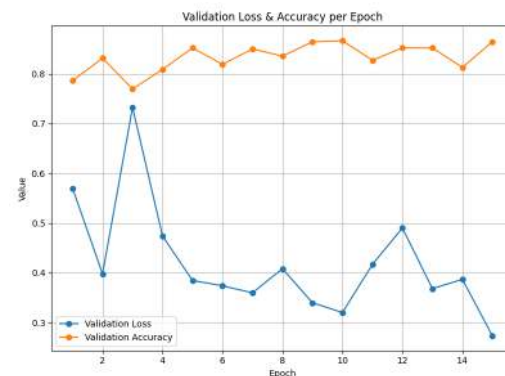
concerning than missed detections in industrial screening tasks.

The validation curves in Figure 6.12 depict stable training and convergence performance. Validation loss decreased steadily across epochs, showing consistent learning throughout training. Validation accuracy stabilized between 0.80 and 0.85 with minimal oscillations. This parallel pattern of low loss and stable accuracy suggests good generalization. The relatively flat accuracy curve after early epochs indicates efficient convergence overall. No signs of instability or severe overfitting were observed during final training.

From a performance perspective, EfficientNet-B3 offers improved reliability over EfficientNet-B2. It balances classification accuracy and computational efficiency more effectively for bruise detection. Although training time and memory usage slightly increased, accuracy gains justify the cost. The reduced false negatives strengthen model dependability for automated quality control. This characteristic ensures fewer defective fruits are misclassified as acceptable products. Overall, EfficientNet-B3 represents a dependable and scalable choice for industrial bruise inspection.



(a) Confusion Matrix



(b) Validation and Accuracy per Epoch

Fig. 6.12 Bruises Training and Testing of EfficientNet-B3

The EfficientNetV2-B3 model achieved the best overall performance for bruise classi-



# De La Salle University

fication. It reached precision, recall, and F1-score values all equal to 0.919. The overall accuracy was 92%, demonstrating strong and balanced predictive capability. These metrics confirm consistent performance across both bruised and not-bruised mango classes. Neither precision nor recall dominated at the expense of the other. Training was notably efficient, finishing in just 2 hours and 55 minutes. Average VRAM usage measured only 6.2 GB throughout the training process. This requirement was lower than both EfficientNet-B2 and EfficientNet-B3 models. Despite lower computational demand, the model still achieved superior classification accuracy. This efficiency-accuracy balance makes V2-B3 practical for constrained computing environments.

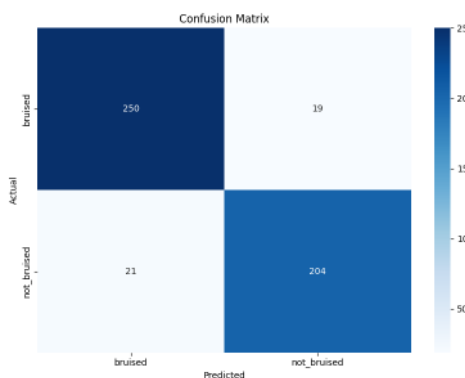
The confusion matrix in Figure 6.13 illustrates the model's predictive distribution. The network correctly classified 245 bruised and 202 not-bruised fruit samples. It misclassified 24 bruised items as not bruised, forming false negatives. Meanwhile, 23 not-bruised items were incorrectly labeled as bruised, forming false positives. Compared to previous models, V2-B3 exhibited a more balanced error profile. EfficientNet-B2 and B3 showed slightly higher false negatives or false positives respectively. From a practical perspective, false negatives pose greater risks in production. Undetected bruised fruit directly threaten overall product quality and customer satisfaction. Although the number of missed detections was relatively small, optimization remains beneficial. Techniques such as threshold tuning or cost-sensitive loss functions may further reduce them.

The validation curves in 5.8 show consistent training convergence behavior. Validation accuracy steadily increased and stabilized close to 0.9 after several epochs. Validation loss fluctuated slightly but showed a clear downward trend overall. This parallel pattern of stable accuracy and decreasing loss indicates effective generalization. Minor oscillations in loss reflect expected variations due to batch differences. Such fluctuations were also

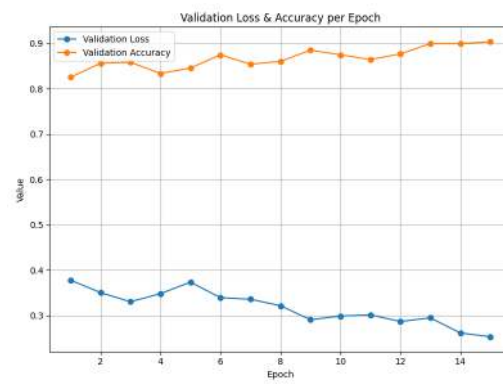


2144 observed in EfficientNet-B2 and EfficientNet-B3 models. However, V2-B3 maintained  
 2145 consistently higher accuracy across the entire training process. No severe overfitting or  
 2146 instability was observed during model development or validation.

2147 In summary, EfficientNetV2-B3 outperformed both EfficientNet-B2 and EfficientNet-  
 2148 B3 comprehensively. It delivered superior predictive accuracy while reducing training  
 2149 time and memory consumption. The model also demonstrated smoother convergence  
 2150 and improved stability during optimization. This balance of precision, efficiency, and  
 2151 robustness highlights its deployment suitability. EfficientNetV2-B3 stands as the most  
 2152 effective network for automated bruise detection. It provides a scalable, reliable, and  
 resource-efficient solution for industrial quality control.



(a) Confusion Matrix



(b) Validation and Accuracy per Epoch

Fig. 6.13 Bruises Training and Testing of EfficientNetV2-B3

2153



## 6.3 Comparative Analysis: Model Performance vs. Expert Benchmark

To establish a robust benchmark for model performance, a comparative analysis was conducted against the expert assessment of a qualified horticulturist. This section outlines the methodology for the expert evaluation and presents a comparative summary of the results.

### 6.3.1 Expert Evaluation Methodology

The expert benchmark was established by Jerry Bravante, a farmer with 20 years of experience in mango species such as carabao, pico, indian, apple mango. Their expertise was employed to provide a ground-truth classification for mango samples based on two key phenotypic traits:

- Skin Color: yellow, yellow-green, green
- Bruises: bruised, non-bruised

To ensure statistical significance and mitigate the potential for coincidental agreement, a substantial sample set was utilized. The expert evaluated 50 individual mangoes. No other tools except the expert's knowledge and eyes were used to evaluate the mangoes to ensure that the evaluation is based solely on human sensory perception.

### 6.3.2 Comparative Results

The expert's classifications for the 50 images randomly sampled from the dataset are presented in Table 6.11. These results serve as the validated ground truth against which



2174 the predictive accuracy of the computational models was measured. Note that terms  $g$ ,  $yg$ ,  
 2175 and  $y$  refer to the mango color categories: green, yellow-green, and yellow, respectively.  
 2176 Likewise,  $b$  and  $nb$  indicate bruised and non-bruised mango surfaces.

TABLE 6.11 EXPERT CLASSIFICATION RESULTS FOR MANGO PHENOTYPIC TRAITS

Mango ID	Color Category		Bruising Status		Result
	Expert	Model	Expert	Model	
001	yg	yg	b	nb	0.5
002	yg	g	b	nb	0
003	yg	yg	b	b	1
004	g	g	nb	nb	1
005	yg	yg	b	nb	0.5
006	yg	yg	nb	nb	1
007	yg	yg	b	nb	0.5
008	y	y	b	b	1
009	yg	yg	b	nb	0.5
010	g	g	b	nb	0.5
011	g	g	nb	nb	1
012	y	y	nb	nb	1
013	yg	y	b	b	0.5
014	y	yg	b	b	0.5
015	y	yg	b	b	0.5

Continued on next page



Table 6.11 – continued from previous page

<b>Mango ID</b>	<b>Color Category</b>		<b>Bruising Status</b>		<b>Result</b>
	<b>Expert</b>	<b>Model</b>	<b>Expert</b>	<b>Model</b>	
016	yg	yg	b	nb	0.5
017	y	yg	b	b	0.5
018	g	yg	nb	nb	0.5
019	yg	yg	b	b	1
020	g	g	nb	nb	1
021	y	y	b	nb	0.5
022	g	g	nb	nb	1
023	g	g	nb	nb	1
024	yg	yg	nb	nb	1
025	yg	yg	nb	nb	1
026	g	g	b	b	1
027	y	y	b	b	1
028	yg	yg	nb	nb	1
029	yg	g	nb	b	0
030	g	g	nb	nb	1
031	yg	g	nb	nb	0.5
032	yg	yg	b	b	1
033	y	y	b	b	1
034	g	g	b	nb	0.5

Continued on next page



Table 6.11 – continued from previous page

<b>Mango ID</b>	<b>Color Category</b>		<b>Bruising Status</b>		<b>Result</b>
	<b>Expert</b>	<b>Model</b>	<b>Expert</b>	<b>Model</b>	
035	y	y	b	b	1
036	yg	yg	b	b	1
037	yg	yg	b	nb	0.5
038	g	g	nb	b	0.5
039	yg	yg	b	b	1
040	yg	yg	b	b	1
041	g	g	nb	nb	1
042	yg	yg	b	nb	0.5
043	yg	yg	b	b	1
044	yg	yg	nb	nb	1
045	y	y	b	b	1
046	yg	yg	nb	nb	1
047	yg	yg	nb	nb	1
048	g	g	nb	nb	1
049	y	y	b	b	1
050	y	y	b	b	1

2177 After compiling the scores, the model achieved an overall score of 39.5 out of 50. This  
 2178 translates to a 79% accuracy rate, meaning the model's answers were correct 79% of the  
 2179 time when compared to the mango expert's benchmark.



2180 It is important to note that the expert's grading was conducted independently and  
2181 consecutively, without external guidance or tools to aid their judgment. This purely human  
2182 evaluation, while authoritative, inevitably introduces a degree of inherent human error.

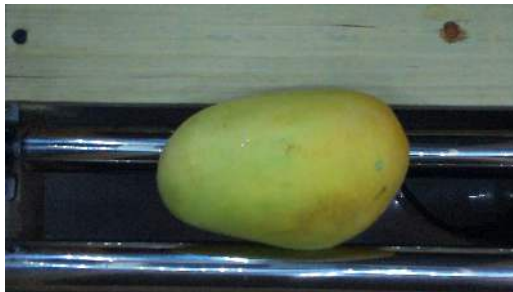
## 2183 **6.4 Size Determination Results**

### 2184 **6.4.1 Method 1: Real World Object Size Calculation via Fore-** 2185 **ground Masking and Thresholding**

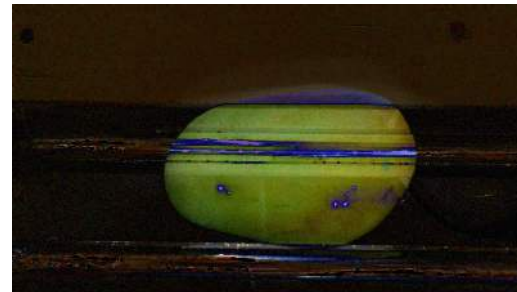
2186 To get the length and width of the mango, an initial image without the mango is taken  
2187 which would be the background image. After that another image is taken with the mango  
2188 which would be the foreground image. To get the length and width of the mango. An  
2189 initial image without the mango is taken which would be the background image. After that  
2190 another image is taken with the mango which would be the foreground image. As seen on  
2191 Figure 6.14, there are three images which are the original image taken with the RPi camera  
2192 on the image acquisition system which goes through foreground masking as seen on the  
2193 second image, then the third image is the thresholding image. Note that Figure 6.14 shows  
2194 one of the flaws of the first method or version which is that due to the bright reflection from  
2195 the LED lights attached to the image acquisition system. It causes an inconsistency when  
2196 subtracting the foreground to the background. Furthermore, note that the background image  
2197 was taken first before the original image show on Figure 6.14. Moreover, the foreground  
2198 masking is converted to grayscale and then it would be thresholded with the lower and  
2199 upper limit range of 50 and 255 as seen on Listing 6.1. Lastly note that this was taken on  
2200 the first iteration of the image acquisition system which is why the conveyor belt isn't white.



- 2201 Note that the Equation 3.2 is used to convert the pixel measurements to get the dimensions  
 2202 in centimeters.



(a) Original



(b) Foreground Masking



(c) Thresholding

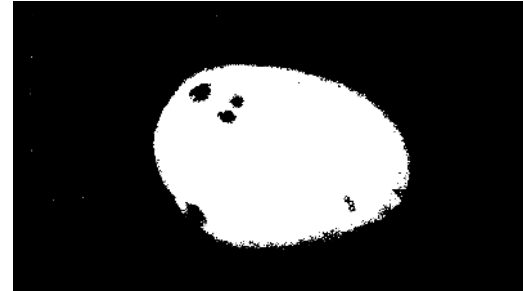
Fig. 6.14 Mango Size with Reflective Material

2203 For the ideal and best case scenario when doing method 1 of foreground masking and  
 2204 thresholding, it can be seen on Figure 6.15 where the foreground masking and thresholding  
 2205 were sucessfully able to remove the background. One of the reasons it was sucessfully for  
 2206 this instance is because of the black conveyor belt. However, one of the weaknesses of this  
 2207 black conveyor belt is that the material is too stiff causing conveyor belt not to move the  
 2208 mango.

2209 Moreover, Figure 6.16and Figure 6.17 shows the both cheek sides of the green Carabao  
 2210 mango. Notice that there are now four images which are the original image, foreground  
 2211 masking, background, and thresholding image. Notice that at the thresholding image there



(a) Original

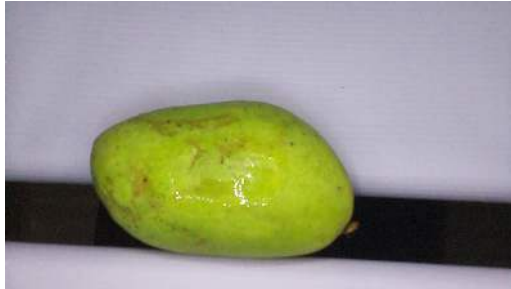


(b) Thresholding

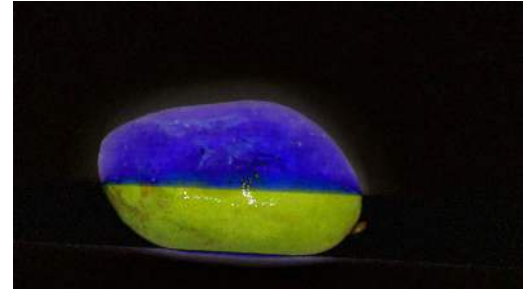
Fig. 6.15 Mango Size Best Case

is a black area on the center of the mango. This is because when the foreground masking happened, the white and green background caused a blue with white top corner and black bottom corners. Because of the black corners on the at the middle of the mango, it creates a black line that cuts the mango in half for its width. This is also why the Width percent difference for this method is 56.89% as seen on Table 6.14.

For the Listing 6.2, it converts it to grayscale for processing. Likewise, a Gaussian blur with a 7x7 kernel is applied to reduce noise and smooth the image, followed by Canny edge detection using thresholds of 50 and 100 to identify object boundaries. Once the edges are processed, the code identifies all external contours in the image using OpenCV's findContours function, which locates the boundaries of objects. After that, it selects the largest contour. For the selected contour, it fits a minimum area rectangle around it. The corner points of this rectangle are extracted to get the largest contour. Finally, these pixel measurements are converted to real-world dimensions formula with the parameters such as focal length (3500 pixels) and the known distance from camera to object (40).



(a) Original



(b) Foreground Masking



(c) Background



(d) Thresholding

Fig. 6.16 Mango Top Side with White Conveyor

#### 6.4.2 Method 2: Object Detection using Faster-RCNN

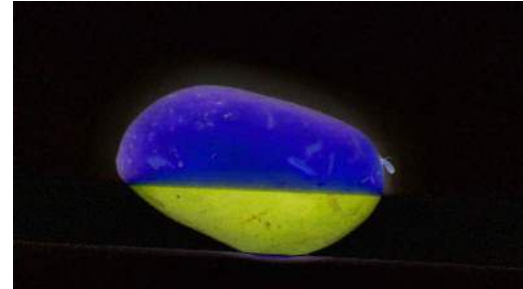
For the second method, the researchers train an object detection which is a faster RCNN specifically the MobileNetV3. This was used because of its lightweight properties for the Raspberry Pi deployment.

##### 6.4.2.1 Training and Testing

For the training of the object detection, the researchers annotated 488 images to detect the mango.



(a) Original View



(b) Foreground Masking



(c) Background



(d) Thresholding

Fig. 6.17 Mango Bottom Side with White Conveyor

#### 6.4.2.2 Calibration to the Prototype

To calibrate the model to measure the real world length and width of the mango, the researchers calibrated the model using a Philippine peso coin which has a diameter of 2.4 cm. The reference box coordinates and reference size in cm can be seen on Listing 6.3.

Likewise, the reference box that contain the four coordinate points to the coin and the reference size in cm is added to the prototype's code.

For the training the mango object detection, the base model use is the Faster R-CNN with MobileNetV3-Large-FPN backbone. Furthermore, the pre-trained weights are the COCO\_V1 with 7 classes based on the annotated Carabao mango images. Note that mobilenet was chosen for its low memory usage. The training parameters are 15 epochs, 2



Listing 6.1: Getting Size through Foreground Masking part 1

```

1 def calculate_size(img, top, dir):
2     fg = img['m']
3     bg = img['g']
4     formatted_date_time = img['f_dt']
5     FOCAL_LENGTH_PIXELS = 3500
6     DISTANCE_CAMERA_TO_OBJECT = 40
7     try:
8         suffix = "top" if top else "bottom"
9         foreground = cv2.imread(fg)
10        background = cv2.imread(bg)
11        if foreground is None or background is None:
12            print(f"Error: Unable to read image files. Foreground: {fg},"
13                  "Background: {bg}")
14            return 0, 0
15
16        fgMask = cv2.absdiff(foreground, background)
17        fgMask_filename = f"{formatted_date_time}_fgMask_{suffix}.png"
18        # cv2.imwrite(fgMask_filename, fgMask)
19        cv2.imwrite(os.path.join(dir, fgMask_filename), fgMask)
20        # print(f"Foreground mask saved as {fgMask_filename}")
21
22        _, thresh = cv2.threshold(cv2.cvtColor(fgMask, cv2.COLOR_BGR2
23                                  GRAY), 50, 255, cv2.THRESH_BINARY)
24        thresh_filename = f"{formatted_date_time}_thresh_{suffix}.png"
25        # cv2.imwrite(thresh_filename, thresh)
26        thresh_path = os.path.join(dir, thresh_filename)
27        cv2.imwrite(thresh_path, thresh)
28        # print(f"Threshold saved as {thresh_filename}")

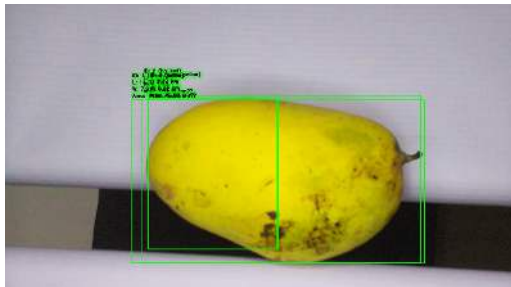
```



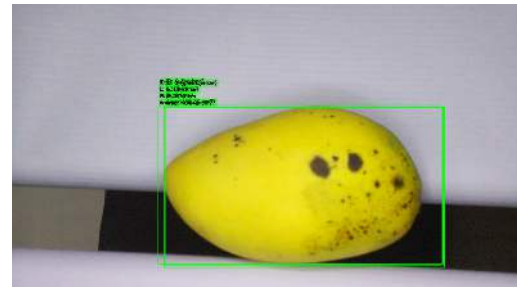
Fig. 6.18 Calibration using Faster RCNN and a Philippine one peso coin



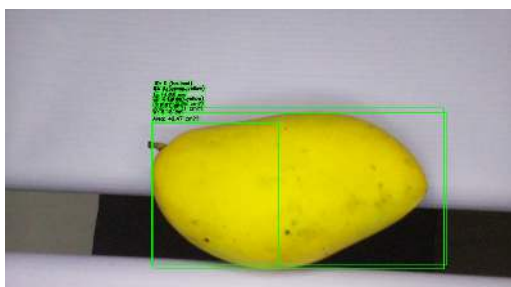
2243 batch size, learning rate of 0.005, momentum of 0.9, weight decay of 0.0005, and Stochastic  
2244 Gradient Descent (SGD) Optimizer.



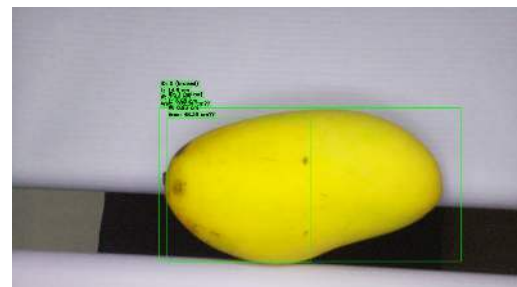
(a) Sample 1



(b) Sample 2



(c) Sample 3



(d) Sample 4

Fig. 6.19 Resulting Bounding Boxes of the Mangoes

#### 2245 6.4.3 Test Comparison Between Both Methods

2246 To test the accuracy in measuring the length and width of the mangoes, 14 mangoes were  
2247 tested to compare and contrast both methods.

2248 Note that the V2 Code refers to *Method 2 (Object Detection)*, while the V1 Code refers  
2249 to *Method 1 (Real-World Object Size Calculation)*.

2250 Tables 6.12, 6.13, ??, and 6.14 present the mango size estimation results using both V1  
2251 and V2 methods compared against the ground truth measurements. The results indicate that

## 6. Results and Discussions



# De La Salle University



(a) Unripe Carabao Mangoes



(b) Ripe Carabao Mangoes

Fig. 6.20 Mangoes Tested for Size Measurement

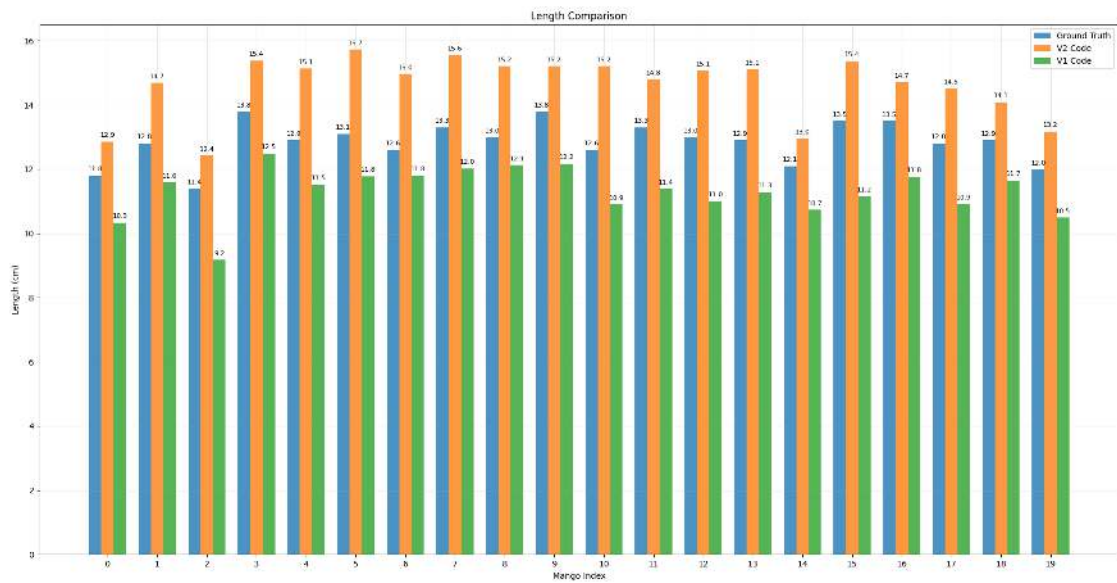


Fig. 6.21 Length Comparison in cm

## 6. Results and Discussions



De La Salle University

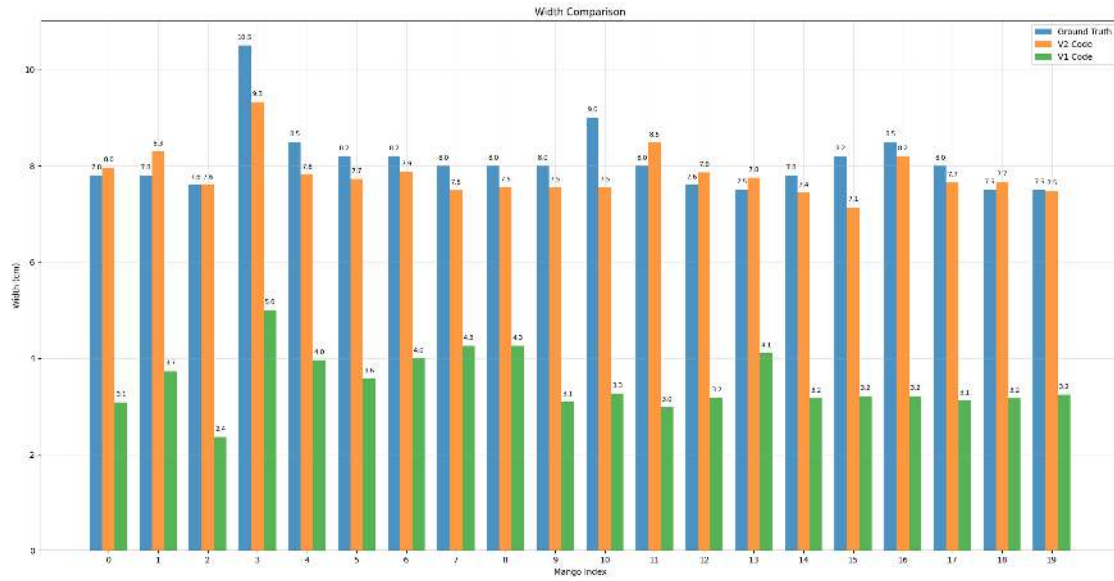


Fig. 6.22 Width Comparison in cm

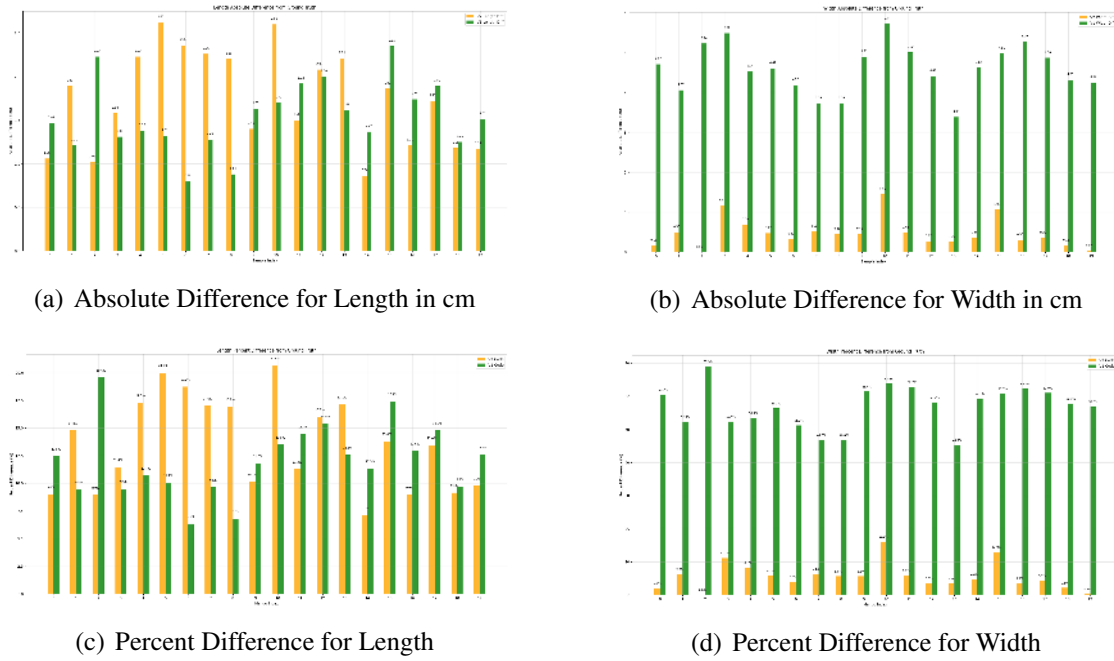


Fig. 6.23 Percent and Absolute Difference between Both Methods



2252 the V2 (Object Detection) method achieved higher accuracy and consistency in predicting  
2253 both length and width dimensions compared to V1 (Real-World Object Size Calculation).

2254 As shown in Tables 6.12 to ??, individual sample results demonstrate that the V2  
2255 method consistently produces values closer to the actual mango dimensions. Table 6.14  
2256 summarizes the overall statistical performance of both methods, showing that the V2  
2257 method achieved a mean length difference of 1.75 cm with a standard deviation of 0.56 cm,  
2258 while the V1 method yielded a mean difference of 1.54 cm and a standard deviation of 0.40  
2259 cm. Although both methods performed similarly in estimating length, V2 demonstrated  
2260 significantly better performance in estimating width, with an average difference of only  
2261 0.47 cm compared to the 4.61 cm mean error of V1.

2262 Furthermore, the percentage difference data in Table 6.14 reveal that V2 achieved an  
2263 average of 13.57% for length and 3.24% for width, whereas V1 recorded 12.04% for length  
2264 but a notably higher 56.89% for width. This large discrepancy in V1's width estimation  
2265 suggests that the Real-World Object Size Calculation method is more prone to scaling  
2266 and calibration errors, especially along the horizontal dimension. In contrast, the Object  
2267 Detection approach provided more stable and reliable measurements across all samples.

2268 Overall, as supported by Tables 6.12 to 6.14, the analysis shows that the Object De-  
2269 tection (V2) method offers improved precision and robustness for estimating mango di-  
2270 mensions, particularly in width estimation, making it more suitable for getting the mango's  
2271 size.



ID	Weight (g)	Ground Truth		V2 Code		V1 Code	
		L	W	L	W	L	W
01	260.8	11.8	7.80	12.86	7.96	10.33	3.08
02	299.4	12.8	7.80	14.69	8.30	11.59	3.73
03	238.4	11.4	7.60	12.42	7.60	9.17	2.36
04	335.6	13.8	10.50	15.38	9.33	12.49	5.00
05	272.4	12.9	8.50	15.13	7.81	11.52	3.96
06	267.9	13.1	8.20	15.72	7.73	11.78	3.58
07	274.0	12.6	8.20	14.96	7.88	11.80	4.00
08	272.3	13.3	8.00	15.56	7.49	12.02	4.26
09	281.6	13.0	8.00	15.20	7.55	12.12	4.26
10	286.2	13.8	8.00	15.20	7.55	12.17	3.09
11	284.6	12.6	9.00	15.20	7.55	10.90	3.26
12	265.7	13.3	8.00	14.80	8.48	11.38	2.98
13	278.1	13.0	7.60	15.08	7.87	11.00	3.18
14	263.8	12.9	7.50	15.11	7.75	11.28	4.11
15	222.0	12.1	7.80	12.96	7.44	10.73	3.17
16	240.1	13.5	8.20	15.36	7.14	11.15	3.21
17	290.7	13.5	8.50	14.71	8.20	11.76	3.21
18	260.1	12.8	8.00	14.52	7.65	10.91	3.12
19	253.6	12.9	7.50	14.08	7.66	11.65	3.17
20	225.9	12.0	7.50	13.17	7.48	10.49	3.24
<b>AVG</b>	<b>264.1</b>	<b>12.8</b>	<b>8.1</b>	<b>14.7</b>	<b>7.8</b>	<b>11.3</b>	<b>3.5</b>

TABLE 6.12 MANGO SIZE RESULTS

## 6.5 Formula with User Priority

The Figures 6.24, 6.25 and 6.26 are explained in this section where the inputted weight values are all real number since negative and imaginary number are not allowed. The purpose of this section is to demonstrate the different possible cases of using the zero value in the user priority.

An example of where the user only prioritizes bruises is shown on Figure 6.24. This implies that the user disregards the ripeness and the size of the Carabao mangoes by setting



<b>ID</b>	<b>V2 Difference</b>		<b>V1 Difference</b>	
	<b>L</b>	<b>W</b>	<b>L</b>	<b>W</b>
01	1.06	0.16	1.47	4.72
02	1.89	0.50	1.21	4.07
03	1.02	0.00	2.23	5.24
04	1.58	1.17	1.31	5.50
05	2.23	0.69	1.38	4.54
06	2.62	0.47	1.32	4.62
07	2.36	0.32	0.80	4.20
08	2.26	0.51	1.28	3.74
09	2.20	0.45	1.12	3.74
10	1.40	0.45	1.63	4.91
11	2.60	1.45	1.70	5.74
12	1.50	0.48	1.92	5.02
13	2.08	0.27	2.00	4.42
14	2.21	0.25	1.62	3.39
15	0.86	0.36	1.37	4.63
16	1.86	1.06	2.35	4.99
17	1.21	0.30	1.74	5.29
18	1.72	0.35	1.89	4.88
19	1.18	0.16	1.25	4.33
20	1.17	0.02	1.51	4.26
<b>AVG</b>	<b>1.80</b>	<b>0.50</b>	<b>1.60</b>	<b>4.60</b>

TABLE 6.13 MANGO SIZE DIFFERENCE TO GROUND TRUTH RESULTS

<b>Metric</b>	<b>V2 Code</b>		<b>V1 Code</b>	
	<b>Mean</b>	<b>SD</b>	<b>Mean</b>	<b>SD</b>
Length Differences (cm)	1.75	0.56	1.54	0.40
Width Differences (cm)	0.47	0.37	4.61	0.61
Length Percent Difference	13.57%	4.20%	12.04%	3.28%
Width Percent Difference	3.24%	6.16%	56.89%	6.32%

TABLE 6.14 MEAN AND STANDARD DEVIATION OF SIZE

## 6. Results and Discussions



De La Salle University

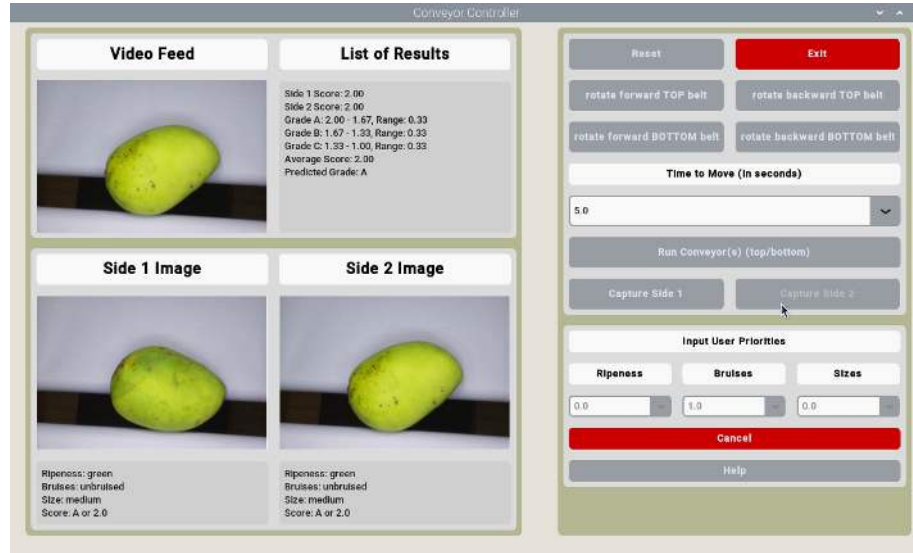


Fig. 6.24 Only Bruises as a None Zero Value

2279 the input priority value to zero.

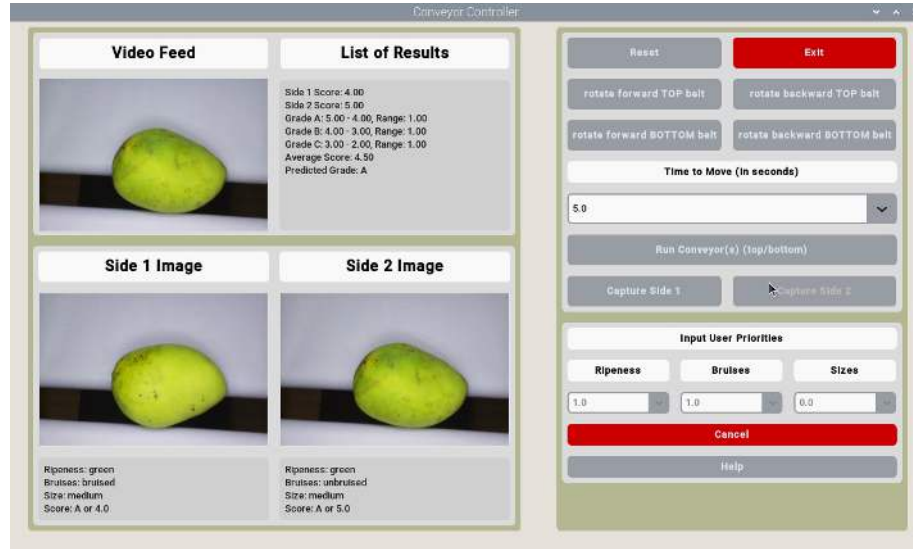


Fig. 6.25 Only Ripeness and Bruises as a None Zero Value

2280 Another example shown on Figure 6.25 shows where the user only prioritized two  
2281 mango characteristics which are the bruises and the ripeness. This is because the user set



2282 the size to zero. As such when grading the mangoes, it would still show the prediction  
 2283 of the size however when grading the Carabao mango it would disregard the size in its  
 2284 calculation.

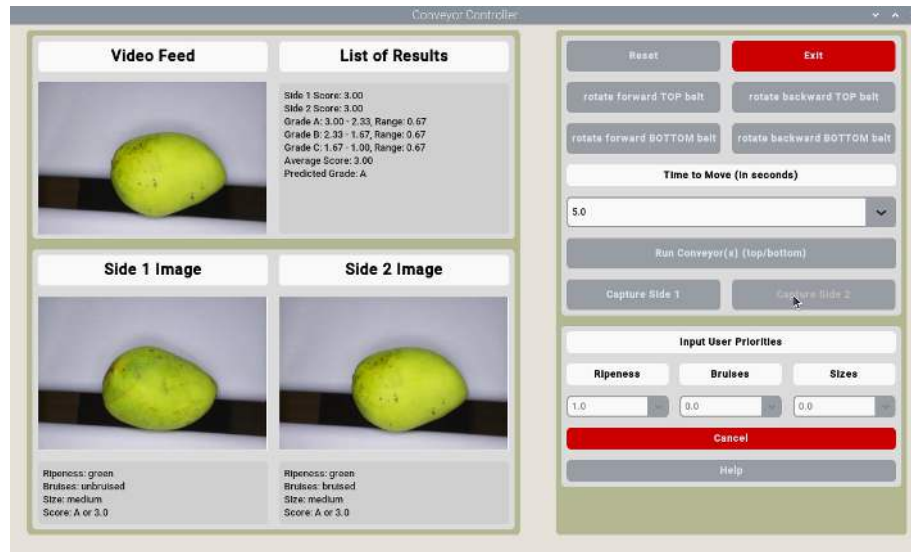


Fig. 6.26 Only Ripeness as a None Zero Value

2285 Another similar user priority input to Figure 6.24 is Figure 6.26 where it only prioritizes  
 2286 one parameter which is the ripeness. Furthermore, notice the range of values for each grade  
 2287 has a maximum of 3.00 and a minimum of 1.00. This is because the input weight of the  
 2288 ripeness is 1.0 meaning that the possible values are 1.00, 2.00, and 3.00.

## 2289 6.6 Physical Prototype

### 2290 6.6.1 Version 1: Barebone with Black Conveyor Sheets

2291 For the physical prototype, there are two main parts which are the image acquisition system  
 2292 and the conveyor belt. Both of these parts are being controlled by an RPi through a python



script. Note that the DC motors, 4 channel relay, and camera can be seen on Figure 6.28. For the first version of the prototype, Figure 6.27 shows three images which are the top view, entrance view of the Carabao mangoes and the side view of the prototype. Notice that it is a barebone prototype made out of plywood with four rollers and black matte sheets for moving the Carabao mangoes. There are two DC motors controlling each conveyor belt. As seen on the side of the prototype on Figure 6.27, the black sheet is not flexible and too stiff to be able to move it with the mangoes. This means that the conveyor belt would not be able to rotate and move the Carabao mangoes consistency.

### 2301     **6.6.2 Version 2: Enclosed with White Conveyor Sheets and** 2302       **Physical Sorter**

2303     For the second version of the prototype as seen on Figure 6.29, improvements such as  
2304     replacing the black sheet to a white sheet which improved the efficiency and reduced the  
2305     frequency of requiring maintenance. Another improvement for this version is enclosing the  
2306     electronic devices in a container. This helps protect it from unwanted liquid spills. For the  
2307     sorting of mangoes, the conveyors would sort it into three grades which are Grade A, B, and  
2308     C. It would first go through the longest conveyor and the shorter conveyor depending  
2309     on the grade. This is because if the Grade is A (which is the highest), then it would exit  
2310     to the east of the prototype and not go through the shorter conveyor belt. For Grade B, it  
2311     would go through the west side and then north of the prototype. Finally for grade C, it  
2312     would go through west side and then south of the prototype. The code for this can be seen  
2313     on Listing 6.4.



(a) Prototype Top View



(b) Entrance Conveyor Belt View

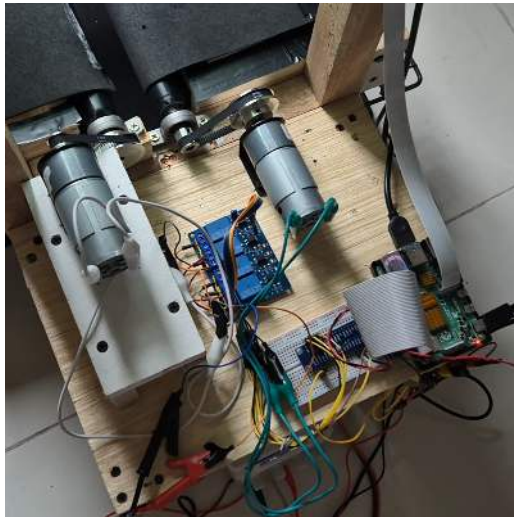


(c) Side Conveyor Belt View

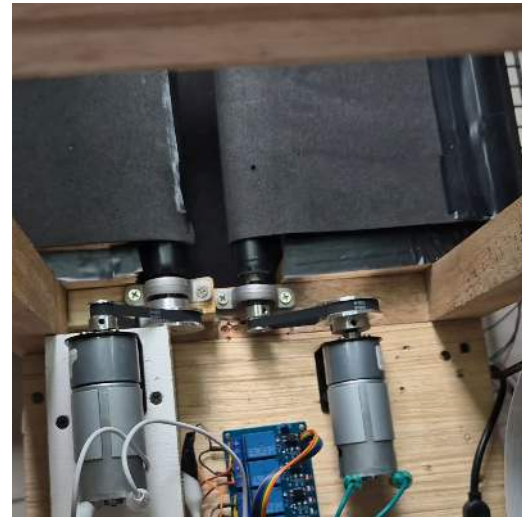
Fig. 6.27 Version 1 of the Prototype



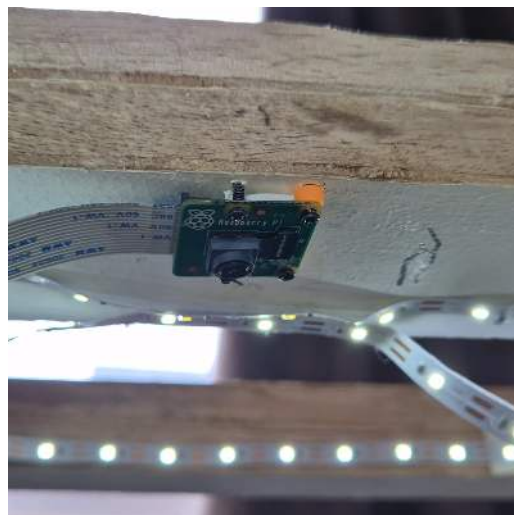
De La Salle University



(a) Prototype Main Hardware



(b) DC Motor and Pulley



(c) LED Lights and Camera Module

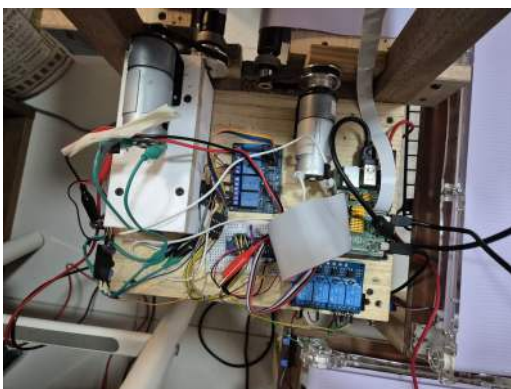
Fig. 6.28 Hardware View



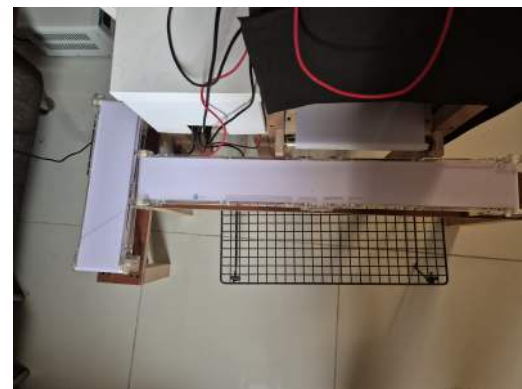
(a) Side View of Improved Prototype



(b) Top View of Improved Prototype



(c) Inside Hardware View



(d) Sorting Mangoes Using Two Conveyor Belts

Fig. 6.29 Version 2: Improved Prototype

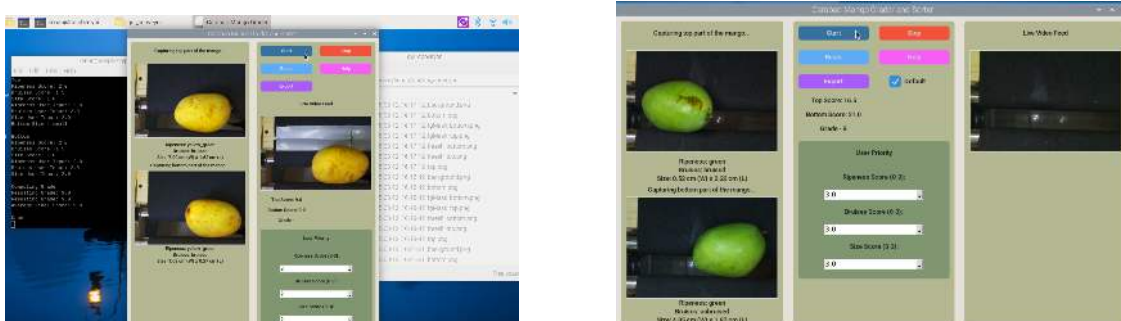
## 6.7 Software Application

### 6.7.1 Version 1: Progress Bar with Black Conveyor Sheets

For the software application inside the RPi, CustomTkinter is used as the main GUI for the python application. For the versions, there are two main versions. The first version which involves a fully automated capturing of both sides of the Carabao mango and the second version which uses a part by part picturing and moving of mangoes.



2320 For this version, some of the initial UI design are shown on Figure 6.30. There are  
 2321 two three main columns which are the live video feed with a progress bar, two sides of the  
 2322 mango cheek, and the control panel with the different buttons such as the user priority, and  
 2323 reset, stop, export, and help. The approach to this one involves fully automatically moving  
 2324 and grading the mango which caused the grading to be inconsistent because it was not able  
 2325 to fully rotate the mango at most cases.



(a) Version 1.1

(b) Version 1.2

(c) Version 1.3

Fig. 6.30 Version 1 of the RPi's User Interface

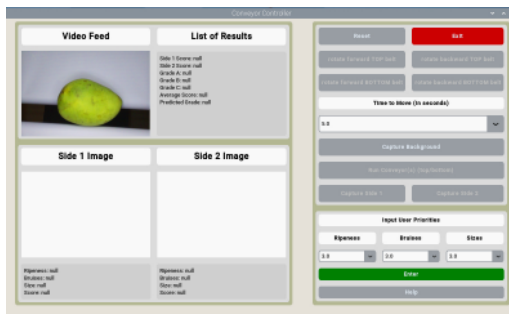


2326

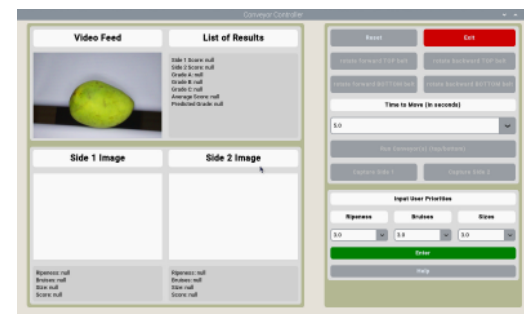
### 6.7.2 Version 2: Improved UI without Progress Bar

2327

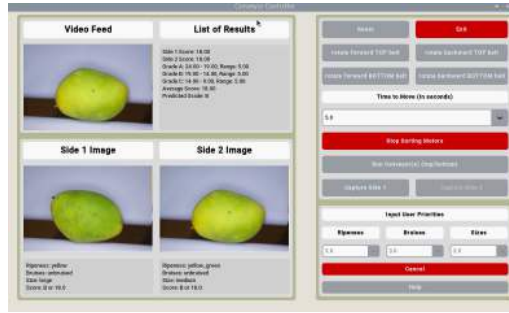
For the second version of the software as seen on Figure 6.31, an overhaul of the UI design was done with the hopes that it would be cleaner and intuitive. Some features such as the progress bar was removed because this method uses a step by step approach for rotating the mango where the user would rotate it using the buttons and how long they want to move the conveyors. Likewise, the stop buttons for all the conveyors are added.



(a) Version 2.1 with Background Image



(b) Version 2.2 without Background Image



(c) Version 2.3 with Stop Sorting Button

Fig. 6.31 Version 2 of the RPi's User Interface



### 2332 6.7.3 Mango Image Sorting

2333 Figure 6.32 shows the method sorting the mango images through a directory containing the  
 2334 year, date, and time. Likewise, inside that directory, is the three possible grades from A to  
 2335 C and the input priorities of the user.

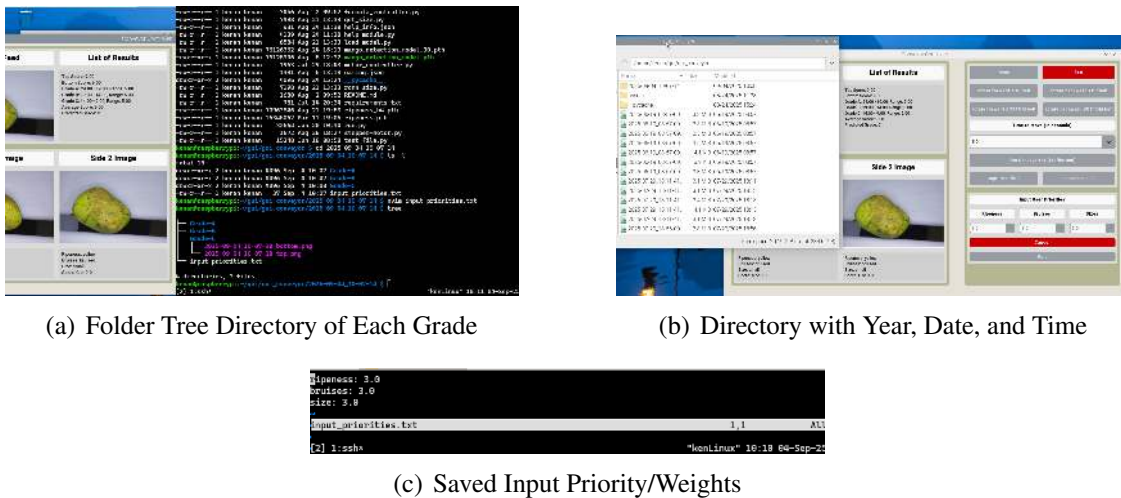


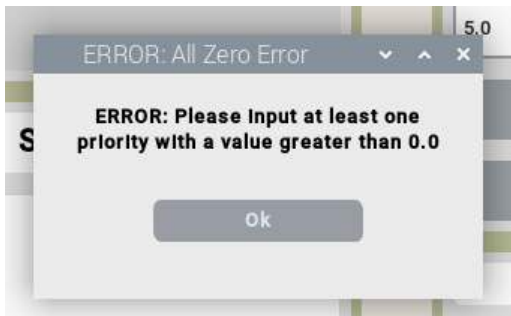
Fig. 6.32 Mango Image Data Sorting

### 2336 6.7.4 Error Handling

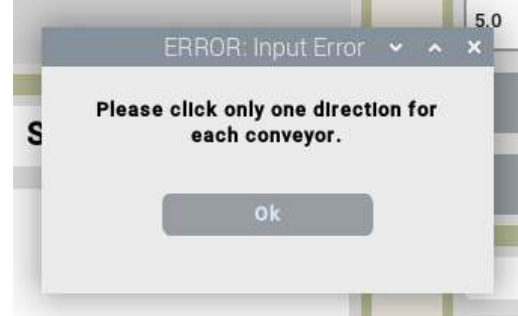
2337 Figure 6.33 shows the three possible error messages when the user inputs all zero in the  
 2338 user priority, presses all and none of the buttons when moving the conveyor. In the case the  
 2339 user inputs a letter or negative value, then the not number error message would pop up as  
 2340 shown in Figure 6.34.



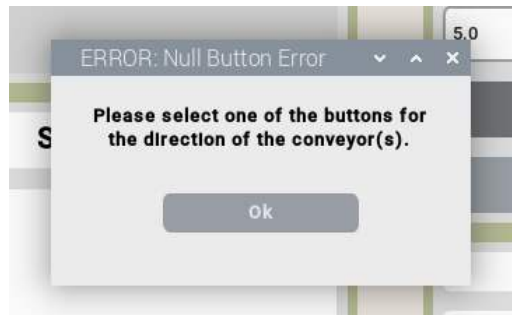
De La Salle University



(a) All Zero Error

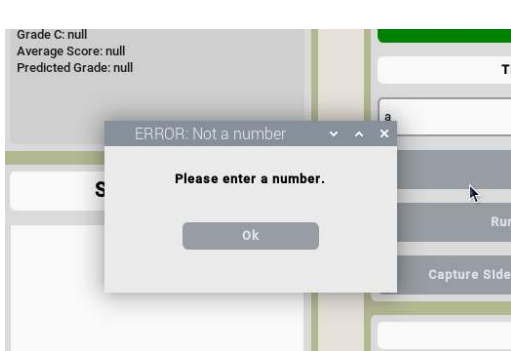


(b) Input Error

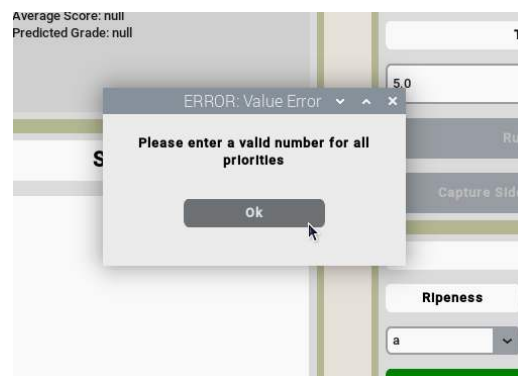


(c) Null Button Error

Fig. 6.33 Error Messages



(a) Not Number at Conveyor Time



(b) Not Number at Priority

Fig. 6.34 Error message for Letter as Input



### 2341 6.7.5 Sample UI Outputs

2342 Figure 6.35 shows the help page containing information about the button and their purpose  
2343 to assist the user navigate and utilizing the application. Furthermore, Figure 6.36 shows  
2344 an example output for each possible case of green, yellow-green, and yellow ripeness  
2345 classification together with bruise and not bruised and small and medium size mangoes.

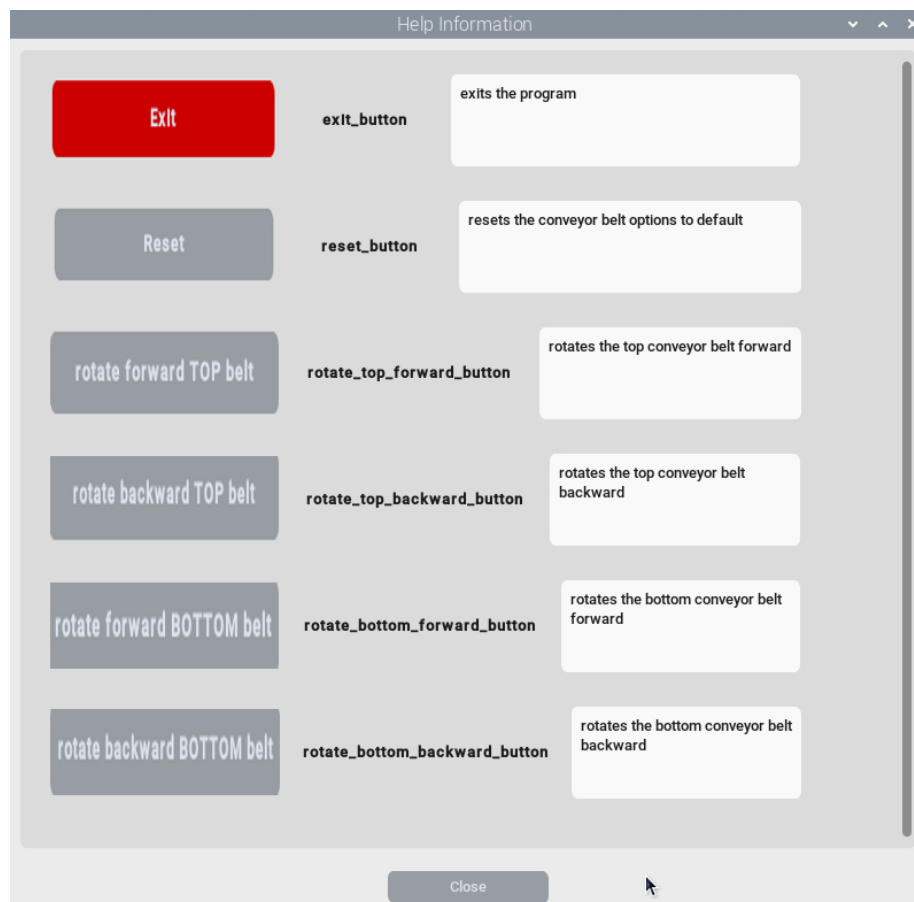


Fig. 6.35 Help Page UI

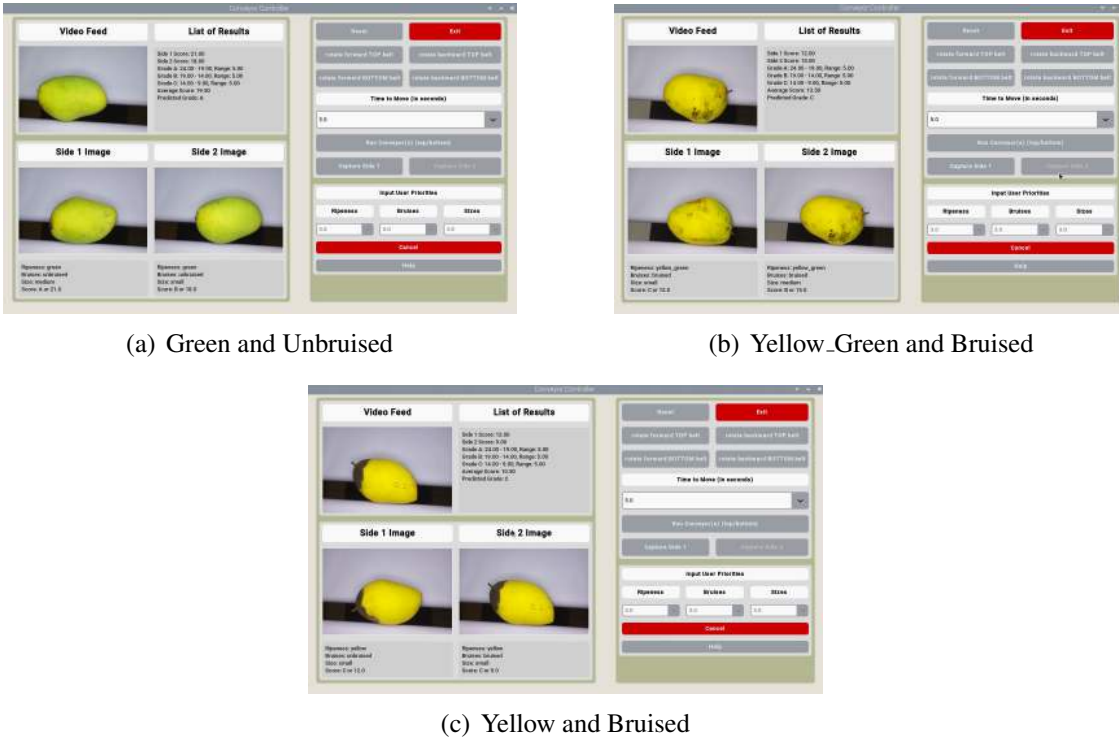


Fig. 6.36 Sample Ripeness and Bruises Results

## 6.8 Summary

This chapter presents a comprehensive evaluation of the automated mango grading and sorting system, demonstrating its successful integration of software intelligence, hardware functionality, and user-centric design. The core of the system's success lies in its high-precision deep learning models, with the final EfficientNetV2-B3 architecture achieving exceptional accuracies of 98% for ripeness classification and 99% for bruise detection. Through extensive benchmarking, modern CNNs like EfficientNet were proven superior, offering an optimal balance of accuracy and computational efficiency. For physical attribute measurement, an object detection method (Faster R-CNN) was established as the most

2346

## 6.8 Summary

2347

This chapter presents a comprehensive evaluation of the automated mango grading and sorting system, demonstrating its successful integration of software intelligence, hardware functionality, and user-centric design. The core of the system's success lies in its high-precision deep learning models, with the final EfficientNetV2-B3 architecture achieving exceptional accuracies of 98% for ripeness classification and 99% for bruise detection. Through extensive benchmarking, modern CNNs like EfficientNet were proven superior, offering an optimal balance of accuracy and computational efficiency. For physical attribute measurement, an object detection method (Faster R-CNN) was established as the most

2348

2349

2350

2351

2352

2353

2354



2355 reliable technique for determining mango size, significantly outperforming a traditional  
2356 computer vision approach. The system's practical validity was further confirmed through a  
2357 comparative analysis with a human expert, achieving a 79% agreement rate, which accounts  
2358 for the inherent subjectivity of manual grading. This robust software is embodied in a  
2359 functional physical prototype that evolved into a refined version with an efficient conveyor  
2360 system and a fully enclosed, three-way sorting mechanism that accurately directs mangoes  
2361 into designated grades. Controlling this hardware is an intuitive software application on the  
2362 Raspberry Pi, featuring a user-friendly interface that allows for custom priority weighting of  
2363 mango characteristics and includes comprehensive error handling and data logging. Overall,  
2364 the results conclusively show that the research has successfully bridged the gap between  
2365 theoretical model development and a practical, deployable system capable of automatically  
2366 and accurately grading Carabao mangoes based on customizable, user-defined standards.  
2367



Listing 6.2: Getting Size through Foreground Masking part 2

```

1  image = cv2.imread(thresh_path)
2  if image is None:
3      print(f"Error: Unable to read threshold image {thresh_
4          filename}")
5      return 0, 0
6
7  gray = cv2.cvtColor(image, cv2.COLOR_BGR2GRAY)
8  gray = cv2.GaussianBlur(gray, (7, 7), 0)
9  edged = cv2.Canny(gray, 50, 100)
10 edged = cv2.dilate(edged, None, iterations=1)
11 edged = cv2.erode(edged, None, iterations=1)
12
13 cnts = cv2.findContours(edged.copy(), cv2.RETR_EXTERNAL, cv2.
14     CHAIN_APPROX_SIMPLE)
15 cnts = imutils.grab_contours(cnts)
16
17 # If no contours found, return zero dimensions
18 if not cnts:
19     return 0, 0
20
21 # Find the largest contour by area
22 largest_contour = max(cnts, key=cv2.contourArea)
23
24 # Only process if the contour area is significant enough
25 if cv2.contourArea(largest_contour) < 100:
26     return 0, 0
27
28 # Process the largest contour
29 box = cv2.minAreaRect(largest_contour)
30 box = cv2.boxPoints(box)
31 box = np.array(box, dtype="int")
32 box = imutils.perspective.order_points(box)
33 (tl, tr, br, bl) = box
34
35 pixel_width = dist.euclidean(tl, tr)
36 pixel_length = dist.euclidean(tr, br)
37 real_width = calculate_real_world_dimension(pixel_width,
38     DISTANCE_CAMERA_TO_OBJECT, FOCAL_LENGTH_PIXELS)
39 real_length = calculate_real_world_dimension(pixel_length,
40     DISTANCE_CAMERA_TO_OBJECT, FOCAL_LENGTH_PIXELS)
41
42 return real_width, real_length
43
44 except Exception as e:
45     print(f"Error in calculate_size: {e}")
46     return 0, 0

```



Listing 6.3: Initializing the Calibration Box

```

1 def __init__(self, model_path, num_classes=7):
2     self.device = torch.device('cuda' if torch.cuda.is_available() else
3                               'cpu')
4     self.model = self.load_model(model_path, num_classes)
5
6     self.class_names = {
7         1: 'bruised', 2: 'not_bruised', 3: 'yellow',
8         4: 'green_yellow', 5: 'green', 6: 'mango', 7: 'background'
9     }
10    # coin object reference
11    self.reference_box = [815, 383, 999, 556]
12    # Known size of reference object in cm
13    self.reference_size_cm = 2.4

```

Listing 6.4: Sorting the Mangoes

```

1 if ave_letter.upper() == 'A':
2     button_state_array = [0, 1, 0, 0]
3     print(button_state_array)
4     self.sort.set_motors(button_state_array)
5 elif ave_letter.upper() == 'B':
6     button_state_array = [1, 0, 1, 0]
7     print(button_state_array)
8     self.sort.set_motors(button_state_array)
9 elif ave_letter.upper() == 'C':
10    button_state_array = [1, 0, 0, 1]
11    print(button_state_array)
12    self.sort.set_motors(button_state_array)

```



2368      **Chapter 7**

2369      **CONCLUSIONS, RECOMMENDATIONS, AND**  
2370      **FUTURE DIRECTIVES**



## 2371 **7.1 Concluding Remarks**

2372 In this Thesis, the prototype is successful in grading and sorting Carabao mangoes based  
2373 on the user priority and machine learning algorithm. More specifically, the prototype is  
2374 successful in classifying Carabao mangoes based on ripeness (Green, Green Yellow, and  
2375 Yellow), size (Large, Medium, Small), and bruises (bruised and not bruised).

### 2376 **7.1.1 Objectives Achieved**

#### 2377 **7.1.1.1 GO: To develop a user-priority-based grading and sorting system 2378 for Carabao mangoes, using machine learning and computer vision 2379 techniques to assess ripeness, size, and bruises.**

2380 For GO, the study successfully developed a user-priority-based grading and sorting system  
2381 for Carabao mangoes by integrating machine learning and computer vision techniques to  
2382 assess ripeness, size, and bruises. The system achieved high accuracy and reliability while  
2383 maintaining a non-destructive process through its hardware and software integration using  
2384 a Raspberry Pi platform.

#### 2385 **7.1.1.2 SO1: To make an image acquisition system with a conveyor belt for 2386 automatic sorting and grading mangoes.**

2387 For SO1, the researchers designed and implemented an automated image acquisition system  
2388 consisting of a Raspberry Pi 4, camera module, LED lighting, and a conveyor belt, which  
2389 ensured consistent lighting and image alignment necessary for precise visual analysis and  
2390 classification.



2391     **7.1.1.3 SO2: To get the precision, recall, F1 score, confusion matrix, and**  
2392       **train and test accuracy metrics for classifying the ripeness and**  
2393       **bruises with an accuracy score of at least 90%.**

2394     For SO2, multiple models were trained and evaluated, with EfficientNetV2 achieving  
2395       precision, recall, and F1 scores of approximately 0.98 and accuracy above 98%, which  
2396       surpassed the target performance threshold and validating the effectiveness of the selected  
2397       machine learning architecture.

2398     **7.1.1.4 SO3: To create a microcontroller-based system to operate the im-**  
2399       **age acquisition system, control the conveyor belt, and process the**  
2400       **mango images through machine learning.**

2401     For SO3, a microcontroller-driven setup using the Raspberry Pi was developed to syn-  
2402       chronize conveyor movement, image capture, and data processing, demonstrating a fully  
2403       automated and self-contained embedded system capable of real-time classification.

2404     **7.1.1.5 SO4: To grade mangoes based on user priorities for size, ripeness,**  
2405       **and bruises.**

2406     For SO4, the grading module incorporated a linear weighting formula that allowed users  
2407       to assign priority values to ripeness, bruises, and size, effectively producing customizable  
2408       grading outcomes that reflected user-defined criteria and market standards.



2409     **7.1.1.6 SO5: To classify mango ripeness based on image data using ma-**  
2410         **chine learning algorithms such as kNN, k-mean, and Naïve Bayes.**

2411     For SO5, various algorithms were implemented and tested, with CNN-based Efficient-  
2412         NetV2 outperforming traditional classifiers, achieving 98% accuracy in categorizing mango  
2413         ripeness into green, yellow-green, and yellow stages based on color and texture features.

2414     **7.1.1.7 SO6: To classify mango size based on image data by getting its**  
2415         **length and width using OpenCV, geometry, and image processing**  
2416         **techniques.**

2417     For SO6, the system utilized OpenCV for contour extraction and geometric calculations,  
2418         and Faster R-CNN for object detection, resulting in an average deviation of 13.57% in  
2419         length and 3.24% in width from ground-truth measurements, indicating reliable dimensional  
2420         estimation.

2421     **7.1.1.8 SO7: To classify mango bruises based on image data by employing**  
2422         **machine learning algorithms.**

2423     For SO7, the implemented CNN models effectively detected and classified visible surface  
2424         bruises, achieving a 99% accuracy rate and demonstrating robustness in identifying varying  
2425         bruise intensities under controlled lighting conditions.

2426     

## 7.2 Contributions

2427     The contributions of each group member are as follows:



- 2428 • BANAL Kenan A.: Scrum Master (Project manager in charge of the hardware  
2429 and software integration, assisted in mango size determination, incharge of dataset  
2430 collection and data augmentation)
- 2431 • BAUTISTA Francis Robert Miguel F.: Front End Engineer (UI/UX Designer in  
2432 charge of software interface and hardware assistant of the Scrum Master, assisted in  
2433 dataset splitting, categorization and collection)
- 2434 • HERMOSURA Don Humphrey L. : Back End Engineer (in charge of mango size  
2435 determination, assisted in machine learning algorithm)
- 2436 • SALAZAR Daniel G.: Product Engineer (Software Engineer in charge of training  
2437 and testing of the machine learning algorithm, assisted in dataset collection and data  
2438 augmentation)

### 2439 **7.3 Recommendations**

2440 The researchers recommend that the prototype be improved in the optimization of the  
2441 machine learning algorithm and the hardware design. The researchers also recommend that  
2442 the prototype be tested in the actual grading and sorting of Carabao mangoes in the market.

### 2443 **7.4 Future Prospects**

2444 Future researchers may consider the following recommendations for future work:

- 2445 1. User testing of the prototype in the actual grading and sorting of Carabao mangoes  
2446 in the Philippine market.



- 2447      2. Additional of weight measurement to the prototype to improve the grading and sorting of Carabao mangoes.
- 2448
- 2449      3. Integration of a custom PCB to improve the hardware design of the prototype.



## REFERENCES

- 2451 Abbas, Q., Niazi, S., Iqbal, M., and Noureen, M. (2018). Mango Classification Using Texture &  
2452 Shape Features. *IJCSNS International Journal of Computer Science and Network Security*, 18(8).
- 2453 Abu, M., Olympio, N. S., and Darko, J. O. (2021). Determination of Harvest Maturity for Mango  
2454 Mangifera indica L. Fruit by Non-Destructive Criteria. *Agricultural Sciences*, 12(10):1103–1118.
- 2455 Adam, J. A. P., Dato, K. S., Impelido, M. C. D., Tobias, R. G., and Pilueta, N. U. (2022). Non-  
2456 destructive microcontroller-based carabao mango ripeness grader. Far Eastern University (FEU)  
2457 College of Engineering.
- 2458 Alejandro, A. B., Gonzales, J. P., Yap, J. P. C., and Linsangan, N. B. (2018). Grading and sorting of  
2459 Carabao mangoes using probabilistic neural network. Bandung, Indonesia.
- 2460 Amna, M. W. A., Guiqiang, L., and Muhammad Zuhair AKRAM, M. F. (2023). Machine vision-  
2461 based automatic fruit quality detection and grading. *Frontiers of Agricultural Science and*  
2462 *Engineering*.
- 2463 Badali, A. P., Zhang, Y., Carr, P., Thomas, P. J., and Hornsey, R. I. (2005). Scale factor in digital  
2464 cameras. *Vision Sensor Laboratory, York University / Topaz Technology Inc. (via ResearchGate)*.  
2465 Discusses the relation between object size and image size via scale factor.
- 2466 Bayogan, E. R. and Secretaria, L. (2019). Enhancing mango fruit quality in asian mango chains:  
2467 Case study – the philippines. Technical report, Australian Centre for International Agricultural  
2468 Research (ACIAR), Canberra, Australia.
- 2469 Bureau of Agriculture and Fisheries Product Standards (2004). Philippine national standard:  
2470 Fresh fruits – mangoes – specification. Technical Report PNS/BAFPS 13:2004, Department  
2471 of Agriculture, Manila, Philippines. Philippine National Standard for Fresh Fruits – Mangoes  
2472 (Mangifera indica Linn.).
- 2473 Bureau of Agriculture and Fisheries Product Standards (2006). Illustrative guide for the philippine  
2474 national standard (pns/bafps 13:2004) – mangoes. Technical report, Department of Agricul-  
2475 ture, Manila, Philippines. Supplementary visual guide for PNS/BAFPS 13:2004, detailing  
2476 classification, defects, and grading criteria for fresh mangoes.
- 2477 Centino, M. F., Castano, M. C. N., and Ebo, J. B. F. (2020). The Current Status of Philippine Mango  
2478 in the Global Value Chain.
- 2479 Chakraborty, S. K., Subeesh, A., Dubey, K., Jat, D., Chandel, N. S., Potdar, R., Rao, N. G., and  
2480 Kumar, D. (2023). Development of an optimally designed real time automatic citrus fruit grading-  
2481 sorting machine leveraging computer vision-based adaptive deep learning model. *Engineering*  
2482 *Applications of Artificial Intelligence*, 120:105826.
- 2483 D'Adamo, G. (2018). The determinants of export quality in the euro area. *Quarterly Report on the*  
2484 *Euro Area (QREA)*, 17(1):23–31. Publisher: Directorate General Economic and Financial Affairs



- 2485 (DG ECFIN), European Commission.
- 2486 de Souza-Pollo, A. and de Goes, A. (2009). Fruit diseases. In Litz, R. E., editor, *The Mango: Botany, Production and Uses*, pages 169–190. CABI Publishing. Covers descriptions of mango diseases including anthracnose, stem-end rot, etc.
- 2488
- 2489 Goodfellow, I., Bengio, Y., and Courville, A. (2016). *Deep Learning*. MIT Press. <http://www.deeplearningbook.org>.
- 2490
- 2491 Guillergan, G., Sabay, R., Madrigal, D., and Bual, J. (2024). Naive Bayes Classifier in Grading Carabao Mangoes. *Technium: Romanian Journal of Applied Sciences and Technology*, 22:14–32.
- 2492
- 2493 Guillermo, M. C. S., Naciongayo, D. S., and Galela, M. G. C. (2019). Determining ‘Carabao’ Mango Ripeness Stages Using Three Image Processing Algorithms.
- 2494
- 2495 Guo, C. and et al. (2024). Cross entropy versus label smoothing: A neural collapse perspective. *arXiv preprint*.
- 2496
- 2497 Howard, A. G., Zhu, M., Chen, B., Kalenichenko, D., Wang, W., Weyand, T., Andreetto, M., and Adam, H. (2017). Mobilenets: Efficient convolutional neural networks for mobile vision applications.
- 2498
- 2499
- 2500 Huang, G., Liu, Z., Van Der Maaten, L., and Weinberger, K. Q. (2017). Densely connected convolutional networks. In *2017 IEEE Conference on Computer Vision and Pattern Recognition (CVPR)*, pages 2261–2269.
- 2501
- 2502
- 2503 Huang, G., Sun, Y., Liu, Z., Sedra, D., and Weinberger, K. Q. (2016). Deep networks with stochastic depth. In *European conference on computer vision*, pages 646–661. Springer.
- 2504
- 2505 Hussein, B. M. and Shareef, S. M. (2024). An empirical study on the correlation between early stopping patience and epochs in deep learning. *ITM Web of Conferences*, 64(12):01003.
- 2506
- 2507 Kadam, J., Shimpi, S., Biradar, R., and Chate, S. (2002). Review on post harvest diseases and management of mango fruits. *J. Plant Pathol. Microbiol*, 13:1000635.
- 2508
- 2509 Knight, R. J. J., Campbell, R. J., and Maguire, I. (2009). *Important Mango Cultivars and their Descriptors*. CAB International, Wallingford, UK.
- 2510
- 2511 Krizhevsky, A., Sutskever, I., and Hinton, G. E. (2012). Imagenet classification with deep convolutional neural networks. In *Proceedings of the 25th International Conference on Neural Information Processing Systems (NIPS 2012)*, pages 1097–1105. Curran Associates, Inc.
- 2512
- 2513
- 2514 Lacap, A., Bayogan, E. R., Secretaria, L., Joyce, D., Ekman, J., and Goldwater, A. (2021). Bruise Injury and Its Effect on ‘Carabao’ Mango Fruit Quality. *Philippine Journal of Science*, 150(6B).
- 2515
- 2516 Lee, S., Moon, G., Lee, C., Kim, H., An, D., and Kang, D. (2024). Check-qzp: A lightweight checkpoint mechanism for deep learning frameworks. *Applied Sciences*, 14(19):8848.
- 2517
- 2518 Loshchilov, I. and Hutter, F. (2016). Sgdr: stochastic gradient descent with warm restarts. *arXiv preprint arXiv:1608.03983*.
- 2519
- 2520 Loshchilov, I. and Hutter, F. (2017). Decoupled weight decay regularization. *arXiv preprint*



- 2521                  *arXiv:1711.05101.*
- 2522                  Ltd, H. A. (2007). Status of mango postharvest disease management: Options and solutions for the  
2523                  australian mango industry. Technical report. Includes description of Dendritic Spot symptoms,  
2524                  epidemiology, and post-harvest behavior.
- 2525                  Markidis, S. and et al. (2018). Nvidia tensor core programmability, performance & precision. *IEEE  
2526                  International Symposium on High Performance Computer Architecture (HPCA) Proceedings.*
- 2527                  Migacz, S. (2020). Performance tuning guide. PyTorch Tutorials Documentation. Accessed [Date  
2528                  of access would normally be provided, but must be excluded per source constraints.].
- 2529                  Moens, V. (2024). A guide on good usage of non\_blocking and pin\_memory() in pytorch. PyTorch  
2530                  Tutorials Documentation. Accessed [Date of access would normally be provided, but must be  
2531                  excluded per source constraints.].
- 2532                  Nguyen, T. M. (2015). Lenticel damage on 'b74' mango fruit. PhD thesis, UQ eSpace. Details on  
2533                  lenticel discoloration symptoms and post-harvest effects.
- 2534                  Patel, K. K., Khan, M. A., Kumar, Y., and Yadav, A. K. (2019). Novel Techniques in Post Harvest  
2535                  Management of Mango- An Overview. *South Asian Journal of Food Technology and Environment*,  
2536                  05(02):821–835.
- 2537                  Paul, R. E. (1993). Postharvest physiology of mango fruit. *University of Hawaii Free Publications*.  
2538                  Mentions sapburn injury as a major post-harvest disorder.
- 2539                  Perez, L. and Wang, J. (2017). The effectiveness of data augmentation in image classification using  
2540                  deep learning.
- 2541                  Philippine Statistics Authority (2023). Major fruit crops quarterly bulletin, april-june 2023. <https://psa.gov.ph/content/major-fruit-crops-quarterly-bulletin-april-june-2023-0>.
- 2542
- 2543                  Richter, M. L., Shenk, J., Byttner, W., Arpteg, A., and Huss, M. (2020). Feature space saturation  
2544                  during training. *arXiv preprint arXiv:2006.08679*. Published in proceedings of ICANN 2021.
- 2545                  Rizwan Iqbal, H. M. and Hakim, A. (2022). Classification and Grading of Harvested Mangoes  
2546                  Using Convolutional Neural Network. *International Journal of Fruit Science*, 22(1):95–109.
- 2547                  Samaniego Jr., L., De Jesus, L. C., Apostol, J., Betonio, D., Medalla, J. D., Peruda Jr., S., Brucal,  
2548                  S. G., and Yong, E. (2023). Carabao mango export quality checker using matlab image processing.  
2549                  *International Journal of Computing Sciences Research*, 7:2080–2094.
- 2550                  Schulze, K., Nagle, M., Spreer, W., Mahayothee, B., and Müller, J. (2015). Development and  
2551                  assessment of different modeling approaches for size-mass estimation of mango fruits (*mangifera  
2552                  indica* l, cv. 'nam dokmai'). *Computers and Electronics in Agriculture*, 114:269–276.
- 2553                  Scott Ledger, R. H. and Cooke, T. (2000). Mango defect guide. Infographic. From Queensland  
2554                  Government, Department of Primary Industries and Fisheries . Published in collaboration with  
2555                  the Australian Mango Industry Association (AMIA) and Horticulture Australia Limited (HAL).  
2556                  Licensed under CC BY 4.0.



- 2557 Shorten, C. and Khoshgoftaar, T. M. (2019). A survey on image data augmentation for deep learning.  
 2558     *Journal of Big Data*, 6(60):1–48.
- 2559 Simonyan, K. and Zisserman, A. (2015). Very deep convolutional networks for large-scale image  
 2560     recognition.
- 2561 Supekar, A. D. and Wakode, M. (2020). Multi-Parameter Based Mango Grading Using Image  
 2562     Processing and Machine Learning Techniques. *INFOCOMP Journal of Computer Science*,  
 2563     19(2):175–187. Number: 2.
- 2564 Szegedy, C., Vanhoucke, V., Ioffe, S., Shlens, J., and Wojna, Z. (2016). Rethinking the inception  
 2565     architecture for computer vision. In *Proceedings of the IEEE Conference on Computer Vision  
 2566     and Pattern Recognition*, pages 2818–2826.
- 2567 Tai, N. D., Lin, W. C., Trieu, N. M., and Thinh, N. T. (2024). Development of a mango-grading and  
 2568     -sorting system based on external features, using machine learning algorithms. *Agronomy*, 14(4).
- 2569 Tan, M. and Le, Q. (2019). EfficientNet: Rethinking model scaling for convolutional neural  
 2570     networks. In Chaudhuri, K. and Salakhutdinov, R., editors, *Proceedings of the 36th International  
 2571     Conference on Machine Learning*, volume 97 of *Proceedings of Machine Learning Research*,  
 2572     pages 6105–6114. PMLR.
- 2573 Tan, M. and Le, Q. V. (2021). Efficientnetv2: Smaller models and faster training. In *Proceedings of  
 2574     the 38th International Conference on Machine Learning*, volume 139 of *PMLR*, pages 10096–  
 2575     10106. PMLR.
- 2576 Tomas, M. C., Celino, J. P. L., Escalambre, I. E., and Secreto, B. P. (2022). Detection of Overall  
 2577     Fruit Maturity of Local Fruits Using Support Vector Machine through Image Processing. In *2022  
 2578     12th International Conference on Software Technology and Engineering (ICSTE)*, pages 96–102.
- 2579 Veling, P. S. (2019). Mango Disease Detection by using Image Processing. *International Journal  
 2580     for Research in Applied Science and Engineering Technology*, 7(4):3717–3726.
- 2581 Zheng, B. and Huang, T. (2021). Mango Grading System Based on Optimized Convolutional Neural  
 2582     Network. *Mathematical Problems in Engineering*.



De La Salle University

2584

## **Appendix A STUDENT RESEARCH ETHICS CLEARANCE**

2585

A. Student Research Ethics Clearance



De La Salle University

2586

RESEARCH ETHICS CLEARANCE FORM <sup>1</sup> For Thesis Proposals	
<b>Names of Student Researcher(s):</b> BANAL, Kenan A. BAUTISTA, Francis Robert Miguel F. HERMOSURA, Don Humphrey L. SALAZAR, Daniel G	
<b>College:</b> GCOE	
<b>Department:</b> ECE	
<b>Course:</b> Computer Engineering	
<b>Expected Duration of the Project:</b> from: January 4 2025 to: January 4 2026	
<b>Ethical considerations</b>  (The <a href="#">Ethics Checklists</a> may be used as guides in determining areas for ethical concern/consideration)	
 <b>To the best of my knowledge, the ethical issues listed above have been addressed in the research.</b>  Dr. Reggie C. Gustilo	
<b>Name and Signature of Adviser/Mentor:</b> <b>Date:</b> February 5, 2025  Dr. Argel Bandala	
<b>Name and Signature of the Department Chairperson:</b> <b>Date:</b> February 6, 2025	

<sup>1</sup> The same form can be used for the reports of completed projects. The appropriate heading need only be used.



De La Salle University

2587

## **Appendix B REVISIONS TO THE PROPOSAL**

2588

## B. Revisions to the Proposal



**De La Salle University**

2589

### PRO1 Panel Comments and Revisions – Appendix Z

#### PRO1 Panel Comments and Revisions

Zoom Recording:

[https://zoom.us/rec/share/mrn9zBtPz3bJ5laVcy2E8-iBno8A6fBRgOCacMrhmzLPCNO0IDxXBHiK\\_xzdicEb.MzbHGzrD7rL3tVgJ?startTIme=1731326444000](https://zoom.us/rec/share/mrn9zBtPz3bJ5laVcy2E8-iBno8A6fBRgOCacMrhmzLPCNO0IDxXBHiK_xzdicEb.MzbHGzrD7rL3tVgJ?startTIme=1731326444000)

Passcode: +7qL6DZE

Panelist's Comments and Revisions	Action Taken	Page Number
Capture both two sides of the mango and not just one to remove error	The image capturing system would only capture the two sides of the mango which are the two largest surface areas of the skin.	18
How will you get large dataset with sweetness and how will you classify it?	Remove Sweetness in the SO	13
Size and weight are not the same.	Remove Weight in objectives but retained size in the SO4 and SO6	
Specify in the specific objectives that it will be automatic sorting	SO1: To make an image acquisition system with a conveyor belt for automatic sorting and grading mangoes.	13
Add what process will be used to get the size classification	SO6: To classify mango size by getting its length and width using OpenCV, geometry, and image processing techniques	13
Add what process the ripeness classification will be	SO5: To classify mango ripeness using kNN or nearest neighbors algorithm	13
Get rid of texture in the general objectives	Texture is removed in the SOs	13
Get rid of CNN in general objectives and replace with machine learning	CNN is removed and replaced with machine learning GO: To develop a user-priority-based grading and sorting system for Carabao mangoes, using machine learning to assess ripeness, size, and bruises.	13
Remove Raspberry Pi on the SO's and generalize to "to create a microcontroller based application"	SO3: To create a microcontroller application to operate and control the prototype.	13
Remove SO4. No need for user testing	Removed user test and the new SO4 is SO4: To grade mangoes based on user priorities for size, ripeness, and bruises.	13
Fix IPO to the correct input and output	Input: Two side image of the Carabao Mango and the User Priority Attributes Process: Machine Learning Algorithm, Grading Formula, and CNN model using a microcontroller Output: Size, Ripeness, and Bruises	20

## B. Revisions to the Proposal



# De La Salle University

2590

### PRO1 Panel Comments and Revisions – Appendix Z

	Classification with its Overall Grade	
Define bruises	The black or brown area of the mango that is visible on the skin of the mango.	6
Dataset should use at least 10,000 images	Added to expected deliverables SO2: To use a publicly available dataset of at least 10,000 mango images for classification of ripeness, and bruises.	14
Add to specific objectives the percentage accuracy	SO2: To get the precision, recall, F1 score, confusion matrix, and train and test accuracy metrics for classifying the ripeness and bruises with an accuracy score of at least 90%.	14
Weight sensor just adds complexity	removed all mention of load sensor, load cell. removed load cell methodology	39,40,41, 42,43,44 previousl y



2591

## PRO1 Panel Comments and Revisions – Appendix Z

### PRO1 Panel Comments and Revisions

Zoom Recording:

[https://zoom.us/rec/share/mrn9zBtPz3bJ5laVcy2E8-iBno8A6fBRgOCacMrhmzLPCNO0IDxXBHiK\\_xzdicEb.MzbHGzrD7rL3tVgJ?startTim=e=1731326444000](https://zoom.us/rec/share/mrn9zBtPz3bJ5laVcy2E8-iBno8A6fBRgOCacMrhmzLPCNO0IDxXBHiK_xzdicEb.MzbHGzrD7rL3tVgJ?startTim=e=1731326444000)

Passcode: +?qL6DZE

Summary:

- Specific Objectives
- Add:
  - what process will be used to get the sweetness classification
  - what process the ripeness classification will be
  - what process will be used to get the size classification
  - Specify in the specific objectives that it will be automatic sorting
- Remove:
  - get rid of texture in the general objectives
  - get rid of cnn in general objectives and replace with machine learning
  - remove Raspberry Pi on the SO's and generalize to "to create a microcontroller based application"
  - remove SO4. No need for user testing

Comments:

\*[00-00] time stamps from recording

- [15:00] Why only the top side of the mango? Isn't the point of automation to reduce human error? Then what about the bottom side wouldn't that just introduce another error if the mango happens to have defects on the bottom?
- [16:09] What is the load cell for? Size is not the same as weight. If size is taken from the weight wouldn't size be also taken from the image. If size then adding a load cell would just introduce more complexity, if weight then load cell is fine. reminder that size is not the same as weight.
- [17:36] When computer vision, state input and output parameters. Output parameters in this case would be sweetness, ripeness, size and bruising. Input parameters would be images.
- [18:12] No mention of how the dataset would be gathered. Would you be gather your own dataset or using a publicly available dataset
- [21:38] Fix IPO based on mention input and output parameters.
- [21:50] Dataset is lacking. Usually in machine learning at least 10,000 images. can take more than one image per mango. after taking an image of mango can make more out of the image using data augmentations.
- [22:48] Add to specific Objectives the mentioned 80%
- [23:09] Consultant that would grade the mangoes as a third party to remove biases. For both the testing and the training
- [24:55] How do you detect the sweetness of mangoes? Add these to the specific objectives. What are the categories of sweetness? Add these to specific objectives. How do



2592

### PRO1 Panel Comments and Revisions – Appendix Z

you detect the correct categorization of sweetness? How to automate the classification of the sweetness.

- [33:10] Why is the dataset destructive but the testing non destructive? Clarify this further to avoid confusion.
- [35:09] What is the basis of sweetness using images? Clarify this further.
- [35:35] How would you know if the classifier is correct or not? What is your ground truth (for the sweetness)?
- [38:55] When can you say you are getting the top side of the mango? How would you know if the mango images showing the top side or the bottom side of both cheeks of the mango can be captured? If it doesn't matter then any side can be captured so why is it in the limitations that only the top side can be captured. Clarify the limitations.
- [48:10] What classifier would you use here? What features would you extract from the images?
- [52:07] Does it explain what process will be used to get the sweetness classification? Add it to the specific objectives
- [54:00] How will ripeness be classified? Will it use the same dataset as the sweetness classification did? How was ground truth obtained?
- [55:44] Why not the nearest neighbor? It is more fit in this scenario. Do not specify CNN in the objectives. The embedded systems as well, do not specify the Raspberry pi unless truly sure
- [57:30] Table is just image processing. Is there a specific objective that would describe how ripeness classification will be done? Add this to the specific objectives.
- [59:10] How is the weight obtained? Add it to the specific objectives. Remember that size is not proportional to weight. Size could be obtained from the image as the camera is from a fixed distance. Add to specific objectives how to get the size
- [1:00:00] get rid of texture in the general objectives. get rid of cnn in general objectives and replace with machine learning. as each parameter will use a different method.
- [1:04:00] remove Raspberry Pi on the SO's and generalize to "to create a microcontroller based application"
- [1:04:37] remove SO4. no more user testing
- [1:05:00] The formula used for grading the mangoes, is this used as industry standard? How do they measure the export quality of mango
- [1:07:00] Specify in the specific objectives that it will be automatic sorting

Here are my comments on my end :)

1. Ensure seamless integration between hardware (sensors, motors, etc.) and software (CNNs, Raspberry Pi). You can consider using a modular approach for easier troubleshooting.
2. How do you gather a comprehensive and diverse dataset for training your CNN. This will enhance the model's robustness and accuracy.
3. Make sure that the weight sensors are calibrated correctly to avoid measurement errors.

## B. Revisions to the Proposal



# De La Salle University

2593

### PRO1 Panel Comments and Revisions – Appendix Z

4. Implement data augmentation techniques to enhance your image dataset, which can improve model generalization and accuracy.
5. Design an intuitive user interface for the Raspberry Pi application.
6. Besides precision, recall, and F1 score, consider incorporating confusion matrices to better understand model performance and error types.
7. Conduct user testing of the application to gather feedback on usability and functionality. This can lead to improvements in design and user experience. Consider how the system can be scaled or adapted for different fruits or larger processing volumes in the future.

Noted by:

  
\_\_\_\_\_  
**Dr. Donabel de Veas Abuan**  
*Chair of Panel*

Date: November 11 2024

---

Note: Keep a copy of this Appendix. It is a requirement that has to be submitted in order to qualify for PRO3 Defense.



De La Salle University

2594

## **Appendix C REVISION TO THE FINAL**

2595



2596

## Thesis Revisions Form – Appendix P



De La Salle University  
 Gokongwei College of Engineering  
 Department of Electronics & Computer Engineering

**PANEL RECOMMENDATIONS PRIOR TO APPROVAL**

TITLE: Non-Destructive Carabao Mango Sorter and Grader based on Physical Characteristics using Machine Learning

Time & Date of Defense: November 8, 2025 Venue of Defense: AG1103

**Revisions:**

Area of Thesis	Comments from Panel	Required Changes / Additions
Objective & Ground Truth	Panel noted confusion on the <i>basis of mango size classification</i> (small/medium/large). Ground truth was unclear.	Clearly define the ground truth reference for mango sizing. State whether classification is based on area, pixel count, bounding box dimensions, or physical calibration (e.g., coin reference).
Size Categorization	Ambiguity in how small, medium, and large are determined. Boundaries between categories not well defined, leading to possible misclassification.	Provide numerical thresholds or ranges for each category (e.g., area in cm <sup>2</sup> or pixel count). Justify with official references or calibration experiments.
Bounding Box vs. Actual Area	Panel highlighted errors when bounding box area was used (includes background pixels, not just mango).	Revise methodology to use segmented mango area instead of bounding box area. Explain error margins and how segmentation reduces misclassification.
Calibration Method	Use of "piso" (coin) as reference was questioned—panel asked what its connection is to mango sizing.	Clarify calibration method. If using coin reference, explain rationale and accuracy. Otherwise, replace with standardized calibration object or direct measurement.
Consistency of Measurement	Inconsistencies noted in how pixel/area measurements were applied.	Ensure consistent measurement approach across all samples. Document error analysis and tolerance levels.



2597

## Thesis Revisions Form – Appendix P

AI vs. Traditional Methods	Panel stressed that AI (YOLO, CNN) is only for detection/tracking, not for actual size measurement.	Revise methodology section: separate AI detection (classification) from size measurement (OpenCV/area computation). Remove claims that CNN/YOLO directly measure size.
Reference to Prior Work	Panel mentioned earlier works as more accurate.	Add a related works section comparing your method with prior studies. Highlight improvements and justify differences.
Color Space & Image Processing	RGB-only processing criticized; suggested conversion to other color spaces (HSV, HSB, etc.) for better segmentation.	Add experiments using HSV/HSB color space for mango segmentation. Document improvements in accuracy.
Error Analysis	Panel emphasized large errors at category boundaries (small ↔ medium, medium ↔ large).	Include error analysis section: quantify misclassification rates at boundaries, propose tolerance margins.
Methodology Documentation	Panel noted missing or unclear steps in methodology (bounding box drawing, pixel extraction, calibration).	Rewrite methodology with step-by-step workflow: detection → segmentation → area measurement → classification. Include diagrams or flowcharts.
Mechanical/Practical Considerations	Mention of conveyor movement and mechanical variation affecting classification.	Add discussion on how the conveyors and sorter position the mangoes.
Final Recommendation	Panel said AI part is acceptable, but sizing concept is the core issue.	Strengthen sizing methodology section. AI classification can remain, but emphasize accurate sizing as the thesis' main contribution.

**Dr. Donabel de Veas Abuan, Ph.D. ECE**  
*Chair of the Panel of Examiners*



De La Salle University

2598

## **Appendix D QUESTIONNAIRE TO THE EXPERT**

2599



2600

## Comparative Analysis: Expert's Assessment

Please fill up the following information.

Full Name: \_\_\_\_\_

Years of Experience: \_\_\_\_\_

Current Role/Position: \_\_\_\_\_

Address of Farm: \_\_\_\_\_ Hectares: \_\_\_\_\_

Mango Varieties Familiar With: \_\_\_\_\_

Experience with Quality Standards: \_\_\_\_\_

Date of Analysis: \_\_\_\_\_

Instructions: Your task is to categorize the mangoes based on its color and bruising. Each image will have checkboxes pertaining to the category. More specifically categorize the mango's color into yellow, yellow-green, and green. And the bruises category into bruised and non-bruised.

---

Name & Signature



2601



Skin Color/Ripeness:

- Yellow
- Yellow-green
- Green
- Bruising:
- Bruised
- Non-Bruised



Skin Color/Ripeness:

- Yellow
- Yellow-green
- Green
- Bruising:
- Bruised
- Non-Bruised



Skin Color/Ripeness:

- Yellow
- Yellow-green
- Green
- Bruising:
- Bruised
- Non-Bruised



Skin Color/Ripeness:

- Yellow
- Yellow-green
- Green
- Bruising:
- Bruised
- Non-Bruised



Skin Color/Ripeness:

- Yellow
- Yellow-green
- Green
- Bruising:
- Bruised
- Non-Bruised

Skin Color/Ripeness:

- Yellow
- Yellow-green
- Green
- Bruising:
- Bruised
- Non-Bruised



2602



Skin Color/Ripeness:

- Yellow
- Yellow-green
- Green
- Bruising:
- Bruised
- Non-Bruised



Skin Color/Ripeness:

- Yellow
- Yellow-green
- Green
- Bruising:
- Bruised
- Non-Bruised



Skin Color/Ripeness:

- Yellow
- Yellow-green
- Green
- Bruising:
- Bruised
- Non-Bruised



Skin Color/Ripeness:

- Yellow
- Yellow-green
- Green
- Bruising:
- Bruised
- Non-Bruised



Skin Color/Ripeness:

- Yellow
- Yellow-green
- Green
- Bruising:
- Bruised
- Non-Bruised

Skin Color/Ripeness:

- Yellow
- Yellow-green
- Green
- Bruising:
- Bruised
- Non-Bruised



2603



Skin Color/Ripeness:

- Yellow
- Yellow-green
- Green
- Bruising:
- Bruised
- Non-Bruised

Skin Color/Ripeness:

- Yellow
- Yellow-green
- Green
- Bruising:
- Bruised
- Non-Bruised



Skin Color/Ripeness:

- Yellow
- Yellow-green
- Green
- Bruising:
- Bruised
- Non-Bruised

Skin Color/Ripeness:

- Yellow
- Yellow-green
- Green
- Bruising:
- Bruised
- Non-Bruised



Skin Color/Ripeness:

- Yellow
- Yellow-green
- Green
- Bruising:
- Bruised
- Non-Bruised

Skin Color/Ripeness:

- Yellow
- Yellow-green
- Green
- Bruising:
- Bruised
- Non-Bruised



2604



Skin Color/Ripeness:

- Yellow
  - Yellow-green
  - Green
- Bruising:
- Bruised
  - Non-Bruised

Skin Color/Ripeness:

- Yellow
  - Yellow-green
  - Green
- Bruising:
- Bruised
  - Non-Bruised



Skin Color/Ripeness:

- Yellow
  - Yellow-green
  - Green
- Bruising:
- Bruised
  - Non-Bruised

Skin Color/Ripeness:

- Yellow
  - Yellow-green
  - Green
- Bruising:
- Bruised
  - Non-Bruised



Skin Color/Ripeness:

- Yellow
  - Yellow-green
  - Green
- Bruising:
- Bruised
  - Non-Bruised

Skin Color/Ripeness:

- Yellow
  - Yellow-green
  - Green
- Bruising:
- Bruised
  - Non-Bruised



De La Salle University

2605



Skin Color/Ripeness:

- Yellow
  - Yellow-green
  - Green
- Bruising:
- Bruised
  - Non-Bruised

Skin Color/Ripeness:

- Yellow
  - Yellow-green
  - Green
- Bruising:
- Bruised
  - Non-Bruised



De La Salle University

2606

## **Appendix E CERTIFICATE FROM FARMERS**

2607



# De La Salle University

2608

## Comparative Analysis: Expert's Assessment

Please fill up the following information.

Full Name: Jesus Redome  
 Years of Experience: 20  
 Current Role/Position: Farmer  
 Address of Farm: Ibaan Batangas Hectares: 4  
 Mango Varieties Familiar With: Piko, Kalabaw, Indian  
 Experience with Quality Standards: 10  
 Date of Analysis: Nov 4, 2021

Instructions: Your task is to categorize the mangoes based on its color and bruising. Each image will have checkboxes pertaining to the category. More specifically categorize the mango's color into yellow, yellow-green, and green. And the bruises category into bruised and non-bruised.

Jesus Redome  
 Jesus Redome  
 Name & Signature

E. Certificate from Farmers



De La Salle University

2609

Name: Jesus Redome Date: Nov 4, 2025  
Position/Role: Farmer

**CERTIFICATION OF CARABAO MANGO SORTING AND  
DATASET VERIFICATION**

This is to certify that the dataset of Carabao Mangoes used in the thesis project entitled "Non-Destructive Carabao Mango Sorter and Grader based on Physical Characteristics using Machine Learning" conducted by AISL-1-2425-C5 of Department of Electronics and Computer Engineering, De La Salle University, has been reviewed and verified.

The mangoes represented in this dataset has been properly sorted based on the standards defined by experts. This verification confirms the dataset's integrity for academic and technical use.

Issued this \_\_\_\_\_, for documentation and thesis validation purposes.

Sincerely,  
Jesus Redome  
Jesus Redome

Name & Signature



# De La Salle University

2610

## Comparative Analysis: Expert's Assessment

Please fill up the following information.

Full Name: Ivan Joseph Palma  
 Years of Experience: 10  
 Current Role/Position: Farmer, Helper  
 Address of Farm: Ibaan, Batangas, Hectares: 4  
 Mango Varieties Familiar With: Carabao, Pico  
 Experience with Quality Standards: 5  
 Date of Analysis: Nov 4, 2025

Instructions: Your task is to categorize the mangoes based on its color and bruising. Each image will have checkboxes pertaining to the category. More specifically categorize the mango's color into yellow, yellow-green, and green. And the bruises category into bruised and non-bruised.

  
 Name & Signature

E. Certificate from Farmers



De La Salle University

2611

V

Name: Ivan Joseph Palma Date: Nov 4, 2025  
Position/Role: Farmer Helper

CERTIFICATION OF CARABAO MANGO SORTING AND  
DATASET VERIFICATION

This is to certify that the dataset of Carabao Mangoes used in the thesis project entitled "Non-Destructive Carabao Mango Sorter and Grader based on Physical Characteristics using Machine Learning" conducted by AISL-1-2425-C5 of Department of Electronics and Computer Engineering, De La Salle University, has been reviewed and verified.

The mangoes represented in this dataset has been properly sorted based on the standards defined by experts. This verification confirms the dataset's integrity for academic and technical use.

Issued this \_\_\_\_\_, for documentation and thesis validation purposes.

Sincerely,

*Ivan Joseph Palma*  
Name & Signature



# De La Salle University

2612

## Comparative Analysis: Expert's Assessment

Please fill up the following information.

Full Name: Ailen Q Redome  
Years of Experience: 10  
Current Role/Position: Farmer Helper  
Address of Farm: T. baan Batangas Hectares: 4  
Mango Varieties Familiar With: Pico, Indian, Kalabaw  
Experience with Quality Standards: 7  
Date of Analysis: Nov 6, 2025

Instructions: Your task is to categorize the mangoes based on its color and bruising. Each image will have checkboxes pertaining to this category. More specifically categorize the mango's color into yellow, yellow-green, and green. And the bruises category into bruised and non-bruised.

Ailen Q Redome  
Ailen Redome  
Name & Signature

E. Certificate from Farmers



De La Salle University

2613

Name: Ailen Q. Redome Date: Nov 4, 2015  
Position/Role: Farmer /keeper

CERTIFICATION OF CARABAO MANGO SORTING AND  
DATASET VERIFICATION

This is to certify that the dataset of Carabao Mangoes used in the thesis project entitled "Non-Destructive Carabao Mango Sorter and Grader based on Physical Characteristics using Machine Learning" conducted by AISL-1-2425-C5 of Department of Electronics and Computer Engineering, De La Salle University, has been reviewed and verified.

The mangoes represented in this dataset has been properly sorted based on the standards defined by experts. This verification confirms the dataset's integrity for academic and technical use.

Issued this \_\_\_\_\_, for documentation and thesis validation purposes.

Sincerely:

Ailen Q. Redome  
Ailen Q. Redome

Name & Signature



# De La Salle University

2614

## Comparative Analysis: Expert's Assessment

Please fill up the following information.

Full Name: JERRY BRAVANTE  
Years of Experience: 50 yrs  
Current Role/Position: FARMER  
Address of Farm: IBAAN, BATANGAS Altitudes: 4  
Mango Varieties Familiar With: CARABAO, PICO, INDIAN, APPLE MANGO  
Experience with Quality Standards: 20 yrs  
Date of Analysis: Sept 26 2015

Instructions: Your task is to categorize the mangoes based on its color and bruising. Each image will have checkboxes pertaining to the category. More specifically categorize the mango's color into yellow, yellow-green, and green. And the bruises category into bruised and non-bruised.



De La Salle University

2615

2616

## **Appendix F DATASET VALIDATION**



# De La Salle University

2617

Name: \_\_\_\_\_ Date: \_\_\_\_\_

Position/Role: \_\_\_\_\_

## CERTIFICATION OF CARABAO MANGO SORTING AND DATASET VERIFICATION

This is to certify that the dataset of Carabao Mangoes used in the thesis project entitled "Non-Destructive Carabao Mango Sorter and Grader based on Physical Characteristics using Machine Learning" conducted by AISL-1-2425-C5 of Department of Electronics and Computer Engineering, De La Salle University, has been reviewed and verified.

The mangoes represented in this dataset has been properly sorted based on the standards defined by experts. This verification confirms the dataset's integrity for academic and technical use.

Issued this \_\_\_\_\_, for documentation and thesis validation purposes.

Sincerely,

\_\_\_\_\_  
\_\_\_\_\_  
\_\_\_\_\_

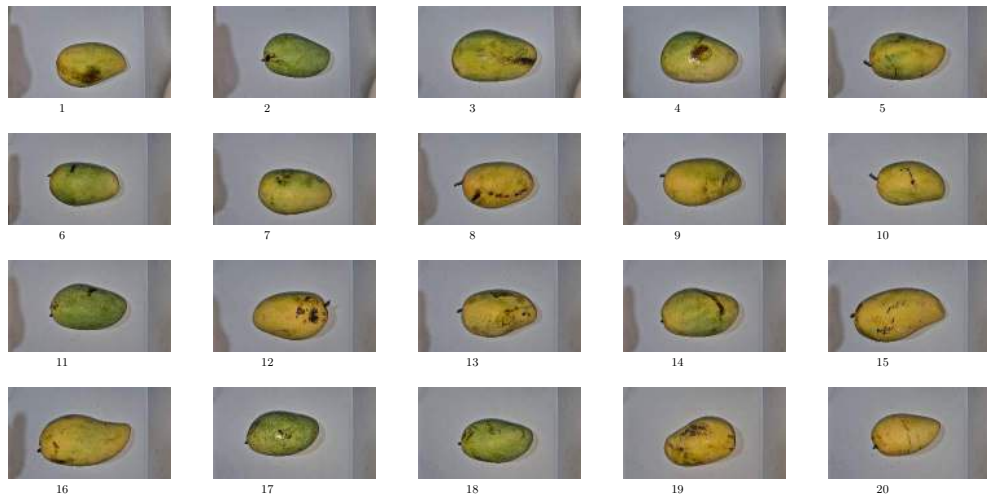
Name & Signature



De La Salle University

2618

Bruised Images (1-20)

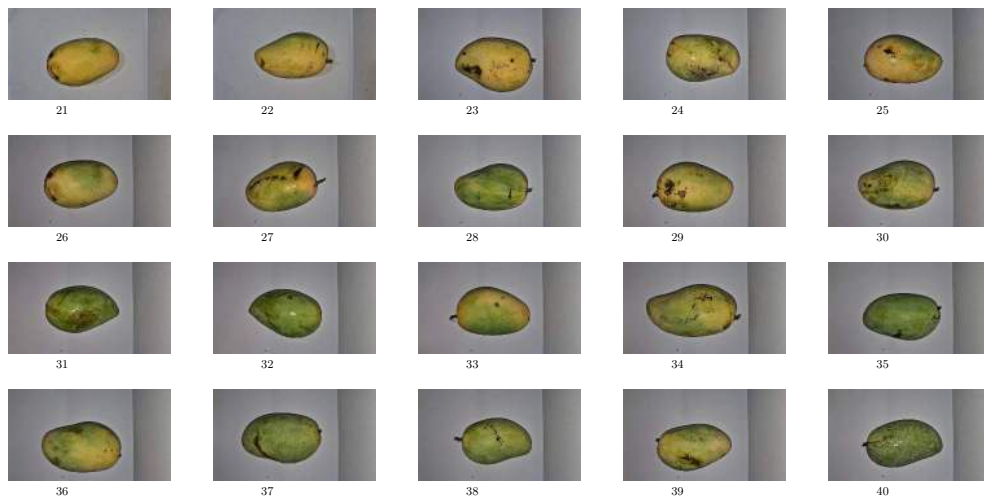




De La Salle University

2619

Bruised Images (21-40)



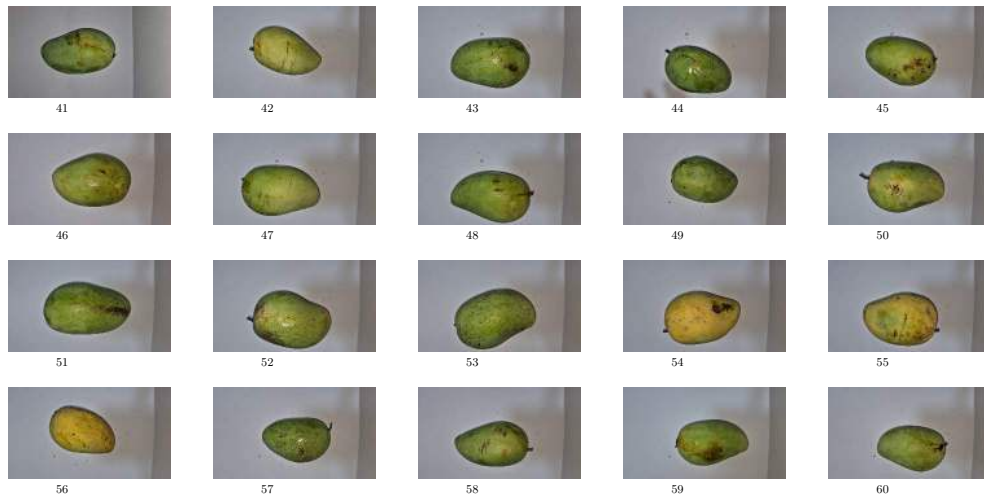
3



De La Salle University

2620

Bruised Images (41-60)

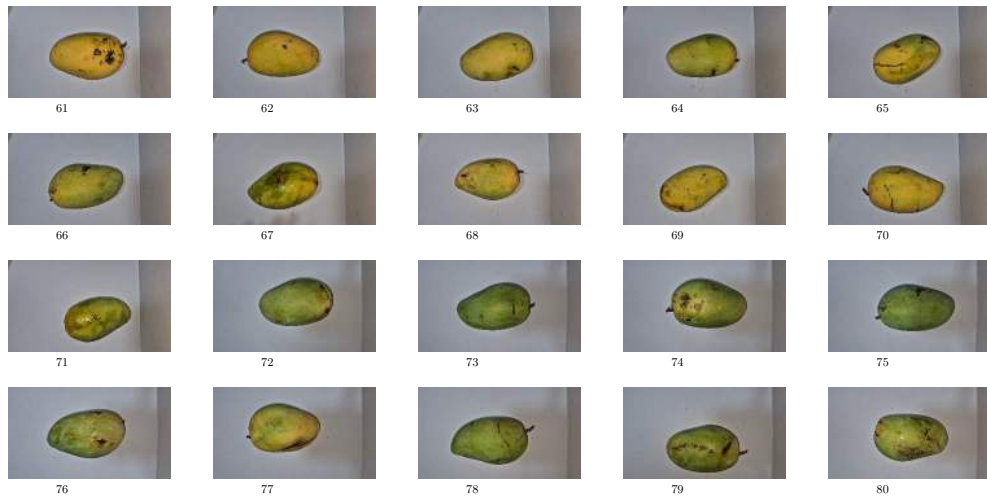




De La Salle University

2621

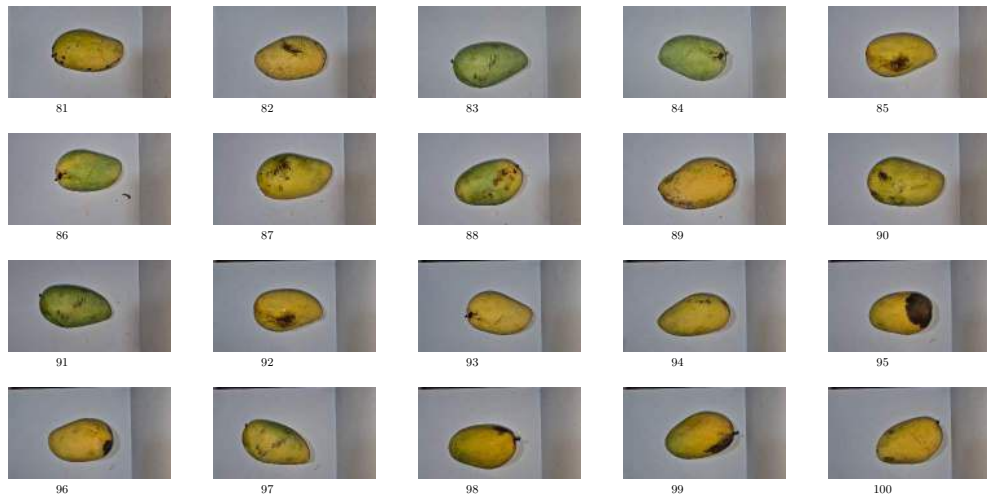
Bruised Images (61-80)





2622

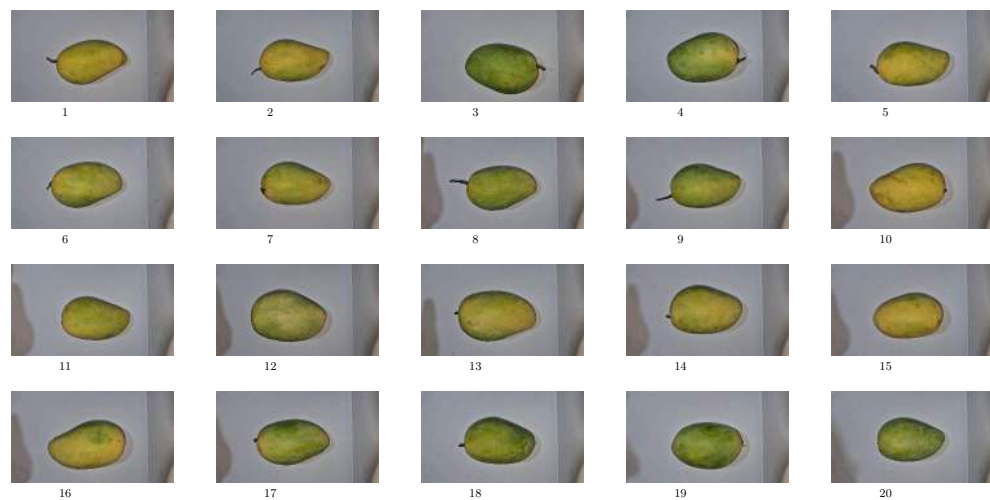
Bruised Images (81-100)





2623

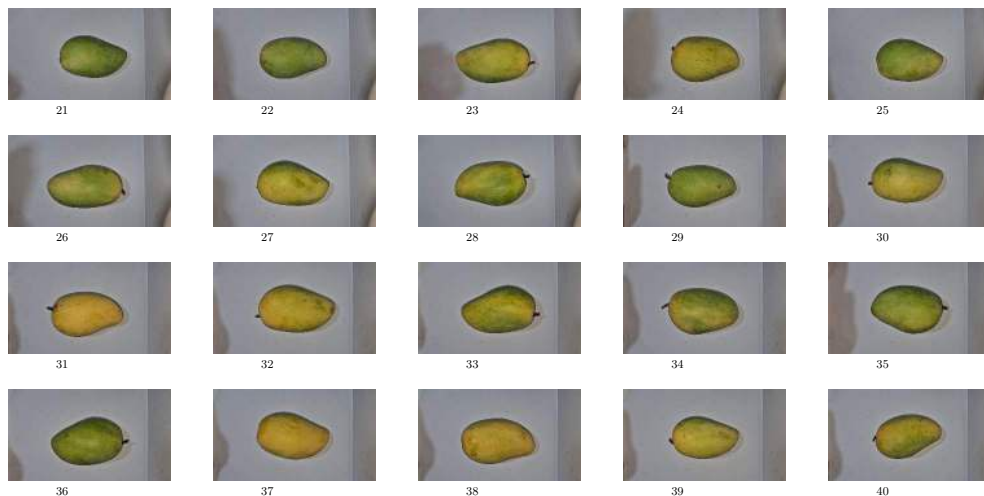
Non-Bruised Images (1-20)





2624

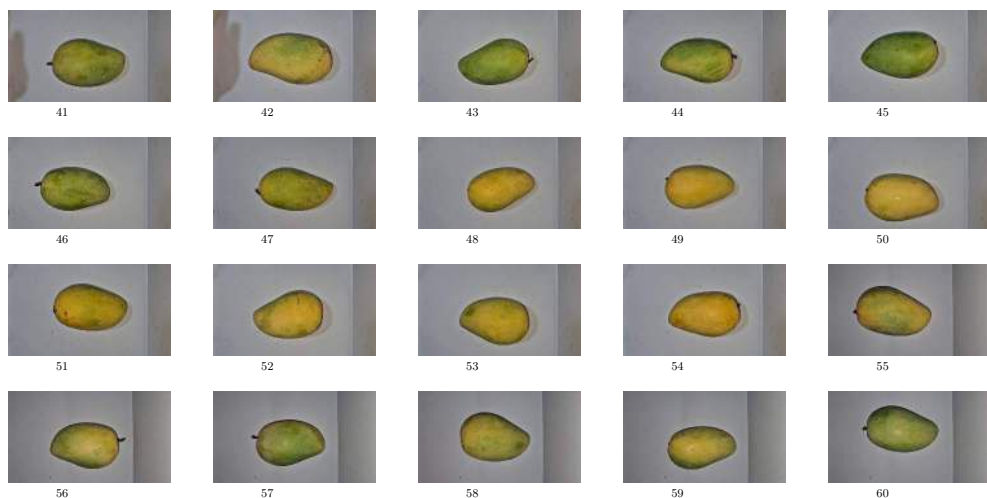
Non-Bruised Images (21-40)





2625

Non-Bruised Images (41-60)

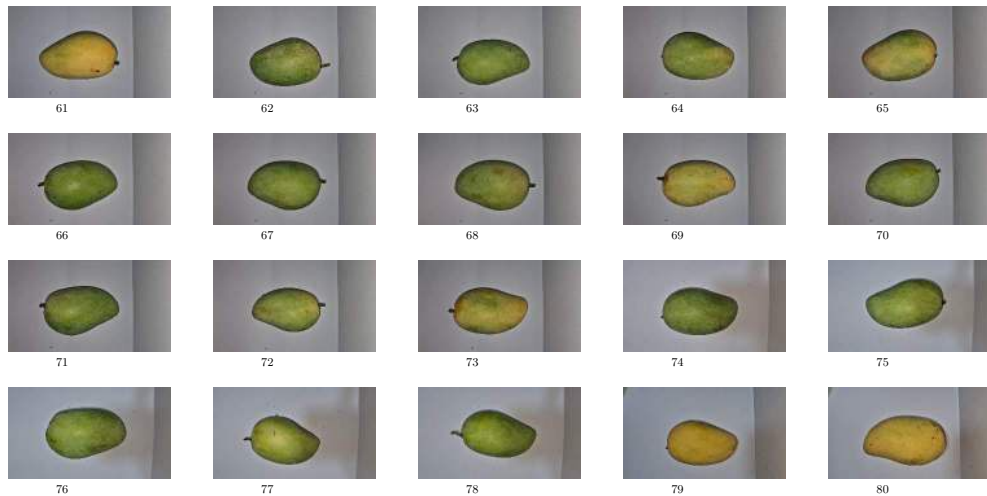




De La Salle University

2626

Non-Bruised Images (61-80)

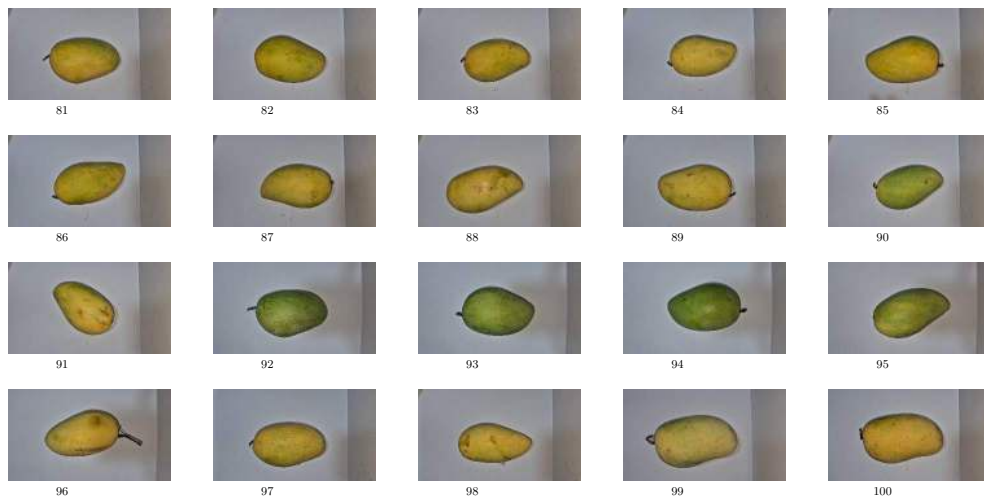




De La Salle University

2627

Non-Bruised Images (81-100)

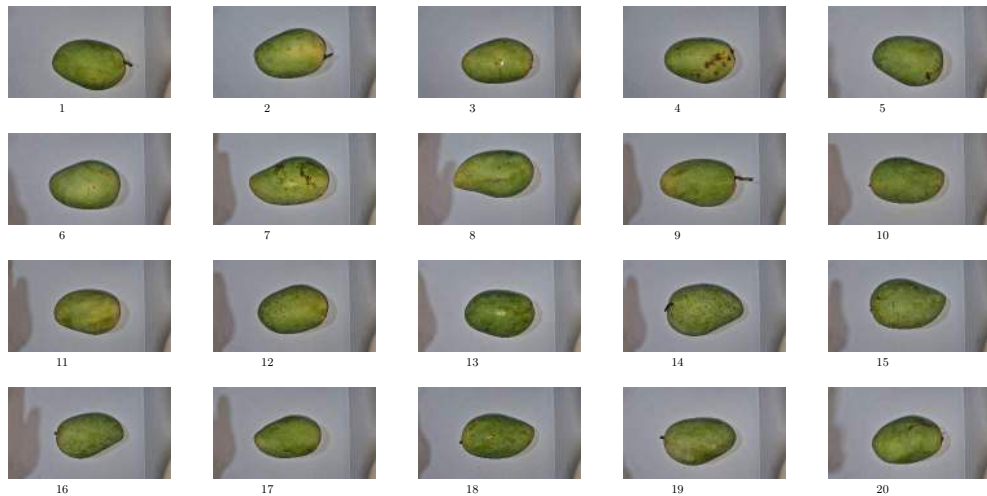




De La Salle University

2628

Green Images (1-20)

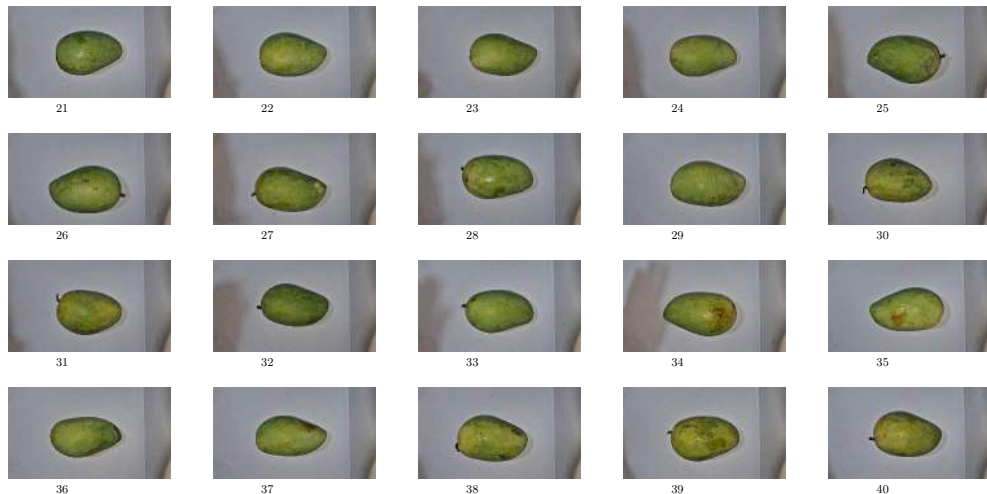




De La Salle University

2629

Green Images (21-40)



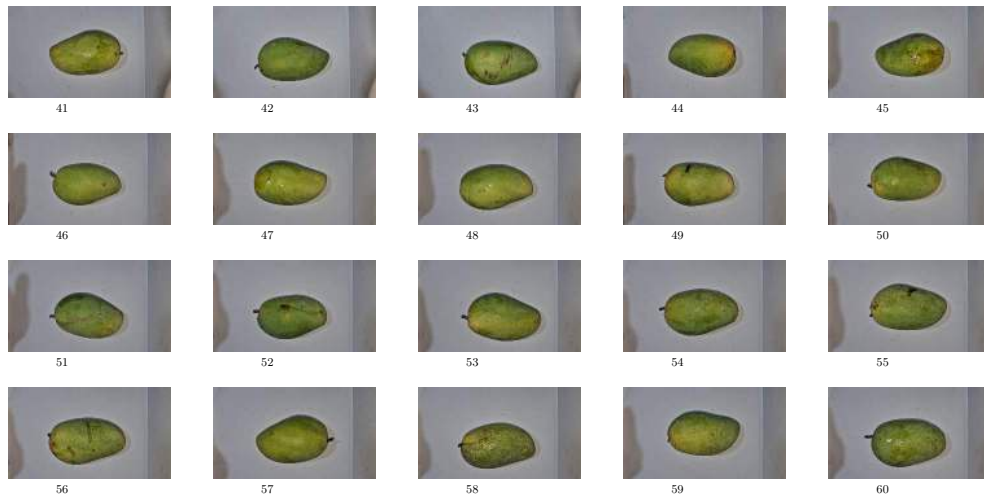
13



De La Salle University

2630

Green Images (41-60)

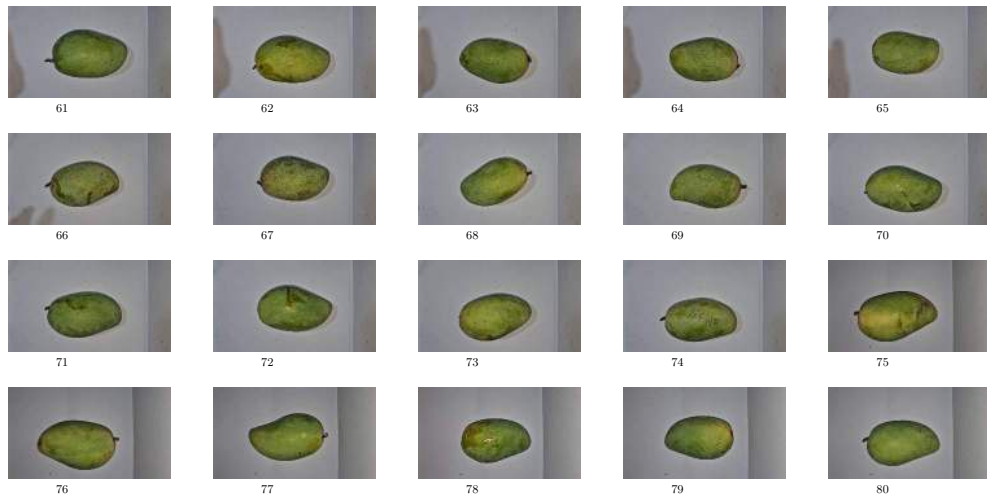




De La Salle University

2631

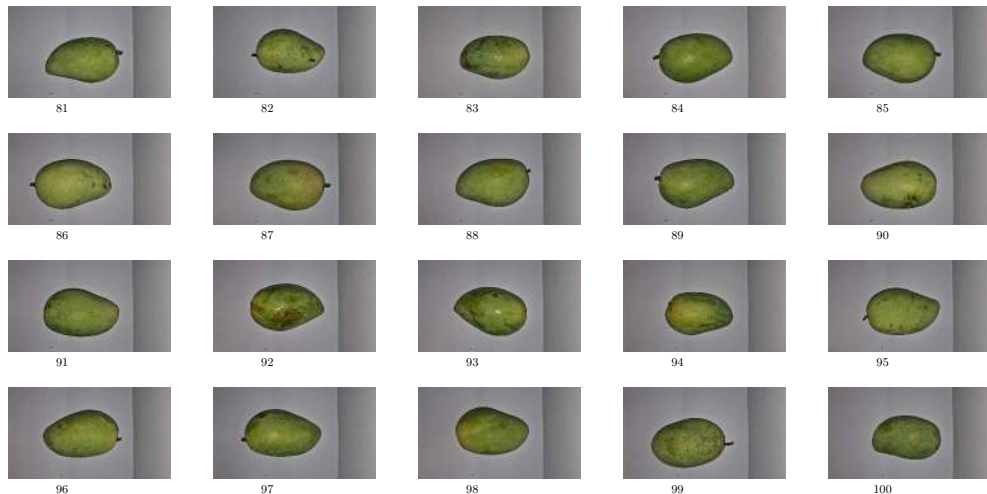
Green Images (61-80)





2632

Green Images (81-100)

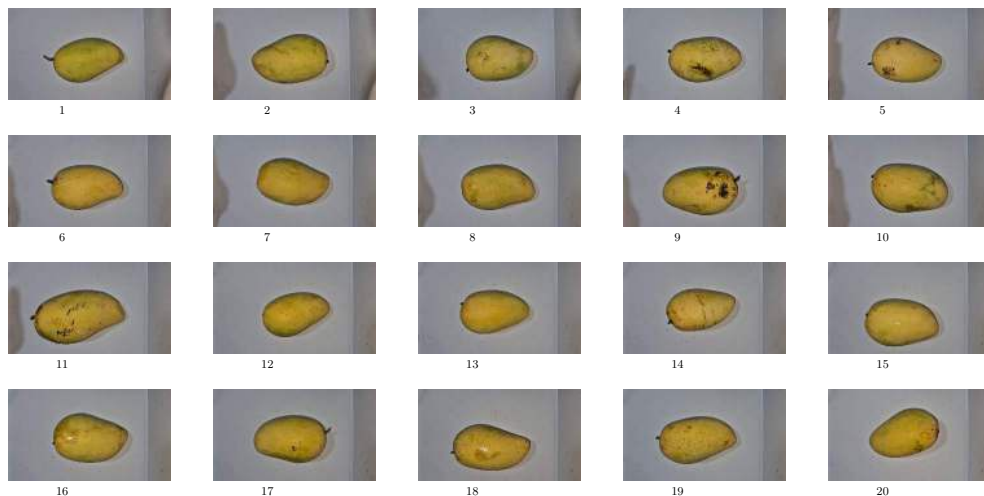




De La Salle University

2633

Yellow Images (1-20)

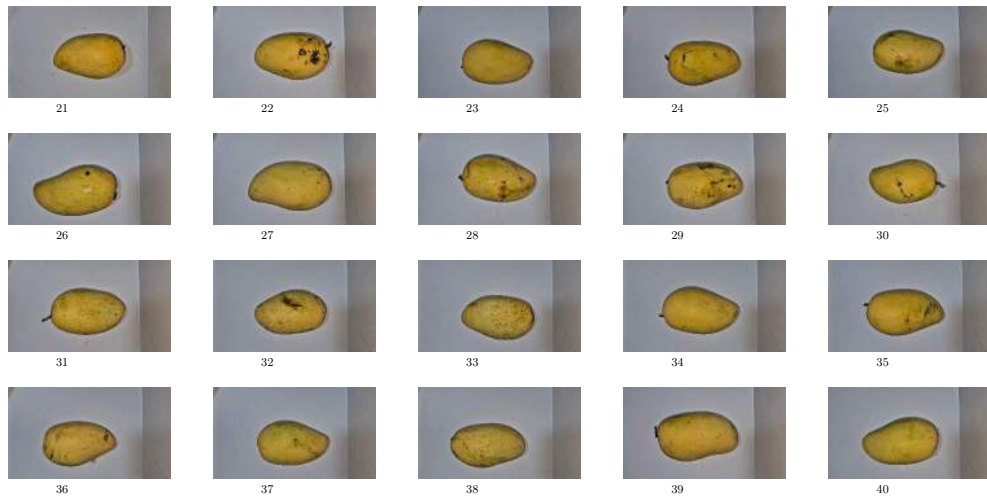




De La Salle University

2634

Yellow Images (21-40)

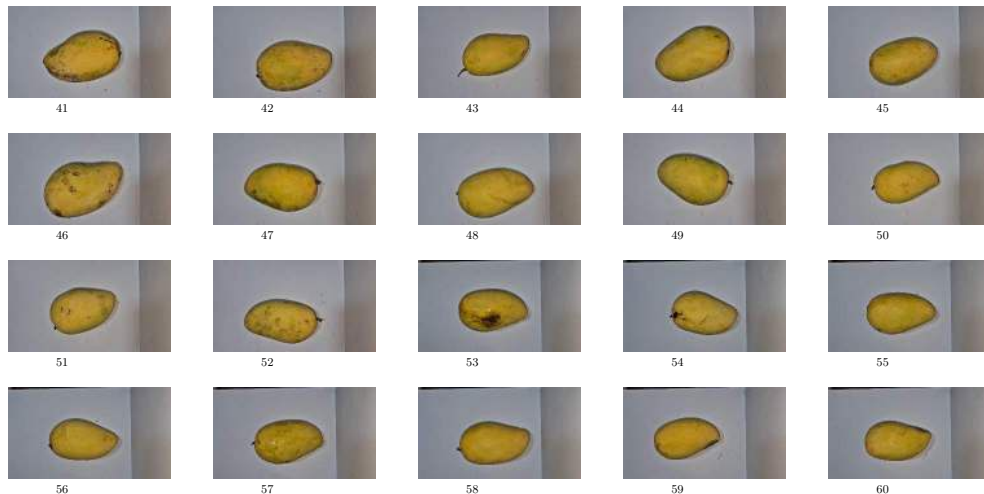




De La Salle University

2635

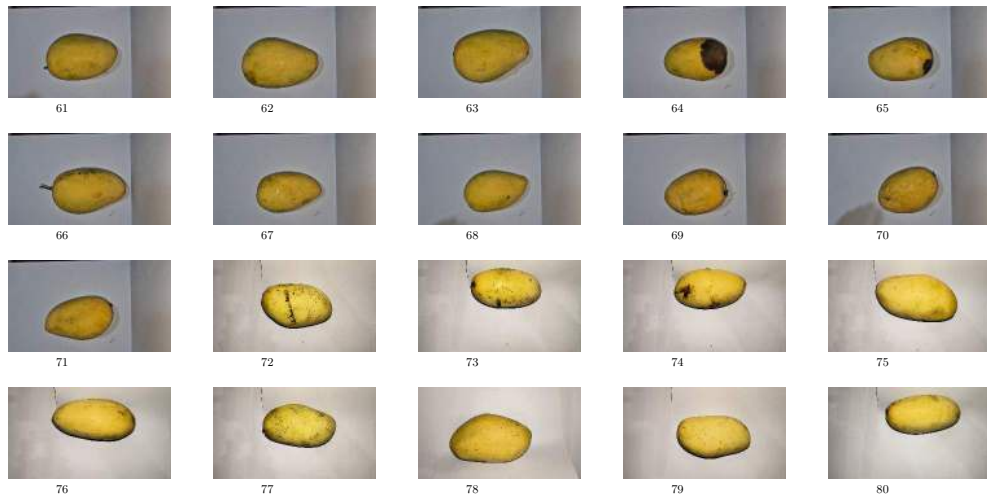
Yellow Images (41-60)





2636

Yellow Images (61-80)





De La Salle University

2637

Yellow Images (81-100)



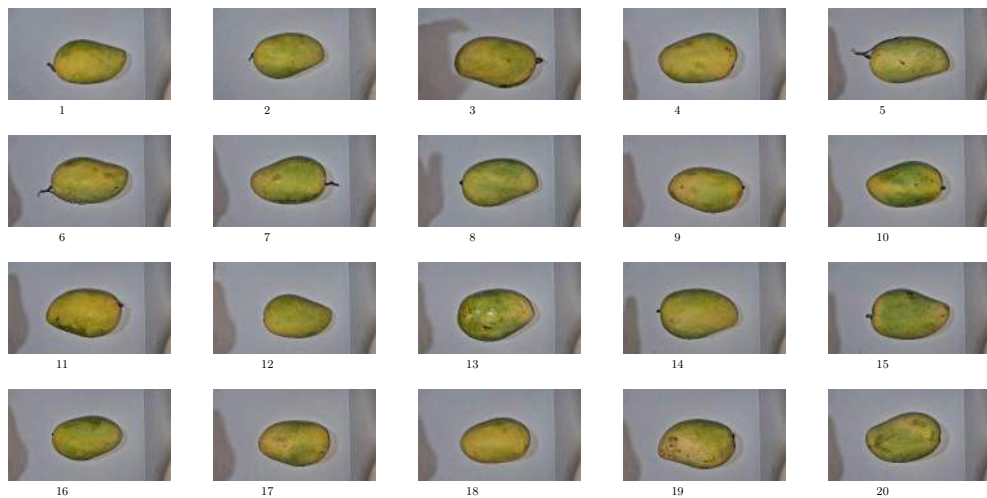
21



De La Salle University

2638

Yellow-Green Images (1-20)

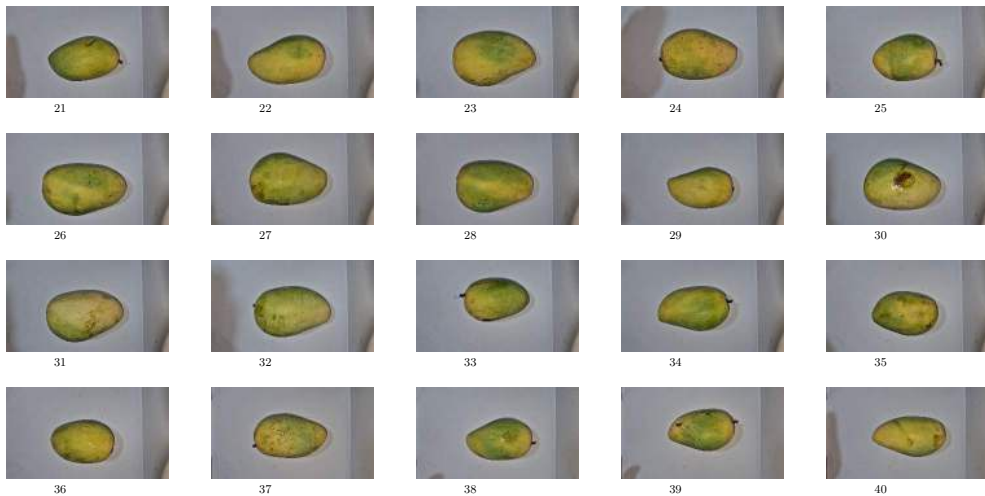


22



2639

Yellow-Green Images (21-40)

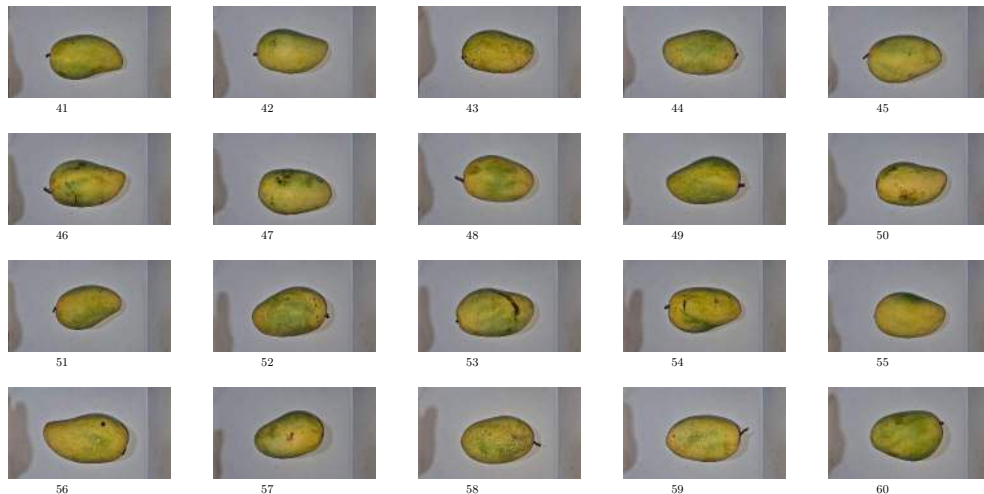




De La Salle University

2640

Yellow-Green Images (41-60)



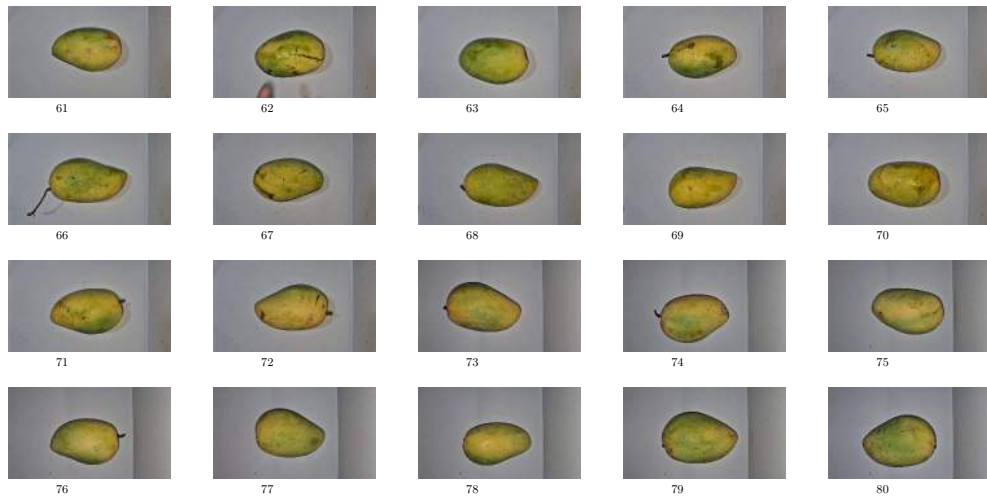
12



De La Salle University

2641

Yellow-Green Images (61-80)



25



De La Salle University

2642

Yellow-Green Images (81-100)

